Draft version February 4, 2003
Preprint typeset using LaTeX style emulateapj v. 11/12/01



# THE COSMOLOGICAL BARYON DENSITY FROM THE DEUTERIUM TO HYDROGEN RATIO TOWARDS QSO ABSORPTION SYSTEMS: D/H TOWARDS Q1243+3047

David Kirkman[1,2,3], David Tytler[1,2], Nao Suzuki[1,2], John M. O'Meara[1,2], Dan Lubin[1,2]

[1] Visiting Astronomer, W.M. Keck Observatory which is a joint facility of the University of California, the California Institute of Technology and NASA.
[2] Center for Astrophysics and Space Sciences, University of California, San Diego, MS 0424; La Jolla; CA 92093-0424
[3] E-mail: dkirkman@ucsd.edu

*Draft version February 4, 2003*

## ABSTRACT

We report the detection of Deuterium absorption at redshift 2.525659 towards Q1243+3047. We describe improved methods to estimate the Deuterium to Hydrogen abundance ratio (D/H) in absorption systems, including improved modelling of the continuum level, the Ly$\alpha$ forest and the velocity structure of the absorption. Together with improved relative flux calibration, these methods give D/H $= 2.42^{+0.35}_{-0.25}\times10^{-5}$ cm$^{-2}$ from our Keck-I HIRES spectra of Q1243+3047, where the error is from the uncertainty in the shape of the continuum level and the amount of D absorption in a minor second component. The measured D/H is likely the primordial value because the [O/H] $= -2.79 \pm 0.05$. This absorption system has a neutral Hydrogen column density log N$_{\rm HI}$ $= 19.73 \pm 0.04$ cm$^{-2}$, it shows five D lines and is mostly ionized. The best estimate of the primordial D/H is $2.78^{+0.44}_{-0.38}\times10^{-5}$, from the log D/H values towards five QSOs. The dispersion in the five values is larger than we expect from their individual measurement errors and we suspect this is because some of these errors were underestimated. We observe a trend in D/H with log N$_{\rm HI}$ that we also suspect is spurious. The best value for D/H is $0.6\sigma$ smaller than we quoted in O'Meara *et al.* (2001) from three QSOs, and although we have more values, the error is similar because the dispersion is larger. In standard big bang nucleosynthesis (SBBN), the best D/H corresponds to a baryon-to-photon ratio $\eta = 5.9 \pm 0.5 \times 10^{-10}$ and gives precise predictions for the primordial abundances of the other light nuclei. We predict more $^4$He than is reported in most measurements, although not more than allowed by some estimates of the systematic errors. We predict a $^3$He abundance very similar to that reported by Bania *et al.* (2002), and we predict 3 – 4 times more $^7$Li than is seen in halo stars. It is unclear if those stars could have destroyed this much of their $^7$Li. The $\eta$ value from D/H corresponds to a cosmological baryon density $\Omega_b h^2 = 0.0214 \pm 0.0020$ (9.3%) that agrees with values from the anisotropy of the Cosmic Microwave Background: $\Omega_b h^2 = 0.021 \pm 0.003$ from the Netterfield *et al.* (2002) analysis of BOOMERANG data and $\Omega_b h^2 = 0.022^{+0.004}_{-0.003}$ from the Pryke *et al.* (2002) analysis of the DASI results.

*Subject headings:* quasars: absorption lines – quasars: individual (cso 0167 = Q1243+3047) – cosmology: observations

## 1. INTRODUCTION

It is well established that the light nuclei hydrogen (H), deuterium (D), $^3$He, $^4$He and $^7$Li are all made during big bang nucleosynthesis. The relative primordial abundances created in the Standard theory of big bang nucleosynthesis (SBBN) for these five nuclei depend on one parameter, the cosmological baryon-to-photon ratio, $\eta = n_b/n_\gamma$ (Kolb & Turner 1990; Walker *et al.* 1991; Schramm & Turner 1998; Nollett & Burles 2000; Olive, Steigman & Walker 2000). A measurement of the ratio of any two primordial abundances gives $\eta$. The three other primordial abundances are predicted once $\eta$ is known and measurements of them test the theory.

SBBN has now been validated in two main ways. First, it successfully accounts for measurements of the approximate relative primordial abundances of all these light nuclei (Boesgaard & Steigman 1985; Walker *et al.* 1991; Copi, Schramm & Turner 1995; Schramm 1998; Schramm & Turner 1998; Tytler *et al.* 2000 and references there in). Second, the baryon density required is roughly consistent with that measured in other ways, including the Ly$\alpha$ forest at high redshifts (Rauch *et al.* 1997; Weinberg *et al.* 1997; Zhang *et al.* 1998; Hui *et al.* 2002), and the baryon fraction in clusters of galaxies (Babul & Katz 1993; Boute & Canizares 1996; Bludman 1998; Rines *et al.* 1999; Arnaud & Evrard 1999; Wu & Xue 2000; Sadat & Blanchard 2001). Recently, the cosmic microwave background (CMB) has given the same baryon density to within 10%.

We use the D I/H I ratio in QSO absorption line systems to estimate $\eta$. This method is attractive because the deuterium abundance is more sensitive to $\eta$ than other light nuclei, the D/H ratio in QSO absorption systems is apparently the primordial value, and we do not apply any corrections for unobserved ions.

We measure D/H by dividing the column densities that we measure for absorbing D I and H I atoms. Since D/H is low, we could see D in only absorption systems that have high H I column densities, at most one per QSO. We would like to measure the column densities to better than 10% accuracy and ideally $< 1\%$ to better test early uni-

verse physics. Echelle spectrographs give ample spectral resolution, and integration times approaching 1 day give the required signal-to-noise ratio (S/N). Once D has been found in a well calibrated QSO spectrum, there are four main factors that limit the measurement accuracy: the continuum level, the Ly$\alpha$ forest, the velocity structure of the absorber, and contamination by absorption other than D.

Each of the factors that complicate the measurement of D/H are hard to model and quantify. We need to know the level of the unabsorbed continuum to measure the amount of absorption. The Ly$\alpha$ and other weak emission lines make it hard to estimate the precise continuum shape, and stochastic Ly$\alpha$ forest absorption only makes matters worse. The Ly$\alpha$ forest H I absorption is random in wavelength and opacity, and is ubiquitous over the redshift intervals in which we can measure D/H from ground based telescopes. All the H and D lines are in the Ly$\alpha$ forest portion of QSO spectra, which introduces confusion and in the worse case can mimic D absorption. The hardest problem is to ensure that we explore all possible velocity structures that might explain a given spectrum. D/H values and their errors are often dictated by the choice of velocity structure.

It appears likely that the measurement errors have been underestimated in at least one of the published D/H values, because these errors are hard to calculate, and the dispersion in D/H measurements is larger than expected. In O'Meara *et al.* (2001) we found that the dispersion between three D/H values that we had measured towards different QSOs was larger than expected from the quoted errors. We concluded that this dispersion was probably not real, and instead a result of our underestimation of the errors. Since then, Pettini & Bowen (2001) have found D in a fourth QSO, Q2206–199 and quote a D/H value which is much less than the previous measurements, while D'Odorico *et al.* (2001) and Levshakov *et al.* (2002) have presented two very different measurements of D/H towards a 5th QSO, Q0347–3819. These new measurements further increase the dispersion in the reported D/H values, and again we suspect that this is because the errors have been underestimated.

In this paper we announce the detection of D in an absorption system at $z = 2.526$ in the spectrum of Q1243+3047. We describe how we have improved our exploration of some factors which determine the measurement errors. In particular we describe improved calibration of relative flux levels, our estimates of the continuum level, our modelling of the velocity structure, and our modelling of the Ly$\alpha$ forest and blended lines.

We present material in the following order: observations and reductions (§2), overview and velocity structure of the absorption system that shows D (§3), measurement of the D column density (§4), evidence that we are measuring D (§5) measurement of the H column density (§6), the metal abundance and ionization in the absorbing gas(§7), the D/H from Q1243+3047 (§8), and from all QSOs (§9), and the deduced cosmological parameters (§10). The summary ends with a discussion of the improvements in methods that we use here, and a list of the issues that remain. In the Appendices we discuss how we model the continuum, our optimizing code, error estimates from the covariance matrix and D/H values from other QSOs.

## 2. OBSERVATIONS AND DATA REDUCTION

We report the detection of D absorption in the QSO Case Stellar Object CSO 0167, which we call by its B1950 coordinate name: Q1243+3047. This QSO was reported as a V = 17 blue object at B1950 RA 12h 43m 44.9s DEC +30d 47.9', with a 15" error, (equivalent to J2000 12h 46m 10.9s +30d 31m 31.2s) in an objective prism photograph by Sanduleak & Pesch (1984), and identified as a QSO at emission line redshift $z_{em} = 2.56$ by Everett & Wagoner (1995). This QSO is not well known. The NASA extragalactic database (NED) gives no other primary references except for a 2MASS QSO search.

We have spectra with three different spectral resolutions, from three spectrographs, summarized in Tables 1 and 2, and shown in Figures 1, 2 and 3.

We obtained five spectra of Q1243+3047 from the Kast double spectrograph on the Lick Observatory 3.1m Shane telescope. These low resolution spectra are used to flux calibrate HIRES spectra. We compare these spectra to check the flux calibration, and we can sum them to improve the S/N. All integrations were obtained using the d46 dichroic that splits the spectrum near 4600 Å, the 830 line/mm grism blazed at 3460 Å for the blue side, and the 1200 line/mm grating blazed at 5000 Å for the red side.

We have one intermediate resolution spectrum from the ESI spectrograph (Epps & Miller 1998; Bigelow & Nelson 1998; Sheinis *et al.* 2000), mounted at the Cassegrain focus of Keck-II. This echellette covers from 3900 – 11,000 Å in a single setting in ten overlapping orders. We also use this spectrum to flux calibrate the HIRES spectra, and to look for metal line absorption at wavelengths larger than those covered in our HIRES spectra.

We have eight high resolution spectra from the HIRES spectrograph (Vogt *et al.* 1994) on the Keck-I 10m telescope. These were obtained using the C5 dekker that has a 1.14" slit width and gives a FWHM of 8.0 km s$^{-1}$ sampled with 2.1 km s$^{-1}$ per pixel on the original HIRES Tektronix 2048x2048 CCD. To improve the relative flux levels along each spectrum, all observations were taken with the spectrograph slits aligned with the local vertical. All but one of these spectra cover down to wavelengths below the Lyman limit break in the absorption system that shows D, while the exception extends to larger wavelengths to cover some metal lines. The S/N per pixel in the summed HIRES spectra (Table 2) increases linearly with wavelength up to 4200 Å, and then rises faster in the Ly$\alpha$ emission line, reaching 105 on either side of the Ly$\alpha$ absorber of the D/H system. The S/N in the center of an echelle order is approximately 1.4 times greater than that at the ends.

We describe the data reduction and flux calibration in detail in Suzuki *et al.* (2003). The error in the wavelength solution for the HIRES spectra is at least 0.05 – 0.1 pixels, or 0.1 – 0.2 km s$^{-1}$, and may be as large as 1 – 2 km s$^{-1}$. Our analysis of other similar spectra (Levshakov, Tytler & Burles 2000) revealed errors of order 1 km s$^{-1}$. We placed all the HIRES integrations on the same logarithmic wavelength scale, which has a constant velocity of 2.1 km s$^{-1}$ per pixel, similar to the original pixel size, and we shifted the Kast and ESI spectra to put them on a similar wavelength scale. All spectra were also converted to vacuum

wavelengths and shifted to the solar rest frame. We applied a relative flux calibration to the HIRES spectra using the Kast and ESI spectra to transfer the flux information from standard stars to the QSO spectra.

## 3. THE $z = 2.526$ SYSTEM THAT SHOWS D

In this section, we discuss the spectrum of Q1243+3047, we introduce the absorption system that shows the D, and we discuss its velocity structure.

### 3.1. *Overview of the Q1243+3047 spectrum*

We observe D in the conspicuous absorption system at $z = 2.526$ that produces both a clear Lyman limit break and has the strongest Ly$\alpha$ absorption line in the spectra, near 4285 Å. We see no flux below the limit that is near 3210 Å in the Kast and HIRES spectra. No flux is expected because the H I column density log $N_{HI}$ is clearly near $\simeq 19$ cm$^{-2}$ from the shape of the Ly$\alpha$ line. The presence of a strong O I line at this redshift also implies that log $N_{HI} > 19$ cm$^{-2}$. In addition to five D absorption lines, this system shows many Lyman series H I transitions, but only a few metal lines, because the metal abundances are approximately 0.001 solar in the main component (see §7). In comparison, HS 0105+1619 has half as much H I, but shows 21 metal lines, as its metal abundance is approximately 14 times larger (O'Meara et al. 2001).

The system at $z = 2.526$ shares some of the properties of both the Lyman limit systems (LLSs) and the Damped Ly$\alpha$ systems (DLAs). It is a LLS because it is optically thick in the Lyman continuum, and it has 25% of the minimum log $N_{HI}$ to qualify as a DLA (Turnshek & Rao 2002). It shows O I like DLAs, but unlike DLAs (Wolfe & Prochaska 2000), it is mostly ionized and the different low ionization lines have different velocity profiles. There is little published work on systems with log $N_{HI} = 18-20$ cm$^{-2}$, (e.g. O'Meara *et al.* 2001; Peroux *et al.* 2002)

The spectrum shows metal lines from unrelated redshifts, none of which effect our D/H measurement. A weaker Ly$\alpha$ absorption line near 3710 Å($z \sim 2.052$) appears to have weak damping wings that imply a high $N_{HI}$.

### 3.2. *How we Measure D/H*

The D/H value is the ratio of two column densities, $N_{DI}$ for the neutral Deuterium (D I) and $N_{HI}$. We must estimate the errors on each of these quantities and show that both measurements apply to the same gas.

We measure the $N_{HI}$ to high accuracy from the Ly$\alpha$ line alone, because the shape of this line is dominated by damping wings that are sensitive to $N_{HI}$, and less sensitive to the velocity information. However, the $N_{HI}$ value is more accurate and reliable when we use accurate velocity information, and hence we measure the $N_{HI}$ last, after we have examined the velocity information. Unlike the $N_{HI}$, the $N_{DI}$ that we measure depends strongly on the velocity information.

We obtain the velocity information from the D I lines themselves, taking guidance from the high order H Lyman lines and the metal lines, especially O I.

### 3.3. *Velocity Structure of the $z = 2.526$ absorption system*

We now discuss the clues that metal line absorption give for the velocity structure. The system at $z = 2.526$ shows many components, with different structure in different ions, but the bulk of the H I is in just two components that we see in absorption by O I.

We expect that the H I and the D I should have identical velocity distributions, except for the effects of thermal broadening. We expect the D/H ratio to be constant from component to component, because the metal abundances are too low for significant destruction of D. We also expect that $N_{DI}/N_{HI} = $ D/H because the D and H should have nearly identical ionization (Savin 2002).

We would like to measure the velocity structure of the H and D separately, allowing for a direct comparison. However, the H lines are all saturated, broad and blended, and give little information. Instead, we use the unsaturated metal lines, especially the O I lines, as guides.

We do not know how closely the metal lines will trace the velocity structure of the H I and D I. We expect to find some H I wherever we find metals, but the metal lines can have different velocity distributions in detail because the ionization and metal abundance can vary from component to component, and perhaps with velocity inside a component (§5.1).

In Figure 3, we present the regions of the spectrum where we expect metal line absorption. We observe strong absorption in only a few metal ions: O I, C II, and Si II. C III and Si III also show absorption, but are poorly constrained since their lines appear saturated and may be highly contaminated by Ly$\alpha$ forest absorption. We see weak C IV and Si IV absorption that has very different velocity structure from the low ionization metals. Al II is seen in the ESI spectrum, but is not covered by our HIRES data. Fe II 1608 is not detected at our S/N, and although some absorption appears near the expected positions of N I, N II, N III, and Fe III, it is very weak, and can readily be accounted for as Ly$\alpha$ forest. We also measure $\log N_{C\ II*} < 12.3$ cm$^{-2}$ in all components.

The O I line suggests that two components will be needed to model the velocity distribution of the gas that shows the D. O I provides the best indication of the velocity distribution of the H I and D I absorption, because O I/H I is similar to O/H in gas of low ionization (O'Meara et al. 2001). The O I 1302 transition is in a high S/N region of the spectrum well separated from other lines. This line is asymmetric, with extra absorption at larger wavelengths. We fit the O I with the two components that we list in Table 3.

In Figures 4 & 5 we show fits to the O I, C II, Si II, C IV, and Si IV lines. Voigt profile fitting usually does not produce unique results, and this is especially true for C II and Si II, which can be synthesized with a variety of components at different velocities that are all heavily blended. The C II and Si II fits listed in Table 3 and shown in Figures 4 & 5. Irrespective of the exact model used, the C II and Si II require gas at $v \simeq -40$, $\simeq 0$, and $\simeq 95$ km s$^{-1}$, blended with additional absorption between 16 and 35 km s$^{-1}$.

The C IV and Si IV lines have a different velocity structure from the low ionization transitions O I, C II and Si II, which means they primarily come from different gas. Both C IV and Si IV show absorption at $v \simeq 40$,

100, and 200 km s$^{-1}$. There is also a component centered near $v \simeq 5$ km s$^{-1}$ for C IV and $v \simeq -10$ km s$^{-1}$ for Si IV.

In summary, the metals indicate that H I may be found in components near: $v = -40$, 0, 13, 20, 40, 95 and 200 km s$^{-1}$. We are confident that the O I marks the velocity of most of the H I. The low ionization lines of C II and Si II have most of their column density at these velocities, and O I is not seen at other velocities.

There is no sign of any metal components near $v \simeq -81.6$ km s$^{-1}$, the velocity that would place H I lines at the position expected for the D I lines. This means that there does not need to be any H I that could contaminate the D lines, although there could be if the metal abundances were very low.

### 3.4. *Velocity Structure of the Gas that Gives D/H*

While the system shows many components, the D/H measurement will depend on just three. We expect to see D I in the two components that we see in the O I, C II and Si II, while the third component is an unfortunate blend that adds uncertainty but does not show D.

- Component 1, near $v = 0$ km s$^{-1}$, is the strongest component in O I, C II, Si II and D I. We will refer to the D I absorption in this component as D-1, with column density N$_{\rm DI}$(D-1) and velocity dispersion $b$(D-1) and similarly for the other ions. The parameters of the O-1 and D-1 components are well determined and they contain approximately 90% of the column density. We use the redshift of the O-1 component, $z$ (O-1)= 2.5256916, to define a reference frame with radial velocity $v = 0$ km s$^{-1}$. In this frame, we measure the velocity of the O-1 as $v = 0.00 \pm 0.14$ km s$^{-1}$, where the error is from the fit alone and ignores the poorly known wavelength scale error.

- Component 2, near $v = 13$ km s$^{-1}$, is seen as an asymmetric extension of the O I that we call component O-2. There is also some C II, Si II near this velocity. We call other associated lines D-2 and H-2. Neither the velocity nor the $b$-value of the O-1 component are well known, and they are correlated. Smaller $b$-values are needed as the line center moves to larger wavelengths. If we have some additional velocity or $b$-value information, then the second component is well determined. For example, if both O I components have the same $b$-value, this value is 6.78 km s$^{-1}$, component 2 is at 13.3 km s$^{-1}$, and its column density at 13% of the total.

- Component 3, near $v = -40$ km s$^{-1}$, is an even weaker component in C II and Si II. We will refer to the H I absorption from this component as H-3, which is at $v(H-3) = -44.3 \pm 7.0$ km s$^{-1}$, with log N$_{\rm HI}(3) = 15.90 \pm 0.03$ cm$^{-2}$ from the higher order Lyman lines. This log N$_{\rm HI}$ value is low enough that we would not expect to see O I or D I and neither is seen. H-3 effects D/H because the short wavelength side of the Lyman lines from H-3 accidentally blend with the long wavelength side of the D-2 lines, and hence some of the absorption near –70 km s$^{-1}$ can be explained by either H-3 or D-2. In Figure 6, we see that D-2 is strongly blended with D-1 and H-3.

There is a large amount of H I absorption, log N$_{\rm HI} \simeq$ 19.7 cm$^{-2}$, near components 1 and 2, but we have little information on the velocity distribution of this H I. In Figs. 7 & 8 we show the Lyman series lines. The spectra require H I Lyman lines corresponding to the metal line components near $v = -40$, 0, 95 and 200 km s$^{-1}$. The spectra are also consistent with, but do not need, components at 13, 20 and 40km s$^{-1}$. The parameters that we find for these components are in Table 3. If there is H I absorption at 40 km s$^{-1}$ with $b > 10$ km s$^{-1}$, the blue edge of the higher order Lyman lines show that it has log N$_{\rm HI} < 16.4$ cm$^{-2}$. Figure 8 shows there is no flux in the range $-40$ to 40 km s$^{-1}$ in lines up to Ly-14, and in higher order lines the S/N is rather low, and the Lyman lines start to overlap. We can measure the shape and width of the higher order lines, but unfortunately this tells us little about the gas at $v = 0 - 13.3$ km s$^{-1}$. The absorption on the negative velocity side of these lines is determined by the H I at –40 km s$^{-1}$ with log N$_{\rm HI} \sim 16$ cm$^{-2}$, and the positive velocity side of these lines may be influenced by log N$_{\rm HI} \sim 16$ cm$^{-2}$ absorption at 40 km s$^{-1}$.

A single component at $v = 0$ km s$^{-1}$ with a $b \simeq 17.7$ km s$^{-1}$ gives a fair fit to all of the H lines without separate lines at $\pm$40 km s$^{-1}$ . This $b$-value is an upper limit on the $b$-value for the H I in component 1, since we must use a lower $b$-value when we include separate lines at $\pm$40 km s$^{-1}$ . We will see below that we can also obtain an excellent fit to the H lines using components H-1 and H-2.

## 4. MEASUREMENT OF THE D COLUMN DENSITY

In this section we explore a variety of models that can account for the spectrum. We estimate the log N$_{\rm DI}$ from the models that fit the spectrum with the lowest $\chi^2$ values (§4.1) and in §4.2 we discuss the many factors that effect the accuracy and reliability of the log N$_{\rm DI}$ value and our estimate of the error.

To make a reliable estimate of the D/H ratio in this system, we must explore the full range of models that can explain the H and D absorption in the spectrum. Different models employ different assumptions about issues such as the velocity structure of the absorber, and whether D or H is making parts of the absorption.

A large part of the uncertainty over the D/H comes from the log N$_{\rm DI}$ in the D-2 component. We can not predict the amount of D in D-2, because we do not know the fraction of the H I in this component, and the O/H need not be the same in the two components. The spectrum requires some absorption near –70 km s$^{-1}$ that can be either D-2 or H-3. We must now determine how much of this absorption is from D-2.

Most of the information on the D is in transitions Ly-2 to 8, which we show in Figure 7. In each transition we see absorption that has all the expected characteristics of component D-1 associated with H-1 and O-1. In Ly-4 to 8 we see a resolved D line that is well separated from the H absorption, while in Ly-2 and 3 the D absorption is fully blended with the H lines, as we expected because the H line is wider. The velocity structure, central velocity, $b$-value and column density are all well determined from Ly-4 to

8, especially since the last few lines are not saturated. The absorption is coming from D in gas with velocity near zero. The D-1 lines are all very narrow, and they can all be fit by a single component.

However, we have less information on the D-2 component, because it is fully blended with the D-1 on its short wavelength side, and H-3 on the other side.

In Figure 9 we show the $b$ and log $N_{DI}$ values that we obtain when we fit each of the D lines individually with a single component. While there is general agreement, the dispersion is clearly larger than expected for the errors that we show. These errors come from the covariance matrix of the $\chi^2$ optimization and we explain in the Appendix §14.1 why such errors are often too small.

Two of the D-1 lines are contaminated by other lines. The Ly-5 D line contains a second narrow Ly-3 line at $z = 2.3987515$ that has log $N_{HI}$ 14.459 cm$^{-2}$ and $b$ = 28.81 km s$^{-1}$. This contaminant is well determined by its other Ly lines and we fit it when we fit the Ly-5 D line. The D Ly-3 line includes a slight contribution from a Ly$\beta$ line with $z = 2.342177$, $b$ = 35.6 km s$^{-1}$ and log $N_{HI}$ = 13.81 cm$^{-2}$.

### 4.1. *Grid Search to Find log $N_{DI}$*

In this section we estimate the log $N_{DI}$ value and its error. We have explored various models that might explain the absorption at all wavelengths relevant to deuterium. When we calculated the $\chi^2$ difference between the simulated spectra from the models and the data we found that there was a well defined set of parameters that give excellent $\chi^2$ values. We obtained log $N_{DI}$ and its error from the set of models that had $\chi^2 < \chi^2_{min} + 1$.

We made a six dimensional grid of models, one model for each combination of the allowed parameter values. We specified these models using six parameters that we vary, because they might change the D/H, and other parameters that we hold constant. We made simulated spectra for 15,750,000 different models, one for each possible combination of the parameter values. We allowed each of the six parameters to have every discrete value given by the (minimum value, maximum value, and the number of uniformly spaced steps), as follows:

- log $N_{DI}$(total) (15.07 cm$^{-2}$, 15.2, 15).
- $N_{DI}$(D-2) / $N_{DI}$(total) (0.01, 0.35, 35).
- $v_{sep}$, the velocity separation of the two D components, (5 km s$^{-1}$, 20, 20). The maximum value lets the D absorption cover the full range of the O I absorption, while we found that log $N_{DI}$(D-2) was insignificant whenever the separation was $< 5$ km s$^{-1}$.
- $b$(D-1) (9 km s$^{-1}$, 9.48, 10).
- $b$(D-2) (4 km s$^{-1}$, 15, 10). The upper limit is guided by the largest value for $b$(H-2) and we discuss the lower limit in §4.2.4.
- $b$(H-3) (15.7 km s$^{-1}$, 19, 15).

We found that the log $N_{DI}$(D-1) varies very little, as expected, because its lines are strong and clear. The main variation in log $N_{DI}$(total) comes from log $N_{DI}$(D-2), and hence the first two parameters are strongly correlated. All except the first and last parameters in the list describe the velocity structure of the D, while the last parameters varies the amount of H absorption near the D-2 lines. In most cases the ranges and the step sizes were chosen by trial and error to sample all models that can give fits with low $\chi^2$. Exploring the range of parameters in this grid search was a computationally intensive task that took over a month and required tens of runs, many of which took over 24 hours on a 1.5Ghz personal computer. We used a similar grid search, with only three parameters, in Kirkman *et al.* 2001.

Several other parameters of the model were not varied, because we believed they would have less effect on D/H, and the computations take approximately ten times longer for each additional parameter. The fixed parameters include:

- The wavelength ranges included in the fit: –40 to –120 km s$^{-1}$ for Ly-2 to Ly-8.
- $v$(D-1) = $-2.8$ km s$^{-1}$, which is well constrained by the spectrum and is also used as the value for $v$(H-1). We discuss why this differs from the O-1 velocity in §5.1.
- The specification of the main H I, including its log $N_{HI}$(total) and its two components, H-1 and H-2. We use the values given in Table 3, some which come from the fits that we will describe in §6. We can fix the main H I because the high order Lyman lines of the H I are all strongly saturated and they do not absorb near the D lines.
- log $N_{HI}$(H-3) is constrained because H-3 does not absorb in the higher order Ly-lines (Figs. 6 & 8) and its precise $N_{HI}$ value does not effect the log $N_{DI}$.
- $v$(H-3) = $-44$ km s$^{-1}$. We found that $b$(H-3) is effectively degenerate with v(H-3), and hence either parameter suffices to explore the range of acceptable models. We changed $v$(H-3) from –50 km s$^{-1}$ to –30 km s$^{-1}$ and found that the $b$(H-3) was larger in compensation, but there was no change in the log $N_{DI}$(total) that gave acceptable $\chi^2$ values. We believe that this is a sufficient range to explore for v(H-3) because a metal component is centered near –41 km s$^{-1}$.
- The continuum shape and height. In Figure 10 we show the continuum that we used near the Ly-limit, while in Figs. 6, 7, 8 & 11 we show the fit to the spectrum using this continuum and absorption by obvious lines. We found that the bumps in the continuum are required to fit the spectrum. We do not claim that the QSO continuum itself is this bumpy, rather that the combination of the QSO continuum, emission lines, broadly distributed and weak blended absorption, and flux calibration errors combine to make this the effective continuum. Had we chosen a smooth or flat continuum across Fig. 10 then we would have also required extra broad absorption distributed like the dips in the continuum in Fig. 10, or emission near 923 Å in the rest frame

of the QSO, to obtain fits similar to those seen in Fig. 11.

- The absorption in the vicinity of D that is H I at different redshifts.

In §4.2 we show that the last two factors are related and have little effect on log $N_{DI}$.

In Figure 12 we show contours of constant $\chi^2$ as a function of the total $N_{DI}$ against each of the other five parameters that we adjust. These plots show projections of the minimum $\chi^2$ values onto the planes specified by the axes, and hence the values of the four other parameters may vary slightly as we move along a particular contour. We found these minimum $\chi^2$ values by stepping each adjustable parameter over its full range, to explore all combinations of all parameters.

Our best estimates for the parameters are the values that together give the minimum $\chi^2$ value, $\chi^2_{min}$. These values are all contained within the innermost contour on each panel. The $m\sigma$ confidence intervals for the parameters are the ranges allowed by the successive contours on the plots, that we have placed at values of $\chi^2_{min} + m^2$. Hence the $1\sigma$ ranges are the smallest and largest values of the parameters that are allowed by the innermost contour, at $\chi^2_{min} + 1$. These critical $\chi^2$ values apply because we have varied all the parameters to find the minimum $\chi^2$ value for each log $N_{DI}$(total). We have only one effective degree of freedom, the log $N_{DI}$(total). The distribution of the $\chi^2$ statistic as a function of log $N_{DI}$(total) is then expected to be approximately the $\chi^2_1$ distribution function, with one degree of freedom. We shall refer to this method of estimating the errors on a parameter as the $\delta\chi^2$ method.

In Figure 13 we show the minimum $\chi^2$ that we found for each log $N_{DI}$. The critical $\chi^2$ values are the same as in Figure 12, for the same reason. Our best estimate for the total D in components 1 and 2, the column density that we will use to get D/H, is

$$\log N_{DI}(total) = 15.113^{+0.042}_{-0.026}\ \mathrm{cm}^{-2}, \qquad (1)$$

which is a $1\sigma$ range of +10% and −6%. This is the log $N_{DI}$(total) value that gives the lowest $\chi^2$ when combined with the following values for the other parameters, all of which are collected in Table 3): $b$(D-1) = $9.2\pm0.2$ km s$^{-1}$, $b$(D-2) = 4 km s$^{-1}$, $v_{sep} = 12^{+2}_{-3.5}$ km s$^{-1}$, $N_{DI}$(D-2) / $N_{DI}$(total) = $0.12^{+0.16}_{-0.05}$, and hence log $N_{DI}$(D-2) = 14.191 cm$^{-2}$.

The $\chi^2_{min} = 271.4$ is reasonable for 274 pixels. We have used 3 degrees of freedom fitting the parameters of each of the two D lines and 2 parameters for the H-3 lines. The continuum, other contaminating lines, and $N_{HI}$(H-3) are well constrained by pixels outside the region used in the grid search, while $v$(H-3) is degenerate with $b$(H-3). There are then approximately 274-8 degrees of freedom. The probability $\chi^2_{266} > 271.3 = 0.40$.

We have a simple explanation for the range of $N_{DI}$(total). The $\chi^2$ distribution is asymmetric, rising more slowly as log $N_{DI}$(total) increases from the best value, because of the contribution from D-2. The log $N_{DI}$(D-1) is well determined and varies little for all models that give a small $\chi^2$ while the log $N_{DI}$(D-2) varies from zero to a well determined maximum. Figure 12 shows an anti-correlation between log $N_{DI}$ and $b$(H-3), which arises because the absorption near –70 km s$^{-1}$ can be explained by various combinations of D-2 and H-3. As log $N_{DI}$(D-2) decreases, the $b$(H-3) can increase to give models with a similar shape and $\chi^2$. The lower bound on log $N_{DI}$ comes from our assumption that the absorption near $v = 0$ is D, which we discuss in section 5. The lower bound on log $N_{DI}$ applies when log $N_{DI}$(D-2) is insignificant and all the absorption in D-1 is D. The upper bound on log $N_{DI}$ is met when D-2 absorbs photons that we see at velocities $\simeq$ 70 km s$^{-1}$. We find a continuous range of acceptable models between these two bounds.

The fit shown in Figures 8, 6, 11, & 7 is that with the minimum $\chi^2$. Other fits with $\chi^2$ values larger by several look indistinguishable in such plots.

We found that we could also find good fits to the D lines using the optimization methods that we describe in §6. Before we conducted the grid search, our best fit had a reasonable $\chi^2 = \chi^2_{min} + 0.7$. After we completed this grid search, we confirmed that the optimization methods can find the same best fit, but only when we limit the parameter to narrow ranges centered on the best fit.

### 4.2. *Discussion of the log $N_{DI}$ Value and its Error*

We now discuss a few of the many factors that can effect the log $N_{DI}$ value and its error. In each case we have made some reasonable choice for the relevant parameters when we conducted the grid search. Here we discuss some of these other options that we did not quantitatively explored in the grid search. In all cases we suspect that these effects are smaller than the error that we quote on the log $N_{DI}$, except for missing D components that might be comparable to the error. Some of these factors could appear as random or systematic errors, depending on details such as potential bias. An error is random if its effect on log $N_{DI}$ is such that the mean log $N_{DI}$ from many spectra and model fits would converge on the true value.

#### 4.2.1. *Flux Calibration*

Flux calibration is a possible cause of the bumpy continuum in Fig. 10. Four different HIRES orders contribute at $\lambda < 3400$ Å. The wavelength scale of the bumps are consistent with the 10 Å correlation length that we expect for flux calibration errors in this part of the spectrum. The amplitude is also consistent, except for the largest bump near 3290 Å that is 6 – 12% in amplitude, two – three times larger than the expected calibration errors. There are two components to the flux calibration error, the S/N of the HIRES integrations, and the S/N of the Kast spectra. We find that the total error in the calibration of the summed HIRES spectrum is approximately a 4% near 3290 Å, and 8% near 3250 Å where the S/N is lower.

The method we used to fit the continuum near the D line should have corrected for the errors in the flux calibration without adding to the error on the log $N_{DI}$. The continuum fitting will also have corrected for any other effects that are correlated over > 10 Å.

#### 4.2.2. *Continuum Level*

We find that the continuum level is not a significant part of the error in the log $N_{DI}$ value. If we multiply the adopted continuum by 1.05, the result is clearly too high for all the D line, while if we multiply by 0.95 the result

is too low, except perhaps for Ly-3. This means that the error in the local continuum is $< 5\%$, and since we fit the continuum independently for each of the 5 main D lines, the corresponding error on the log $N_{DI}$ is $< 5\%/\sqrt{5}$, which we will ignore.

#### 4.2.3. *Velocity Error*

We took $v(D-1) = -2.8$ km s$^{-1}$ and we did not vary this value, to account for the error of 0.6 km s$^{-1}$ from the fit to D-1 or the wavelength scale error. If the D-1 were not centered at this velocity, it would have a smaller log $N_{DI}$ and some additional narrow D or H absorption would be needed to account for all the absorption. This does not seem a likely way to change the log $N_{DI}$ value.

#### 4.2.4. *Could b(D-2) be very Low?*

The grid search hints that $b$(D-2) could be very small. The model with $\chi^2_{min}$ had $b$(D-2) = 4 km s$^{-1}$, but with a $1\sigma$ range extending to 12 km s$^{-1}$. The minimum $b$ value that we considered in the grid search was 4 km s$^{-1}$ because the instrumental resolution is similar, and hence $b < 4$ km s$^{-1}$ has little effect on the spectrum.

Small values for $b$(D-2) do not allow very large log $N_{DI}$(D-2). The spectrum places an upper limit on the opacity near –70 km s$^{-1}$, and a weaker limit on the equivalent width. We can then trade $N_{DI}$(D-2) against $b$(D-2) to find acceptable fits for a wide range of $b$(D-2). Solutions with low $b$(D-2) tend to have low $N_{DI}$(D-2), the opposite of the situation for lines with constant equivalent width. Fortunately the optical depth prohibits large log $N_{DI}$(D-2), and hence the uncertainty in the $b$(D-2) value has little effect on log $N_{DI}$(D-2), as seen in the third panel of Figure 12 .

Low $b$(D-2) values require temperatures that are unlikely. If $b$(D-2) $< 4$ km s$^{-1}$, the absorbing gas would have $T < 1900$ K, and it should be neutral if ionized by intergalactic radiation. However, the C II/O I and Si II/O I ratios appear to be higher near to component 2 than in component 1, which implies that component 2 is more ionized, and less likely to be neutral (§7.2).

#### 4.2.5. *Velocity Structure*

When we calculated the maximum log $N_{DI}$ in D-2, we assumed that both D-2 and H-3 were Voigt profiles. More complex velocity distributions could give different column densities, a topic that has been explored by Sergei Levshakov and collaborators (Levshakov *et al.* 2003). This is unlikely to be a major effect for H-3, which is wide enough (Fig. 12) that its profile is dominated by thermal motions, and hence should be insensitive to the detailed velocity distribution. The same argument wil apply to D-2 if its $b$-value is close to the $1\sigma$ upper limit of 12 km s$^{-1}$, but not if $b$(D-2) is near 4 km s$^{-1}$.

#### 4.2.6. *Missing D Components*

The D/H would be systematically low if we have included velocity components in log $N_{HI}$(total) that are not detected in D I because the D I is hidden by H I absorption.

We see no evidence that we have missed D components, and we do not know how to estimate the chance that they exist, and hence we will not include them in the error on log $N_{DI}$. However, they could exist and have a major effect on log $N_{DI}$, even doubling the D/H if their metal abundances are very low.

We need to examine the D and H lines in detail to establish the velocities that could contain missing D components. Fig. 8 shows that the H I included in the total log $N_{HI}$ all lies well within the range –40 to 40 km s$^{-1}$. At other velocities, log $N_{HI} < 17$ cm$^{-2}$ because see flux at the expected positions of one or more of the higher order Lyman lines. Figs. 7 & 11 show that there are no significant D lines from components at –40 km s$^{-1}$ $< v < 0$ km s$^{-1}$, except for D-1. At positive velocities there are opportunities to hide D. Component 2 was hard to detect, some of component H-3 could be D, and there might also be significant D between the two, at $13 < v < 40$ km s$^{-1}$, where we see C II, Si II, C IV and Si IV.

The H I lines alone allow that a major portion of the total log $N_{HI}$ is at velocities approximately 16 – 25 km s$^{-1}$. H I lines alone do not give the $v$ of the main H I to within approximately 25 km s$^{-1}$ because the core of the Ly$\alpha$ contains many other components, and the higher order Lyman lines are blended on both sides. However, the C II, S II and especially the O I all indicate that most of the H I is in component H-1. The H I in components other than 1 and 2 is probably $< 10\%$ of the total because we do not see O I at other velocities. If D/H is a constant, we expect that any missing D is also less than 10% of the total. We would have seen the O I from any component with more than 10% of the total log $N_{HI}$ provided it had [O/H] $> -3$.

We do not know whether the absence of O I and other metals is sufficient to rule out missing components that contain $> 10\%$ of the total column density. Abundances $< -3$ are very rare for absorption systems as a whole. Not one of 34 DLAs listed by Pettini *et al.* (1997) had [Zn/H] $< -2$, although several were upper limits and some systems with lower abundances are known (e.g. Fan & Tytler 1994). However, we know little about the abundances in components of systems.

Although H-3 might contain as much optical depth in D as D-1, H-3 is predominantly H and not D because a distinct component of C II and Si II is centered near $v = -40$ km s$^{-1}$ (Table 3, Figure 4).

#### 4.2.7. *Contamination of the D-1 component by H*

In §5 we explain why it is unlikely that the D-1 lines are contaminated by H, other than the blends that we mentioned above with D Ly-3 and 5. Several of the D lines seem relatively free of close contamination and hence we do not expect that the way in which we fitted the contaminants to D Ly-3 and 5 is a significant source of error.

#### 4.2.8. *Validity of the Model and the $\chi^2$ Constraint*

The error we quote for log $N_{DI}$ comes from the range of fits with $\chi^2 < \chi^2{}_{min} + 1$. The log $N_{DI}$ and the error will be unreliable if: (1) the model or the parameters with the lowest $\chi^2$ are unrealistic, or physically unacceptable; (2) we did not fully explore the parameter space of the model; (2) we did not explore a wide enough range of models, for example allowing D in enough components or at enough velocities.

We believe that the log $N_{DI}$ value and its error are reasonable. We explored a relatively large range of possible

models using coarse grids before we settled on the fine grid presented above. However, we may have misunderstood the velocity structure because the S/N is low near the Lyman limit and we did not explore more complex models because they would have taken too long to compute.

## 5. THE ABSORPTION NEAR THE D-1 POSITION IS MOSTLY D

Several lines of argument imply that the absorption that we identify as D-1 is mostly D. The evidence is convincing, but not as strong as for some other QSOs.

Ideally, we would compare the velocity structures of the D I and H I lines, which would be identical if we have correctly identified the transitions and there is minimal contamination. This comparison is not possible for Q1243+3047 because the velocity structure of the H I is not observed, and hence we are less certain that we have seen D than we were in other QSOs.

The only reasonable identifications for D-1 are D and H, because D-1 shows a Lyman series.

If the D-1 absorption is H, $b$(D-1) implies a very low temperature of $< 5130$ K. This temperature is much too low for low density gas photoionization by the intergalactic ionizing UV radiation. It is certainly too low for the Ly$\alpha$ forest and perhaps for components with log $N_{HI}$= 15 cm$^{-2}$ in DLAs and LLS, unless they are shielded from the radiation by H I. There are no metals at the redshift of H at the position of D-1, but this is not significant, since metals would not be seen if their abundances were low.

There are three main reasons why D-1 is D: its velocity, line width, and column density are all close to the values that we expect.

The column density of the absorption near D-1 could have been orders of magnitude different from the measured value. D-1 is likely to be D because it has a log $N_{DI}$ that gives D/H similar to the values found toward four other QSOs. The converse is not true: we would not reject a D line that gives a different D/H value if it otherwise appears to be D.

### 5.1. *Velocity Agreement*

The wavelengths of the centers of the D, O and H lines indicate that the D-1 absorption is D, but they also suggest that O/H varies with velocity.

In the frame of the main component of the O-1, D-1 is at $-2.8 \pm 0.6$ km s$^{-1}$, where the error is from the line fit alone. This is close enough to show that D-1 is mostly D, since the D-1 and O-1 lines overlap in velocity.

The O-1, D-1 velocity difference of 1.3 pixels is larger than we expect from measurement errors, but we have been surprised in the past by wavelength scale errors in HIRES spectra. The error might be with the single O I line, rather than the D lines, since the several D lines appear at the same velocity (Figs. 6 & 7).

The H I velocity is consistent with that of the D I, but it is not known well enough to show that the D-1 line is D.

#### 5.1.1. *Does O/H Increase with Velocity?*

The O I might have a different velocity structure from the H I and the D I if O/H varies and is correlated with velocity. For example, we can imagine that all of the H I, D I and O I come from a single component. This component might have a Gaussian distribution of velocities. The O-1 component would be centered at +2.8 km s$^{-1}$ in the frame of the D-1 because O/H is larger at larger velocities, and the O-2 component might arise from the O/H gradient alone. In this case we should model the H and D with a single component. We do not favor this model, because C II and Si II show components 1 & 2. However, we can fit to the H I lines with a single component (§3.4), and this can have a $b$-value that is consistent with the D and O lines (§5.2). If we have a single component the log $N_{HI}$ is unchanged (§6), while the D/H is lower because log $N_{DI}$ tends to be lower when we loose D-2 (§4.1).

#### 5.1.2. *Metal Abundance Gradients in Other Absorbers*

There is almost no published information on the variation of metal abundances or metal line kinematics in components of absorption systems with log $N_{HI} \simeq$ 19 cm$^{-2}$, especially on velocity scales of a few km s$^{-1}$. The closest analogue is HS 0105+1619 where we found that ions C II, N II, Si II and Fe II did not come from the same gas as the H I, D I and O I, because the line centers differed by 1 – 2 km s$^{-1}$ and the lines widths were different (O'Meara *et al.* 2001). Toward absorption systems with much lower $N_{HI}$ we have found that the abundances can vary greatly between components with similar velocities and relatively high ionization. Toward PKS 1937–1009 Tytler, Fan & Burles (1998) found that two components separated by 15 km s$^{-1}$ had very different metal abundances: [Si/H] = −2.7 and −1.9. Toward Q1009+2956 Burles & Tytler (1998) found that two components also separated by a similar amount had abundances of [Si/H] = −2.7 and −2.4. Hence for these two QSOs the metal lines do not give a sufficient description of the H I and D I. Toward DLAs with log $N_{HI} > 20.3$ cm$^{-2}$, Wolfe & Prochaska (2000) find that different low ionization ions show similar velocity distributions, which implies that both the ionizations and relative abundances are similar, but does not constrain the absolute abundances. In those cases the differences were in different components, but for Q1243+3047 the velocity offset would require structure within component 1, for which we have no other evidence.

#### 5.1.3. *Velocity Agreement for D-2*

We suspect that D-2 is D for three reasons, but the case is weak, because D-2 is not well determined. First, the absorption that we fit with D-2 is very narrow, narrower then typical H I lines. Second, the separation of D-2 from D-1, 12 km s$^{-1}$, with a $1\sigma$ range of 8.5 – 14 km s$^{-1}$, matches the separation of the O I components, that is $\simeq$ 13.3 km s$^{-1}$. In the grid search we examined D separations from 4 – 20 km s$^{-1}$, and the D separation could have been different from that of the O I. However, this argument is weak, in part because the D-1 and O-1 are at slightly different velocities. Third, the fraction of the D in D-2 ($0.12^{+0.16}_{-0.05}$) matches the fraction of O in O-2, 0.13, when we force $b$(O-1) = $b$(O-2).

### 5.2. *Line Width Agreement*

The widths of the D I, H I and O I lines indicate that the D-1 absorption is D. If the D I, H I and O I arise

in the same homogeneous gas, and the velocity distribution in this gas is described by a single temperature, and a Gaussian distribution of turbulent velocities, then we can predict the $b$-value of the D from the H and O $b$ values. Following O'Meara *et al.* (2001), the intrinsic $b$ value of the lines, $b_{int}$ is given by $b_{int}^2 = b_{temp}^2 + b_{turb}^2$, where the temperature term is $b_{temp}^2 = 2kT/m = 166.41(\mathrm{km\ s^{-1}})^2(T/10^4\ K)/\mathrm{mass\ (amu)}$, where T is the gas temperature and $b_{turb}$ represents the bulk turbulent motions, and $m$ is the mass in atomic mass units. The $b$ values in this paper are all intrinsic values, since we have convolved the intrinsic line profiles by the instrumental broadening before we fit to the spectrum.

The observed width of the D-1 component agrees with the prediction from the widths of the O-1 and H-1 components, given in Table 3, and shown in Fig. 14. The straight line that fits $b^2$ against $1/m$ gives $T = 1.1 \pm 0.6 \times 10^4$ K and $b_{turb} = 5.8 \pm 0.6$ km s$^{-1}$, both reasonable values, similar to those that we found in other D/H systems. This fit predicts $b$(D-1)$= 11.3 \pm 1.8$ km s$^{-1}$, $1.2\sigma$ larger than the observed $b$(D-1)$= 9.2 \pm 0.2$ km s$^{-1}$. This agreement suggests that D-1 is D and not H. However the evidence is weak because the $b$(H-1) value and its error, from the covariance matrix, are both poorly constrained, and because the velocity difference of the D-1 and O-1 components may mean that the model we used to predict $b$(D-1) is too simplistic.

When we accept that the D-1 component is D, we can use D-1 together with the H-1 and O-1 to improve our estimates of the gas properties. We find $T = 0.55 \pm 0.04 \times 10^4$ K, which is low but reasonable for the large log N$_{\rm HI}$, and $b_{turb} = 6.3 \pm 0.2$ km s$^{-1}$. The data are also fully consistent with this fit, which we show as the dashed line in Fig. 14. Compared to this line, the measurements give $\chi^2 = 1.38$ for one degree of freedom, where $\mathrm{Prob}(\chi_1^2 > 1.38) = 0.24$.

## 6. MEASUREMENT OF THE H COLUMN DENSITY

In this section, we describe the measurement of the Hydrogen column density in the system that shows D, along with new methods that we developed to improve the accuracy and reliability of N$_{\rm HI}$ measurements. We first find the approximate log N$_{\rm HI}$ value (§6.1), then a detailed model that fits the spectrum (§6.2), and then we examine other models that give acceptable fits (§6.3). We find the log N$_{\rm HI}$ value and its error in §6.4, and we discuss these values in §6.5.

Most information on the N$_{\rm HI}$ comes from the shape of the damped Ly$\alpha$ line at 4285 Å that we will call the DLA because it shows damping wings, although its log N$_{\rm HI}$ value is less than the usual definition for a DLA system. Compared to the methods we used to get log N$_{\rm DI}$, for the log N$_{\rm HI}$ we use different ways to fit the continuum and Ly$\alpha$ forest, to explore the parameter values and to assign an error to log N$_{\rm HI}$.

### 6.1. *The Approximate log $N_{\rm HI}$ Value*

We can quickly establish that the DLA has log N$_{\rm HI}\simeq$ 19.7 cm$^{-2}$. If we fit the HIRES spectrum by a Ly$\alpha$ line with a lower column density, there remains unexplained absorption which looks like damping wings. This is very clear when log N$_{\rm HI}\leq$ 19.5 cm$^{-2}$, and can still be seen at larger log N$_{\rm HI}$. On the other hand, when we fit with log N$_{\rm HI}$= 19.8 cm$^{-2}$ we absorb flux which is seen, which is un-physical. To allow this extra absorption, the QSO continuum, including any emission line flux, would have to bend upward, on either side of the damped line, near 4288 Å and 4293 Å, which is best seen when we divide the spectrum by the line profile. We then know that 19.5 $<$ log N$_{\rm HI}$ cm$^{-2}$ $<$ 19.8, where the larger limit is twice the smaller, a range that is 20 times the $1\sigma$ range on the log N$_{\rm DI}$(total).

### 6.2. *An Initial Model for the Spectrum Near the DLA*

We now describe how we made an initial model of the spectrum. In §6.3 we will use this model as a starting point when we explore alternative models.

A model of the flux in the spectrum is determined by three main factors: the flux emitted by the QSO, the Ly$\alpha$ forest and the DLA. We developed our own software to control these coupled factors. We can change the model manually, or automatically, optimizing over parameters to give models that have the smallest $\chi^2$ difference from the spectrum. These tools are described in Appendices I and II.

To construct our model, we first placed a DLA at $z = 2.526$ with log N$_{\rm HI}$ = 19.7 cm$^{-2}$. We then set a preliminary continuum level from 4200Å to 4350Å, such that the continuum plus DLA touched most of the peaks in the spectrum. This continuum was defined by 10 control points: six between 4320Å and 4340Å to define the top of the Ly$\alpha$ emission line, two at $\lambda < 4250$ Å to define the continuum far from the emission line, and two between 4260 Å and 4325Å nearest to the DLA. This continuum has enough freedom to take on a wide variety of shapes in the crucial region where the DLA is strongly absorbing. In addition, we add Ly$\alpha$ forest absorbers where we see lines. We then made made small modifications to the continuum, the log N$_{\rm HI}$ of the DLA and the Ly$\alpha$ forest, until we arrive at a model that appeared to accurately reproduce the spectrum. This model used log N$_{\rm HI}$ = 19.695 cm$^{-2}$. Finally, we used this model as the starting point for an automatic optimization that returned log N$_{\rm HI}$ = 19.73 cm$^{-2}$. This model, shown in Figure 15, has a reasonable $\chi^2$ , a smooth looking continuum, the Ly$\alpha$ forest absorbers are not unusual, and there is little discernible structure in the residuals.

The error on the log N$_{\rm HI}$ from the optimization covariance matrix, $\sigma$(log N$_{\rm HI}$) = 0.0002 cm$^{-2}$, is too small for at least two reasons: (1) the final covariance matrix has significant off-diagonal term involving the N$_{\rm HI}$, and (2) the $\chi^2$ manifold may have multiple minima. We believe that errors derived from the covariance matrix will be too small for all similar models that contain many correlated parameters. We discuss this issue in §14.1.

The initial model has two problems. First, we do not know the error on the log N$_{\rm HI}$ value, and second, we have no reason to believe that it is unique.

### 6.3. *Restarting the Optimization to Find the $N_{\rm HI}$ Range*

We now try to determine the robustness and uniqueness of our fits by seeing if, for a variety of input values for the parameters, we return to our best value of log N$_{\rm HI}$ = 19.73 cm$^{-2}$. A fit is robust if it can be found when we start from

a wide variety of input parameters. A fit is unique if there are no other fits which have significantly lower $\chi^2$. Although we can readily find local minima in the manifold of parameters, it is well known that there are no simple ways of showing that we have found the unique, or global minimum. On the contrary, we expect that there are other fits, which may have different log $N_{HI}$ values, and similar or lower $\chi^2$ values.

We used the optimizing code to searched for fits with low $\chi^2$ values. We performed thousands of optimizations, each beginning with different parameter values. We added random numbers, selected from normal distributions (NDs), to the parameter values of our initial model (§6.2). The ND for the continuum control points had $\sigma = 1$ unit of flux. Since the continuum near the damped line is 12 units of flux, these input continua usually have significant bumps and dips. The ND for the log $N_{HI}$, $b$, and $z$ of each Ly$\alpha$ forest line had a $\sigma$ equal to the prior measurement error.

We allowed the optimizer to move the two continuum points between 4260 Å and 4325 Å (shown as squares in Figure 15) in both wavelength and flux. The optimizer also varied the flux, but not the wavelengths of all the other continuum points. Some examples of the starting continua are shown in Fig. 16.

We found that the velocity structure of the H I has little effect on the log $N_{HI}$ value. For all optimizations, we distributed the total log $N_{HI}$ of the DLA between the two velocity components seen in the O I line, and we put 13% of the total log $N_{HI}$ in the second component at $v = 13.3$ km s$^{-1}$. This proportion is similar to that seen in O I and D I. However, we measured the same total log $N_{HI}$ if all of the H I is in one component. Our fits to the DLA give log $N_{HI}$(total) that excludes the H I from components 3, 4 and 5. We fit these other components separately with the results listed in Table 3. We did not fit separate components near 20 and 40 km s$^{-1}$ because they are poorly constrained, none are needed near 40 km s$^{-1}$, and gas in this range should have log $N_{HI}$< 17 cm$^{-2}$.

The total log $N_{HI}$ was not allowed to vary in any of the optimizations. However, the input log $N_{HI}$ was different in different optimization re-starts.

We conducted thousands of re-starts for each chosen $N_{HI}$ value. The $\chi^2$ at the starts were typically $10^5$, while at the end, depending on the $N_{HI}$ value, 5700-6700, similar to the degrees of freedom. We found reasonable solutions with low $\chi^2$ values for a wide variety of $N_{HI}$ values. In Figure 17 we show the $\chi^2$ values for these re-starts.

Some of the final solutions found by the re-start procedure had Ly$\alpha$ forest absorbers that are not typical of those seen in the Ly$\alpha$ forest of other QSOs (Pettini *et al.* 1990; Hu *et al.* 1995; Kirkman & Tytler 1997). In particular, many of the solutions with log $N_{HI} < 19.68$ cm$^{-2}$ had very wide Ly$\alpha$ forest absorbers near to 4295Å. We do not believe that these solutions indicate that there may be wide Ly$\alpha$ forest absorption near to the LLS, but rather that the optimizer can, if it needs to, use Ly$\alpha$ forest absorption with large $b$ values to compensate for low values of $N_{HI}$ in the LLS. For this reason we have rejected, from the bottom panel of Figure 17, all fits that included Ly$\alpha$ forest lines with $b > 150$ km s$^{-1}$. In Figure 18 we show the effect of one broad Ly$\alpha$ forest line on a portion of the spectrum.

### 6.4. *The Best Estimate for log $N_{HI}$ and its Error*

We now discuss our best estimate for the log $N_{HI}$ value and its error.

We found that the re-starts with log $N_{HI}$= 19.73 cm$^{-2}$ consistently gave the lowest $\chi^2$ values. If our re-starts had fully explored the parameter space, we would have concluded log $N_{HI}$= 19.73 ± 0.005 cm$^{-2}$, where the error is the range of log $N_{HI}$ values have fits with $\chi^2 < \chi^2_{min} + 1$, the $\delta\chi^2$ method that we used for the log $N_{DI}$ in §4. For no other values of log $N_{HI}$, including 19.72 and 19.74 cm$^{-2}$ did we find fits with $\chi^2$ within 10 of the minimum, let alone 1.

We do not use this method to estimate the log $N_{HI}$ error because our optimization process is not efficiently finding fits with the lowest $\chi^2$ values. For each log $N_{HI}$ value, Figure 17 shows a range of $\chi^2$ values of approximately 200, and the lowest $\chi^2$ is often 10 lower than the second lowest. To define the error on log $N_{HI}$ using $\delta\chi^2 = 1$, we would require many fits with $\chi^2$ values within 1 of the minimum, and we would also have to prove that we had adequately explored all relevant models and parameter ranges (§4.2.8).

We determine the error on the log $N_{HI}$ value by testing the hypothesis that there is at least one acceptable fit for a given log $N_{HI}$ value. We accept an log $N_{HI}$ value if the restarts include one or more models with an acceptable $\chi^2$ value. We accept a $\chi^2$ if there is > 5% probability of a larger value when the hypothesis, that the data came from the model, is true. We fit 5048 pixels near Ly$\alpha$ with 289 parameters, leaving 4759 degrees of freedom and hence the maximum acceptable $\chi^2$ value is 4920.6. We increased this maximum acceptable $\chi^2$ by a factor of 1.23, to 6052.3, for reasons discussed in §6.5.4.

We found acceptable fits for the re-starts for log $N_{HI}$= 19.68 – 19.78 cm$^{-2}$ when we reject fits with Ly$\alpha$ forest lines with $b > 150$ km s$^{-1}$, and 19.70 – 19.78 cm$^{-2}$ when we reject $b > 100$ km s$^{-1}$. Therefore, we choose 19.68 – 19.78 cm$^{-2}$ as the range of acceptable log $N_{HI}$ values.

It is helpful to assign a probability distribution function to summarize the range of likely log $N_{HI}$ values. We made the following choices: a normal function, centered at 19.73 cm$^{-2}$, with an 80% probability that the true log $N_{HI}$ is in the range 19.68 – 19.78 cm$^{-2}$. We choose 80% because we guess that there is of order a 20% chance that the true log $N_{HI}$ is not in the range 19.68 – 19.78 cm$^{-2}$, and because we do not want the function to be too sharply centered on 19.73 cm$^{-2}$.

Our best estimate for the column of the H I in components 1 and 2, that is associated with log $N_{DI}$ in the same components, is then

$$\log N_{HI}(total) = 19.73 \pm 0.04 \text{ cm}^{-2}, \quad (2)$$

which is a $1\sigma$ error of 9%, similar to the error on the log $N_{DI}$.

### 6.5. *Discussion of $N_{HI}$ Value and its Error*

We now discuss our log $N_{HI}$ value and its error. We discussed a similar set of issues for the log $N_{DI}$ value in §4.2.

### 6.5.1. *The Coupling of the Continuum, Lyα forest and the log $N_{HI}$*

The flux emitted by the QSO varies smoothly over scales of thousands of km s$^{-1}$. Its precise shape is unknown *a priori* and is hard to gage from spectra because of the absorption and emission lines.

The Ly$\alpha$ forest lines are narrow relative to the uncertainties in the shapes of the continuum and the DLA. We can identify and fit these lines individually, and we can distinguish their effects from the shape of the emitted flux and the DLA. It is unlikely that such lines would have the velocities and column densities which make absorption that varies smoothly over hundreds or thousands of km s$^{-1}$, however the optimizer will attempt to do this to accommodate errors in the log N$_{\rm HI}$ and the continuum.

The damped Ly$\alpha$ line has a very well determined shape that gives the log N$_{\rm HI}$. The information on the N$_{\rm HI}$ comes from the whole profile of the damped Ly$\alpha$ line. While the line is most conspicuous over the central 20 Å, the damping wings extend much further, and continue to absorb about 1% of the flux from approximately 4233 Å to 4340 Å. This range covers approximately $\pm$3700 km s$^{-1}$ in either direction from the line center, or 3500 pixels in total, and extends over the peak of the QSO Ly$\alpha$ emission line at 4331 Å.

In Fig. 19 we show the change in the flux corresponding to a change in log N$_{\rm HI}$ of 0.04 cm$^{-2}$, the 1$\sigma$ error that we quote. This is the derivative of the flux with respect to the column density, in different units. The change in the flux is largest $\pm$5.4 Å or 380 km s$^{-1}$ from the line center, where the line absorbs 60% of the flux. The change in the flux decreases nearer to the line core because little flux remains there. The fractional change in the flux keeps increasing toward the line center, but we can not detect this. The information in the spectrum that gives log N$_{\rm HI}$ comes from the whole of the Ly$\alpha$ line. The change in the flux is significant in the core where there is almost no flux, and also far from the core where we can integrate over a wide wavelength range.

The error on the log N$_{\rm HI}$ value for the DLA is larger than would be thought from considering just the change in the spectrum produced by changing the DLA line alone, because the Ly$\alpha$ forest and continuum can be adjusted to accommodate some of the effect of changing the log N$_{\rm HI}$.

Figure 19 shows the change in flux required of a fit to the spectrum when the log N$_{\rm HI}$ changes slightly. If we start with a model that gives a good fit to the spectrum and then increase log N$_{\rm HI}$, we could maintain a good fit if we add bumps to the continuum approximately 5.4 Å from the center of the DLA. For small changes in log N$_{\rm HI}$ the optimizer is able to avoid adding bumps, and instead it can find good fits using different smooth continua shapes, and different amounts of Ly$\alpha$ forest absorption; less where the dips were expected and more on either side of them. The optimizer adjusts all parameters of the model so that the residuals appear uniformly distributed. This is one type of behavior that explains why the errors on log N$_{\rm HI}$ are greater than we expect by varying log N$_{\rm HI}$ alone.

We now discuss in more detail the connection between the error on log N$_{\rm HI}$ and how we fit the Ly$\alpha$ forest and the continuum.

### 6.5.2. *Fitting the Lyα forest*

The models accommodate different log N$_{\rm HI}$ values by changing both the continuum and the Ly$\alpha$ forest together. We must be careful to not allow the optimizer too much freedom to adjust the Ly$\alpha$ forest parameters to simulate smoothly varying absorption, to accommodate an excessive range of log N$_{\rm HI}$. For example, when we divide the spectrum by a DLA with log N$_{\rm HI}$ = 19.8 cm$^{-2}$ we make a spike in the flux near 4293 Å that is unlike any feature seen in QSO spectra. Hence, we should not allow the optimizer to obtain acceptable fits for this log N$_{\rm HI}$ value by raising the continuum over a wide wavelength range and using smooth Ly$\alpha$ forest absorption to remove this extra flux everywhere, except at the spike. This is reason that we require all of the Ly$\alpha$ forest $b$-values to be less than 150 km s$^{-1}$.

We may have over-estimated the error on the log N$_{\rm HI}$ if we have allowed the Ly$\alpha$ forest lines to have more variety than is typical. The Ly$\alpha$ forest can accommodate changes in the log N$_{\rm HI}$ in two ways: by making a few lines unusually broad, and by using more lines than normal. We rejected the fits that used lines with $b >$ 150 km s$^{-1}$, a value that is not well defined. If we instead reject fits with $b <$ 100 km s$^{-1}$, we reduce the allowed range of log N$_{\rm HI}$.

Alternatively, we may have underestimated the error on log N$_{\rm HI}$ because we did not adequately explore the Ly$\alpha$ forest absorption. We began all restarts using the parameter values that deviated about the values of the initial fit. Perhaps the deviations that we gave to the Ly$\alpha$ forest lines were too small to allow them to adequately fit the continum required for differing log N$_{\rm HI}$. The deviations that we gave to the Ly$\alpha$ forest parameters were uncorrelated, so that increased absorption by one line would tend to cancel decreased absorption by its neighbors. We might have explored the Ly$\alpha$ forest more thoroughly if we had used correlated deviations.

We have not performed any quantitative checks of whether we have used an accurate Ly$\alpha$ forest absorption model, but the excessive $\chi^2$ value of our model (§6.5.4) suggest that we may have systematically used too few components in our Ly$\alpha$ forest model. We suspect that the effect this has N$_{\rm HI}$ is systematic, though we do not know in which direction. We also suspect the effect is small, in part because two of us developed independent models of the Ly$\alpha$ forest absorption, both of which gave the same log N$_{\rm HI}$ = 19.73 cm$^{-2}$. It's hard to proceed quantitatively with this issue because it is extremely difficult to develop alternative models of the Ly$\alpha$ forest absorption (number of lines, their approximate positions, etc) which are equally compelling to the one we used.

### 6.5.3. *Continuum Shape*

Because the DLA absorbs over a very large wavelength range, we suspect that the largest class of systematic errors which might affect the N$_{\rm HI}$ are those where the flux emitted by the QSO can not be adequately fit by our continuum model. This might occur, for example, if there are weak emission lines or high frequency errors in the relative flux calibration, in the vicinity of the DLA.

The continuum shape can be effected by errors in the flux calibration. These errors are approximately 3% near the DLA, from comparison of HIRES spectra that we cal-

ibrated in different ways. We find the same log $N_{HI}$= 19.73 cm$^{-2}$ gives the lowest $\chi^2$ values when we fit the DLA in HIRES spectra that we calibrated in different ways.

The models described above all used only two continuum control points that were free to move in both flux and wavelength near the DLA. We also performed re-starts with three such continuum control points in the region between 4260 Å and 4325 Å. The results of these re-starts are shown in Figure 20. The top panel contains a number of fits that are unreasonable, having either very unusual Ly$\alpha$ forest absorption (like some fits in the top panel of Fig. 17), or very bumpy continua that we could not make with only two continuum points.

We filter the results using 3 continuum control points to exclude the unreasonable fits, leaving the results shown in the bottom panel of Figure 20. As with the two continuum point re-starts, we first removed all fits containing Ly$\alpha$ forest absorbers with $b > 150$ km s$^{-1}$. In addition, we removed models having continuum bumps larger than we expect to be present due to either weak emission lines, broad shallow absorption or errors from the relative flux calibration.

To help us decide what size of bumps and dips were reasonable in QSO continua, we fitted the Ly$\alpha$ forest of three other QSOs in a similar manner to Q1243+3047. Our HIRES spectra of these QSOs had similar, or in two cases a bit lower S/N. Near the position of the DLA in Q1243+3047, approximately 3000 km s$^{-1}$ from the peak of the Ly$\alpha$ emission line, we did not require any bumps or dips in the continuum that exceeded approximately 2% in amplitude, similar to the error in the relative flux calibration for Q1243+3047.

The filter that we used to reject bumpy continua was guided by this result, but it was imperfect in its treatment of the Ly$\alpha$ emission line. Examples of continua that it ejected are shown in Figure 21, and those that it accepted in Figure 22.

We find that the results from the models with two- and three-control point in the continuum are similar. This suggests that we have explored an adequate range of continuum shapes to accommodate the emitted flux, weak emission lines, broad shallow absorption and errors in the relative flux calibration.

The first thing that we note is that the best model with three-continuum points has log $N_{HI}$ = 19.73 cm$^{-2}$, the same value as with two control points. Second, the range of solutions is also approximately the same; log $N_{HI}$ = 19.71 to just above log $N_{HI}$ = 19.78, which was unfortunately the highest log $N_{HI}$ we explored with three points.

The third finding is that most of the filtered 3-point continua with acceptable $\chi^2$ had shapes similar to those from the 2-point fits. In Figure 23 we compare the continua from the two and three-point continua, for the models with that gave the lowest $\chi^2$ values for log $N_{HI}$= 19.69 cm$^{-2}$, the value 1$\sigma$ below our estimate for log $N_{HI}$. They differ by at most $< 1\%$ in flux, which is less than the error from the flux calibration. In Figure 24 we show the same for log $N_{HI}$= 19.783 cm$^{-2}$, our best estimate for log $N_{HI}$. The differences are at most $\simeq 0.3\%$. For log $N_{HI}$= 19.783 cm$^{-2}$, shown in Figure 25, the differences are $< 3\%$.

We use the 2-point rather than the 3-point continua to define the log $N_{HI}$ because we have explored the former in more detail, and the latter give a large number of fits with unacceptably bumpy continua, that we can not readily filter.

Although the 2 and 3-point continua give very similar results, we are not certain that we have explored an appropriate range of continua. We might have allowed either too much or too little freedom to represent the continuum, and we do not know how such errors might effect the log $N_{HI}$ value and its error.

#### 6.5.4. *The Largest Acceptable $\chi^2$ Value*

As we stated in §6.4, we increased the maximum acceptable $\chi^2$ by a factor of 1.23. We did this scaling because we found that when we fit a similar region of the Ly$\alpha$ forest without unusually strong lines, we obtained a $\chi^2$ value of 6111 over 5290 pixels using 336 parameters. This is $\chi^2$ per degree of freedom is much larger than we would expect.

One possible explanation is that we are under-fitting the Ly$\alpha$ forest. This is reasonable because we fit lines only where they are clearly required. We did not fit lines that changed the residuals by less that approximately 1$\sigma$, and hence we have underfit the Ly$\alpha$ forest because the need for such lines would be apparent where the S/N higher. We did not fit such lines because the spectrum gives little guidance in how to obtain a lower $\chi^2$. The residuals, like those shown in Figure 15, do not show the need for distinct lines.

A less likely explanation is that the error array associated with the spectrum is systematically too small. When we fit 5882 pixels to the red of the Ly$\alpha$ emission lines, using just 32 parameters, we found a $\chi^2$ value of 5264, or 0.90 per degree of freedom, which suggests that the errors are on average too large.

Several factors will determine the $\chi^2$ value we obtain when we fit the Ly$\alpha$ forest. The $\chi^2$ will decrease when we add lines. As the S/N increases, we need more lines to reach a given $\chi^2$ per pixel, and the higher S/N helps show that these lines are needed. The S/N decreases systematically with decreasing wavelength in our HIRES spectrum, and hence we do not know if the 1.23 factor applies at all wavelengths. In addition, the Ly$\alpha$ forest evolves, with more absorption at higher redshifts, until we near the QSO, where the proximity effect reverses the trend, further complicating the issue.

Although we can not readily determine the accuracy of the correction factor of 1.23, Fig. 17 shows that the log $N_{HI}$ range is rather insensitive to the precise maximum acceptable $\chi^2$ value.

#### 6.5.5. *Speculation on the Errors Associated with the $\chi^2$ Range*

The portion of the error on the log $N_{HI}$ that comes from only the quality of the fit and the S/N of the spectrum, might be up to an order of magnitude smaller than 0.04 cm$^{-2}$. We speculate this because the 0.04 cm$^{-2}$ error corresponds to a range of $\chi^2$ of 250, while we could have used a range of $\chi^2$ of 1 had we adequately explored both the parameter and model space. Because we have not done the required exploration, we do not know the shape of the $\chi^2_{min}$ as a function of log $N_{HI}$ to the required accuracy. If we make the guess that the shape remained similar to that suggested in Fig. 17, then the range of log $N_{HI}$ corre-

sponding to $\delta\chi^2 = 1$ would be much less than 0.04 cm$^{-2}$. Of course, the central value could end up anywhere in the range indicated by Equation 2.

## 7. ABUNDANCES AND IONIZATION OF THE HEAVY ELEMENTS IN THE ABSORBING GAS

In this section we discuss the metal abundance, ionization, and physical conditions in the components (1 and 2) where we measure D/H. In §7.3 we discuss the components at −40 and 100 km s$^{-1}$.

We modelled the level of photoionization using CLOUDY version 94.00, developed by G. Ferland (Ferland, 1991). We used the solar Oxygen abundance log O/H = −3.31 from Allende, Prieto, Lambert & Asplund (2001). For other elements we used the CLOUDY defined solar abundance ratios. We assumed a plane-parallel geometry and we approximated an isotropic background by placing a point source at a very large distance. We used the Haardt-Madau (Haardt & Madau, 1996) ionizing spectrum at $z = 2.526$. The ionization is given by the parameter $\log U$, where $U \equiv \phi/cn_H = J_{912}/4\pi hcn_H$, $\phi$ (cm$^{-2}$ s$^{-1}$) is the surface flux of ionizing photons, and $J_{912}$ is the intensity of the incident radiation at 1 Rydberg. We set $J_{912} = 10^{-21}$ ergs cm$^{-2}$ s$^{-1}$ Hz$^{-1}$ sr$^{-1}$ , a typical, if slightly high value for the intensity of the intergalactic radiation field (Scott *et al.* 2000; Hui *et al.* 2002; but see Prochaska 1999). The gas density, $n_H$ cm$^{-3}$, is then related to the ionization by $\log U = -4.34 - log\ n_H$ (cm$^{-3}$).

### 7.1. *Metal Abundance in Components 1 & 2*

Photoionization models show that the gas in components 1 & 2 has relatively low ionization and hence we used O I/H I to find [O/H] ≃ −2.79.

We ran a set of CLOUDY models for log N$_{\rm HI}$= 19.73 cm$^{-2}$ and metal abundance [X/H]= −2.77, similar to the value we expected to find based upon the observed O I/H I ratio. We considered all the gas in components 1 and 2 together because there are large errors on the fraction of each ion in component 2. Figure 26 shows the predicted column densities for ions of interest as a function of gas density.

The absence of strong C IV and Si IV shows that the density is high enough that the metal abundance can be taken from the O I/H I ratio. The components that we fit to C IV and Si IV nearest to $v = 0$ km s$^{-1}$ have $b \simeq 38$ km s$^{-1}$ , very different from the $b \simeq 7$ km s$^{-1}$ that we expect for components 1 & 2. In Table 3 we list upper limits on the column densities that could be associated with components 1 & 2, obtained when we fit lines with fixed $b = 7$ km s$^{-1}$ and $v = 0$ km s$^{-1}$. The spectrum allows these column densities, but not much larger values. We also list upper limits that we found for Si III and Al II. These limits all require relatively high densities: $\log n_H$ (cm$^{-3}$) > –2.3 (Al II), –1.7 (Si IV), –1.6 (Si III) and –1.5 (C IV).

We obtain the [O/H] from the observed O I/H I, making a slight adjustment for ionization. The O I column density in components 1 & 2, $13.63 \pm 0.02$ cm$^{-2}$, equals the model prediction for [O/H] = −2.77 and log $n_H = -2.24$ cm$^{-3}$. Since the density is relatively high, the [O/H] is insensitive to the precise density. The other ions prefer a higher density of $\log n_H \simeq -1.5$ cm$^{-3}$, where the predicted O I column density is 0.02 cm$^{-2}$ higher than we observe. Hence we conclude [O/H] = $-2.79 \pm 0.05$, which includes the error on log N$_{\rm HI}$. Had we chosen a much higher density of $\log n_H = +1$ cm$^{-3}$, the [O/H] would decrease by only 0.01. We checked that that the [O/H] value is insensitive to the shape of the ionizing spectrum.

### 7.2. *Ionization, Size and Mass of Components 1 & 2*

Overall, the column densities of the ions indicate $\log n_H \simeq -1.5$ cm$^{-3}$, or $\log U \simeq -2.84$. Although a lower density of $\simeq -2.1$ cm$^{-3}$ is preferred by Si II and is allowed by Al II, the C IV and Si IV rule this out, and the C II prefers a higher density, log $n_H \simeq -0.44$ cm$^{-3}$. We used the column densities in the components at the velocities that we footnote in Table 3. The fit is improved if we add C II at $v = -5.6$ km s$^{-1}$, or if C is slightly underabundant and Si is over-abundant, but none of these differences are significant because the column densities are not well known.

The level of ionization indicated by the ions implies that the gas is mostly ionized. Figure 27 shows the neutral fraction is of order 21% for $\log U = -2.84$.

The $\log n_H$ value implies an absorbing region of typical size and mass. The bottom half of the Fig. 27 shows the size for a given ionization, for either constant $n_H$ or constant $J_{912}$. For a given $\log U$, $n_H$ is proportional to $J_{912}$ by definition, the size is proportional to $n_H^{-1}$, and the mass to $n_H^{-2}$. For an ionization of $\log U = -2.84$ and $J_{912} = 10^{-21}$ ergs cm$^{-2}$ s$^{-1}$ Hz$^{-1}$ sr$^{-1}$ , the size is 2700 pc along the line of sight, and the mass of H in a sphere with this diameter, and the density $\log n_H = -1.5$ cm$^{-3}$ is $8.0 \times 10^6$M$_\odot$.

Both the size and mass of the absorbing region are uncertain by at least an order of magnitude because $J912$ and especially the gas density are uncertain. Consider three types of change we can make to lower the sizes and masses: we can increase the density, we can decrease the ionization, or we can increase the density and the $J_{912}$ in proportion to maintain the ionization, which we prefer. For example, if we increase both the $J_{912}$ and the $n_H$ by 10 times, the ionization is unchanged, the size drops by 10 times, and mass by 100 times.

If we consider low ionization solutions, we can have high gas densities that give small sizes and masses. We view this alternative as unlikely, because at lower ionization we expect less Si II than we see, and less Al II than allowed by the upper limit. This is possible if most of the absorption from these ions is from different gas. However, this would also require C II to come from different gas, yet Fig. 4 suggests that much of the O I, C II and Si II do some from the same gas, and the ionization model is consistent with this. But if we do consider lower ionization solutions and we keep the density constant at $\log n_H = -1.5$ cm$^{-3}$, the size comes down by at most a factor of 5, and the mass by a factor of 125. This is because the gas becomes neutral, at which point the size depends only on the density.

The properties of the gas that shows D towards Q1243+3047 are typical. Table 4 summarizes the inferred total gas column densities, sizes and gas masses of six D/H absorbers. For consistency we scaled the gas densities, and hence sizes and masses so that the observed ionization was obtained for $J_{912} = 10^{-21}$ ergs cm$^{-2}$ s$^{-1}$ Hz$^{-1}$ sr$^{-1}$. We

see that the total gas column densities, log H, may all be very similar. The sizes are of order 1 kpc, but with a huge range covering over a factor of 1000, while the masses cover an even larger range.

Finally, CLOUDY provides estimates for the gas temperature that we show in Fig. 28. For $\log U \simeq -2.84$ we expect an equilibrium gas temperature near 10,000 K. At this temperature we expect $b$(D-1) > 9.1 km s$^{-1}$, similar to the observed value. We saw in §5.2 that the widths of the O-1, D-1, and H-1 components together indicate $T = 0.55 \pm 0.04 \times 10^4$ K, which is lower, perhaps because the gas is, after all, neutral or the ionizing spectrum is softer than the one we used.

### 7.3. *Abundances in other components*

Photoionization calculations suggest, with large uncertainty, that components 3 near $v \simeq -40$, and 4 near $v \simeq +100$ km s$^{-1}$, have different metal abundances from each other and from components 1 & 2.

We performed additional photoionization calculations for a metal abundance $[X/H] = -1.5$ and $n_H = 0.001$ cm$^{-3}$ and log N$_{\rm HI}$= 16.00 cm$^{-2}$ (component 3) and log N$_{\rm HI}$= 16.50 cm$^{-2}$ (component 4). The $n_H$ was determined using the relation between column density and physical density as given by Hellsten et al. (1998). Figure 29 illustrates the results.

For component 3 we estimate [C/H] = −0.5 to −1.5, from Si II/C II and the lack of Si IV and C IV. The ionization is in the range $-5 < \log U < -2.75$, and the Si is not enhanced. The equilibrium temperature requires $13.36 < b_H < 17.50$ km s$^{-1}$, when we assume a turbulent velocity width of 3 km s$^{-1}$, as implied by the widths of the Si II and C II absorption. This range is consistent with the grid search value $b(H-3) = 16.3 \pm 0.7$ km s$^{-1}$(§4.1).

For component 4 we estimate [Si/H] ≃ [C/H] ≃ −1.9 with a large uncertainty, because different ions suggest different ionization. If Si is enhanced by 0.3 dex, C II/Si II suggests $\log U \simeq -1.8$ and [Si/H] ≃ [C/H] ≃ −1.7. However, C IV/C II and C IV/Si IV indicate higher ionization, $\log U \simeq -2.6$, and [Si/H] ≃ −2.1.

Three of the components of the absorption system at $z \simeq 2.526$ appear to have very different abundances: −2.79 for the gas in components 1 & 2, −2 for component 4 and −1 for component 3. We note that the component with the most H I and the lowest ionization also has the lowest metal abundance.

## 8. BEST FIT VALUES FOR Q1243+3047

We have made the following estimates for the parameters that describe the gas in which we measure D/H:

- The velocity structure of the gas has two main components that we see in the asymmetry of the O I line.
- Our grid search of models that fit the D lines showed that the components are separated by 12 km s$^{-1}$, with a 1$\sigma$ range of 8.5 – 14 km s$^{-1}$, consistent with the asymmetry of the O I line.
- The main D component, D-1, is at $z = 2.525659$ and has $b = 9.2 \pm 0.2$ km s$^{-1}$.
- The wavelength, $b$-value and column density show that D-1 is D absorption. We believe that the D-2 component is D because it is very narrow, the separation of the D-1 and D-2 components is the same as that of the O-1 and O-2 components, and the fraction of the D in D-1 is similar to the fraction of the O in O-1 (§5). However, these arguments are weak because D-2 is not well defined.
- The grid search also indicated that component D-2, at the larger redshift, contains 12% of the total D column density, with a range of 7% to 28% depending on how much of the absorption near component 2 is H in another component, H-3.
- Total log N$_{\rm DI}$= $15.113^{+0.042}_{-0.026}$ cm$^{-2}$, (i.e. +10%, −6%) where the error range includes fits with $\chi^2 < \chi^2_{min} + 1$. The errors are larger for higher values of log N$_{\rm DI}$ because of the second component can make a significant contribution.
- Total log N$_{\rm HI}$= $19.73 \pm 0.04$ cm$^{-2}$ (9%), where the error is a Gaussian distribution centered on the log N$_{\rm HI}$ value that consistently gave the best fits. We set the width of the Gaussian to give an 80% chance that the true log N$_{\rm HI}$ lies in the range 19.68 – 19.78 cm$^{-2}$ where we found acceptable fits to the Ly$\alpha$ line, the continuum and Ly$\alpha$ forest.
- log (D/H) = $-4.617^{+0.058}_{-0.048}$ (+14%, –10%).
- D/H = $2.42^{+0.35}_{-0.25} \times 10^{-5}$ cm$^{-2}$.
- [O/H] = $-2.79 \pm 0.05$.
- The absorber is probably mostly ionized, with of order 21% of H atoms neutral (§7).

## 9. THE PRIMORDIAL D/H RATIO

In this section we compare D/H measurements from different QSOs, we discuss the dispersion in these value, and whether D/H might correlate with metal abundance or N$_{\rm HI}$, and we give our estimate for the primordial D/H value.

### 9.1. *The Weighted Mean D/H from Five QSOs and the Dispersion of the Values*

We find the weighted mean of the D/H values from five QSOs and we show that the individual values show more dispersion than we expect. In Tables 5 & 6 we list all reported D/H measurements that remain viable. We have previously measured D/H in three QSOs (Tytler, Fan & Burles 1996; Tytler & Burles 1997; Burles & Tytler 1998a; Burles & Tytler 1998b; O'Meara *et al.* 2001), and placed a strong upper limit on D/H in a fourth (Kirkman *et al.* 2000). We will also use the D/H measurement by Pettini & Bowen (2001) towards Q2206–199, although this measurement is less secure because the HST spectra are of much lower S/N and resolution than those from the ground. We discuss Q2206–199 and QSOs that we will not use in Appendix III (§15).

The weighted mean of the first five log D/H values from Table 6 is,

$$log\ D/H = -4.556, \qquad (3)$$

where the weights we use are the $1\sigma$ errors on the quantity $Y_i = log(D/H)_i$. We use log values because they were used to find all but one of the individual D/H values and errors. We obtain a slightly smaller mean D/H if we instead work with the linear D/H values.

The D/H measurements towards the five QSOs are more dispersed than we expect. In O'Meara *et al.* (2001) we noted that the dispersion in the first three measurements was larger than expected, with a 3% chance of a larger $\chi^2$ value. We interpreted this to mean that we had underestimated one or more of those errors. With the addition Q1243+3047 the dispersion of log D/H remains approximately 0.10, but adding the low D/H from Q2206–199 increased the dispersion to 0.14, the $\chi^2$ value for all five measurements increases to 12.35 for 4 degrees of freedom, and the probability that we would have obtained a larger $\chi^2$ value by chance drops to 1.5%.

### 9.2. *Factors that Determine Measurement Errors on D/H Values*

The accuracy and reliability of a D/H value will depend on many factors, that fall under three main headings:

- The details of the absorption system: the $N_{HI}$ value, the number of velocity components, their velocities, column densities and $b$-values, the chance placement of Ly$\alpha$ forest lines and other contamination, the redshift and the flatness of the continuum near the key lines.

- The quality of the spectrum: the spectral resolution, the S/N, the ions observed, and the accuracy of the wavelengths and relative flux calibration.

- The adequacy of the model: Have all possible velocity structures been explored? Have alternative line identifications been considered? Where contaminating and blended lines fit? Were the hidden components explored? Is the continuum over- or under-fit? Have the continuum, Ly$\alpha$ forest and the lines that give D/H been fit simultaneously?

The dominant error with any particular D/H value might depend on any of these factors, or some combination of them. Many of these factors are different between the D/H values, and hence each value can have a different dominant error. We do not expect the measurement errors, or any uncorrected systematic errors to correlate with a single parameter, such as the $z_{abs}$, $N_{HI}$ or metal abundance. Although unlikely, we do not know enough to rule this out.

The errors that are associated with any D/H value could be too small for any of the factors in the list above, such as: poor flux calibration, especially near the Lyman limits, inadequate fitting of the Ly$\alpha$ forest, and inadequate modelling of the continuum and velocity structure, and especially, inadequate exploration of all possible models. The error on a D/H value could be larger than that deduced from the $\chi^2$ values for any of these reasons.

### 9.3. *The Dispersion in the D/H Values May Come from Measurement Errors*

We suspect that the dispersion in the D/H values arises from measurement errors and is not real. If the measurement errors have been underestimated for at least one QSO, then we can explain the excess $\chi^2$ value.

The dispersion of the D/H values is not much larger than we expect. In Table 6 we list $X_i = (Y_i - \mathrm{mean})/\sigma(\mathrm{Y_i})$, the deviation of each measurement from the weighted mean, in units of the individual measurement errors. The D/H from Q1009+2956 is $1.95\sigma$ above the weighted mean, while the D/H from Q2206–199 is $2.17\sigma$ below. A $\chi^2 < 9.5$ would have been expected if all five log D/H values were consistent with the weighted mean, since $\mathrm{Prob}(\chi^2_4 > 9.5) = 0.05$. We would obtain $\chi^2 < 9.5$ if either Q1009+2956 or Q2206–199 were within $1\sigma$ of the mean, or if the measurement errors on all five QSOs were increased by 1.14, both small changes. However, to obtain a typical $\chi^2 = 3.36$, where $\mathrm{Prob}(\chi^2_4 > 3.36) = 0.5$, 3 or more D/H values, or their errors, would need to change, or the measurement errors on all five QSOs would need to increase by a factor of 1.92. These are a large, but still credible changes.

The methods that we introduced in this paper have allowed us to explore some of the issues that effect a D/H value more thoroughly that in past work. We see many ways in which the errors might have been underestimated, both here, and in past work. In §4.2 and §6.5 we discuss factors that might change the $1\sigma$ error that we give for the D/H value from Q1243+3047 by a factor of two. We further believe that the D/H value for Q1243+3047 has benefited from the most thorough exploration of these error related issues. We would not be surprised if the errors on some of the other D/H values were too small by a factor of two.

We are now more confident that measurement errors explain the dispersion in D/H values than we were in O'Meara *et al.*. Our work on Q1243+3047 better illustrates the many ways in which errors can be underestimated. We see that the three D/H values that we suspect are the least reliable are also the values farthest from the mean. For PKS 1937–1009 and Q1009+2956 some of the data reduction and analysis methods were less reliable than those that we used for HS0105+1619 and Q1243+3047, and for Q2206–199 there is much less data available.

### 9.4. *How D/H Depend on Metal Abundance: D/H Chemical Evolution*

The mean D/H from QSOs is similar to the primordial D/H value that we would predict from the D/H and metal abundance in the local interstellar medium (LISM) using standard Galactic chemical evolution. However, chemical evolution can not account for the dispersion in the D/H values from QSOs.

With the two latest D/H measurements, there is no longer a hint of a correlation between D/H and metal abundance in the QSO absorbers that we noted in O'Meara *et al.* (2001). Prantzos & Ishimaru (2001) showed that standard chemical evolution could not reproduce the correlation, while Fields *et al.* (2001) discussed an unconventional scenario that could. In Fig. 30 we show D/H values against metal abundance, mostly measured with Si when the ionization is high, and O otherwise (Table 6).

With the elimination of the correlation, Galactic chemi-

cal evolution more clearly supports the idea that our D/H measurement towards Q1243+3047, and the mean D/H from five QSOs are very close to the primordial D/H value. We include two curves in Fig. 30 that show the expected decrease of D/H against metal abundance in a simple closed box model, without in-fall, and with the instantaneous recycling approximation (Tinsley 1974; Tinsley 1980; Ostriker & Tinsley 1975). We normalized the two curves in different ways. The solid curve uses the mean D/H from Eqn. 3 as the primordial D/H and predicts D/H as a function of metal abundances, including that in the LISM. The dotted curve is normalized to give the D/H abundance in the LISM (Moos *et al.* 2002; Oliveira *et al.* 2002) and it then predicts the primordial D/H abundance, $(D/H)_p$. To draw these curves, we use the equation

$$D/H = (D/H)_p \times \exp\left(-\frac{Z}{y}\frac{R}{1-R}\right), \quad (4)$$

and the values for two parameters from Prantzos & Ishimaru(2001); the returned mass fraction $R = 0.31$, and the yield $y = 0.6$, where $Z$ is the metallicity, or metal abundance in solar units, on a linear scale. These parameters were derived from a Salpeter IMF and the yields of Woosley & Weaver (1995). The choice of parameters and D/H chemical evolution are discussed in Steigman & Tosi(1992), Vangioni-Flam, Olive & Prantzos (1994), Galli & Palla (1995), Prantzos (1996) and Prantzos & Silk (1998).

Both curves connect the D/H values towards Q1243+3047 and HS 0105+1619 to the D/H in the LISM, over three orders of magnitudes in metallicity. The curves show that the decline in D/H, as stars eject gas that lacks D, is insignificant when metal abundances are low; e.g. [O/H] $< -1$. The simple closed box model (Eqn. 4) predicts that by the metal abundance of Q1243+3047, $(D/H) = 0.9987(D/H)_p$, and for HS 0105+1619, 0.986. We have not applied these corrections because they are much smaller than our measurement errors.

We predict the primordial D/H when we normalize the simple model to give the D/H in the LISM. Ostriker & Tinsley (1975) predicted the primordial D/H would be 1.5 – 2 times that in the LISM. With the modern parameters given above, the same model predicts 1.62 times, again without using any D/H measurements. Using the D/H and $Z$ measurements in the LISM from FUSE and HST spectra, $D/H_{LISM} = 1.52 \pm 0.07 \times 10^{-5}$, and [O/H] $= -0.189$ or $Z = 0.647$ (Oliveira *et al.* 2002, and using the solar $\log O/H = -3.310$ from Allende Prieto, Lambert & Asplund 2001), the predicted primordial abundance is $D/H = 2.47 \pm 0.13 \times 10^{-5}$, very similar to the value from Q1243+3047 and from Eqn. 3: $2.78 \times 10^{-5}$. The errors on the prediction are substantial. When we allow the two parameters to simultaneously take values that maximize the change in D/H, from $0.26 < R < 0.36$ and $0.5Z_\odot <$ yield $< 0.9Z_\odot$ (Prantzos, private communication), we find $D/H = 1.94$ – $3.16 \times 10^{-5}$. The range is further increased when we consider in-fall of gas to the Galactic disk (Lubowich *et al.* 2000) and dispersion of D/H in the LISM (Vidal-Madjar *et al.* 1998; Sonneborn *et al.* 2000). Hence, although the D/H values from both Q1243+3047 and HS 0105+1619 are closest to the predicted D/H, we can not use the chemical evolution model to rule out primordial D/H values that are suggested by the measurement to the other QSOs.

### 9.5. *Does D/H Depend on $N_{HI}$?*

The D/H values appear to decline with increasing $\log N_{HI}$. We do not believe that this correlation is real, because we suspect that the dispersion in the D/H values is not real (§9.3). We will discuss potential systematic errors, and then potential cosmological and astrophysical origins for a correlation.

In Figure 31 we see a clear trend of declining D/H with $N_{HI}$. This trend was apparent with just the three D/H values discussed by O'Meara *et al.* (2001) and it was accentuated by Q2206-199 from Pettini & Bowen (2001). The trend rests upon the relatively high D/H for the two LLS (PKS 1937–1009 and Q1009+2956), and the relatively low D/H for Q2206–199 and Q1243+3047 that we will call DLAs.

#### 9.5.1. *Systematic Measurement Errors that Depend on $\log N_{HI}$*

We are not aware of any systematic error in the measurements of PKS 1937–1009, Q1009+2956, HS 0105+1619 and Q1243+3047 that could readily account all of the trend with $N_{HI}$. Rather, we expect that potential errors are complex, and specific to each spectrum (§9.2). However, we can think of three types of systematic error that might depend on $N_{HI}$.

One possibility is that we have included absorption by H in the D measurements, making D/H too large. Hydrogen absorption is more likely to appear like D in the LLS compared to the DLAs for three reasons. First, the LLS have weaker D lines, and hence small amounts of H can have a larger effect than with the DLAs. Second, in the LLS we see only the D Ly$\alpha$ line, and hence we have less information on the D velocity structure than we have for the DLAs. Third, the $b$ values for the H and D lines in the LLS are larger than those in the systems with higher $N_{HI}$ values, which makes the D lines less different from common H lines. A strong argument against this possibility is that the D lines in both PKS 1937–1009 and Q1009+2956 had $b$-values that were smaller than Ly$\alpha$ forest lines, and that agreed with predictions from their H and metal lines that we collect in Table 5.

A second possibility is that we have underestimated the $N_{HI}$ for the two LLS. The method of measuring $N_{HI}$ is different for the LLS than for the systems with higher $N_{HI}$, hence this could be a systematic effect.

A third possibility is that we have missed some of the components of D, making D/H too low in some QSOs (§4.2.6). D components at positive velocities can hide in the parts of the spectrum where the main H absorbs. This can happen in any system where the $v$ distribution of the H I is poorly known, and the H absorption extends over nearly 82 km s$^{-1}$, enough that the H with large positive velocities has D that lies among the absorption of the H with negative velocities.

We do not know whether missing components are more likely at low or high $\log N_{HI}$. It would be header for this effect to go undetected in systems with the lowest column densities and unsaturated Ly series lines, like Q1009+2956. We might expect this effect to be worst in systems with the highest $\log N_{HI}$ because the H lines are

then widest. However two other factors make it easier to find components of the systems with higher log $N_{HI}$ values: the components then have enough gas to show metal lines, and the $b$ values for the H I are smaller than for the LLS.

### 9.5.2. *Both LLS and DLAs can give Reliable D/H*

In general, both DLAs and LLS can give accurate D/H values, and both can have significant advantages. On the other hand, both LLS and DLAs can, in specific cases, give unreliable D/H values. If we had many more D/H measurements, we could determine observationally the fraction of DLAs and LLS that had given errors, but we can not estimate this today.

The DLAs have the advantages that we see several D lines, the $b$ values can be much lower than in the LLS or the Ly$\alpha$ forest, the D lines are strong enough that they are less effected by the Ly$\alpha$ forest alone, and we can see many metal lines that can help us understand the velocity structure.

The LLS with the lowest log $N_{HI}$ also have major advantages. They have unsaturated H lines that give the velocity distribution of the H. We can also measure the log $N_{HI}$ independently the drop in flux across the Lyman break, as we did for PKS 1937–1009 (Burles & Tytler 1997) and Q1009+2956 (Burles & Tytler 1998b). These two advantages make the log $N_{HI}$ much easier to measure than in other systems. We can also directly compare the velocity distributions of the H and D, proving that the absorption is D, and guaranteeing that we are measuring the D and H in the same gas, and not missing components of either the D or the H. These advantages are offset by the greater similarity between the D and H lines.

### 9.5.3. *Cosmological and Astrophysical Reasons why D/H Might Depend on log $N_{HI}$*

If D/H were correlated with log $N_{HI}$, the explanation might involve inhomogeneous BBN, or the creation, removal or destruction of D. No such plausible mechanisms are known.

If we ignore measurement errors, the correlation in Fig. 31 suggests that the D/H ratio has a range of approximately a factor of 2.4.

Although the correlation is seen against log $N_{HI}$, this might not be the most readily interpreted parameter. In Table 4 we list approximate, order of magnitude estimates for the physical conditions where we measure D/H. The log $N_{HI}$ values correlate with the ionization of the gas, and with the approximate density and size and mass of the absorbing region. The highest log $N_{HI}$ values (low D/H values) tend to correspond to low ionization, higher gas density and smaller, less massive absorbing regions. Q1243+3047 stands apart from the trend because it has both a high log $N_{HI}$ and it is ionized, giving a large size and mass, perhaps the largest of any of the D/H regions. Most of the masses are large, $10^5$ – $10^9$ $M_\odot$, which makes it hard to make or destroy the D in local events, unless they effect a large fraction of the higher density portions of the universe.

In SBBN the range in D/H values would correspond to a range of approximately 2 in the $\eta$ value. This range might arrive is the universe is has inhomogeneous $\eta$ on large scales at the time of BBN (Kainulainen, Kurki-Suonio, & Sihvola 1999). The scale of the inhomogeneity would need to be $> 1$ kpc, and perhaps, for the log $N_{HI}$ values of the D/H absorbers, $> 100$ kpc (Mike Norman, private communication), to avoid mixing before the time of observation. The scale is also but is limited to $< 1$ Mpc by the near isotropy of the CMB (Jedamzik & Fuller 1995; Copi *et al.* 1998; Jedamzik 2002). The 1 Mpc scale corresponds to a baryon mass of $5.9 \times 10^9$ $M_\odot$ that is larger than the typical masses of baryon in the gas showing D/H. Inhomogeneity can produce varying D/H, but the power spectrum of the fluctuations should be cut off at both small and large scales to prevent the overproduction of $^4$He and $^7$Li, and to avoid CMB constraints. The lack of variation of the $^7$Li/ H in stars in the halo of our galaxy is a weak argument against inhomogeneities on these scales, since we expect that the gas that we see in QSO absorption systems is the type of gas that makes the halo stars. The argument is weak because the $^7$Li in the halo stars may not be the primordial value (§10.1).

Dolgov & Pagel (1999) present a different scheme (discussed by Kurki-Suonio 2000; Whitmire & Scherrer 2000 and Dolgov 2002) that is inhomogeneous on scales of 100 – 1000 Mpc, small enough to give variation in D/H to QSOs, but large enough to avoid large variations in existing $^4$He and $^7$Li measurements that are all in local objects. They employ inhomogeneities of the different neutrino flavors that add up to give a constant total energy density, thus avoiding the CMB constraint.

We can speculate that significant D has been destroyed in those parts of the universe that, by the time of observation, had the largest H I column densities. These are regions with larger over-densities relative to the mean density. Fields *et al.* (2001) discuss a highly unconventional chemical evolution models and find three constraints on the conditions required to destroy significant D while keeping metal abundances very low. Most observed baryons must have been inside an early generation of stars, the early stars must all have had intermediate initial masses in the range $2 - 8 M_\odot$, and they must not have ejected much C or N.

Other astrophysical explanations seem equally unlikely (Epstein *et al.* 1976; Jedamzik & Fuller 1997; Fuller & Shi 1997; Famiano, Boyd & Kajino 2001; Pruet, Guiles & Fuller 2002; Jedamzik 2002). We can not hide significant D in dust or molecules because neither are abundant enough in typical absorption systems. We would require $> 10\%$ of all the gas to be molecular if $HD/H_2 \simeq 10^{-4}$, or a large proportion of all heavy elements to be in dust, neither of which are likely, except in molecular clouds.

## 9.6. *Our Estimate for the Primordial D/H from all QSOs*

We believe that the best value for primordial D/H is the weighted mean (§9.1) of the log D/H values for the first five QSOs listed in Table 5:

$$logD/H = -4.556 \pm 0.064, \qquad (5)$$

($1\sigma$ error of 15%), which is equivalent to D/H= $2.78^{+0.44}_{-0.38} \times 10^{-5}$, where the errors are the $1\sigma$ errors on the mean, given by the standard deviation of the five log D/H values divided by $\sqrt{5}$. We use this error on the mean instead of the usual error on the weighted mean because the individual

D/H values show more dispersion than we expect. The error on the mean depends on just the dispersion of the D/H values, and the number of measurements, but not on the errors on the values. Had the D/H values been consistent with a single value (§9.1) we would have used the error on the weighted mean, and if the errors on the individual values were also unchanged, this error would have been 0.023, or 1/3 of the error we quote.

The new D/H is $0.6\sigma$ lower than the value we gave in O'Meara *et al.* (2001), $\log \mathrm{D/H} = -4.52 \pm 0.06$, because the two new values since that paper are both lower. However, the error, which is the error on the mean in both cases, has not changed significantly. Although the dispersion in the D/H values is now larger, the error on the mean is not larger because we have two more measurements, Q2206–199 and Q1243+3047.

When we take the primordial D/H from the weighted mean, we assumed that the quoted errors on each D/H value are too small by the same factor. However, if this assumption is not true, other ways of combining the measurements of D/H will give a better estimate of the primordial D/H. As an example, we could speculate that Q1243+3047 and HS 0105+1619 give the two most reliable D/H values because Q1243+3047 has the most thorough treatment of the errors, and HS 0105+1619 is the simplest measurement with the most supporting evidence. A similar line of argument was explored by Pettini & Bowen (2001) when they derived a D/H value using three DLA systems alone, although the value they gave is no longer acceptable because the D/H to Q0347–3819 has since increased and now seems the least secure (§15.2). The best estimate of the primordial D/H might now be the weighted mean of the D/H values from HS 0105+1619 and Q1243+3047 alone. We might then reject the other three measurements because they have less data and they were less thoroughly evaluated (§11.1). This alternative, two-QSO, mean D/H is not very different: $\log D/H = -4.604 \pm 0.032$ (7.6% error), or $\mathrm{D/H} = 2.49 \times 10^{-5}$, and the corresponding parameters from SBBN are $\eta = 6.30 \pm 0.30 \times 10^{-10}$ and $\Omega_b h^2 = 0.0230 \pm 0.0011$, all $0.8\sigma$ different from the values that we quote in §10, in units of the errors in that section.

## 10. BBN RELATED COSMOLOGICAL PARAMETERS

We use SBBN calculations to obtain the $\eta$ and $\Omega_b h^2$ values that correspond to the primordial D/H. We use this $\eta$ value to predict the abundance of the other light nuclei, and we compare with measurements. There are differences that may be caused by systematic errors. We also compare with other estimates of the $\Omega_b h^2$ and find good agreement.

Using the SBBN calculations of Burles, Nollett & Turner (2001), our best estimate for primordial D/H leads to the following predictions: $\eta = 5.9 \pm 0.5 \times 10^{-10}$, $\Omega_b h^2 = 0.0214 \pm 0.0020$ (9.3%), $Y_p = 0.2476 \pm 0.0010$ (predicted mass fraction of $^4$He), $^3\mathrm{He/H} = 1.04 \pm 0.06 \times 10^{-5}$ and $^7\mathrm{Li/H} = 4.5^{+0.9}_{-0.8} \times 10^{-10}$ . In the above, the error on $Y_p$ is the quadratic sum of 0.0009 from the error on the D/H measurement and 0.0004 from the uncertainty in the $Y_p$ for a given $\eta$ (Lopez & Turner 1999). We obtain slightly different central values if we use values from Esposito *et al.* (2000a,b). The differences are 10% or less of the error from D/H alone, except for $^7$Li/H (Esposito *et al.* equations give $4.05 \times 10^{-10}$) and $^3$He/H ($1.06 \times 10^{-5}$). In Fig. 32 we compare the predicted abundances with some recent measurements. The vertical band shows the range of $\eta$ and $\Omega_b h^2$ values that SBBN specifies for our primordial D/H value. Measurements of primordial $^3$He are consistent, but all $^7$Li and most $^4$He measurements prefer lower $\eta$.

### 10.1. *Comparison with the Abundances of other light nuclei*

Here we discuss the other light nuclei produced during BBN – $^3$He, $^4$He, and $^7$Li– and why we believe that D/H is preferred over these elements to determine $\Omega_b$.

For several years it appeared that the primordial $^3$He had not been measured, because of chemical evolution. Now Bania *et al.* (2002) report a limit on the primordial $^3$He/H ratio from their detailed long term study of 60 Galactic H II regions and 6 planetary nebulae. They argue that low mass stars have neither destroyed nor released significant $^3$He, because $^3$He/H changes little with metal abundance. In 17 Galactic H II regions for which the ionization corrections were relatively simple, they find a mean $^3\mathrm{He/H} = 1.9 \pm 0.6 \times 10^{-5}$, which will be an upper limit on the primordial ratio if stars have not on average destroyed $^3$He. They propose that the best value for the upper limit on the primordial $^3$He/H is the value they measured for one H II region that has the lowest metal abundance in their sample, the third lowest $^3$He/H ratio, excellent data and a small ionization correction of 22%. They then quote $^3\mathrm{He/H} < 1.1 \pm 0.2 \times 10^{-5}$ that is consistent with the value predicted by D/H and SBBN. Given the potential complexity of the chemical evolution of $^3$He, the relatively small range and high mean metal abundance in the gas where they have made measurements ($0.1 < [\mathrm{O/H}] < -0.5$), and the other possible ways of extracting the primordial abundance from the data, we suspect that the errors are larger than quoted, as with D and $^4$He.

The main isotope of He, $^4$He, is measured in many tens of extragalactic H II regions to much higher accuracy than either D or $^3$He. But $^4$He is fairly insensitive to $\eta$ and the differences between the measurements allow a large range of $\eta$, probably including the value indicated by D/H. It is likely (Skillman *et al.* 1994; Olive & Skillman 2001) that the systematic errors were underestimated for many measurements. Pagel (2000) stated "systematic errors up to about 0.005 are still not excluded", and "$\mathrm{Y}_p$ is very probably between 0.24 and 0.25", while Fields *et al.* (2001) state: "the systematic uncertainties in the $^4$He abundance make it difficult to exclude $\mathrm{Y}_p$ as high as 0.25". The upper end of this range includes the $\mathrm{Y}_p$ expected from D/H and SBBN. However, Peimbert *et al.* (2002) argue that the systematic errors can be ten times smaller. Compared to other measurements, Izotov & Thuan (1998) report relatively high values for $^4$He/H that are closest to the D/H prediction, but at $\mathrm{Y}_p = 0.2443 \pm 0.0013$ they are still approximately $2\sigma$ below our prediction from D/H (in units of their error). Thuan & Izotov (2002) estimate that their 1998 $\mathrm{Y}_p$ value may be to small by 0.0005 – 0.0010, which still leaves $\mathrm{Y}_p$ $1.5\sigma$ below the prediction from D/H. Ballantyne, Ferland & Martin (2000) reject nebulae from the Izotov & Thuan (1998) sample that may have significant ionization corrections and find a very high $\mathrm{Y}_p = 0.2489 \pm 0.0030$, which is consistent with D/H, but they use an unaccept-

able decrease in $^4$He/H as O/H increases. Although Izotov & Thuan found absorption lines that might explain why Olive, Steigman & Skillman (1997) found less $^4$He in some objects, it is uncertain whether the $Y_p$ is as high as indicated by D/H.

$^7$Li also prefers a lower $\eta$ than the value given by SBBN and D/H. There are many tens of high accuracy measurements of $^7$Li in the atmospheres of metal poor halo stars. There is very little scatter, and hence the abundance ratio in these stars is well determined at $1 - 2 \times 10^{-10}$ (Ryan *et al.* 2000; Bonifacio & Molaro 1997; Thorburn 1994). With the recent measurement of D/H, $^3$He and the $\Omega_b h^2$ from the CMB, it is looking increasingly likely that the $^7$Li in these stars is not the primordial value, but rather a factor of 3 – 4 less (Tytler, Fan & Burles 1996; Charbonnel 2002). Authors differ on whether this much depletion is reasonable. Pinsonneault *et al.* (2002) quote a primordial $^7\mathrm{Li/H} = 2.51^{+1.74}_{-0.93} \times 10^{-10}$ from models of stellar rotational mixing and the measurements of Ryan *et al.* (1999). This value is $1\sigma$ below the D/H prediction. However, Ryan *et al.* (2000) claim that the depletion correction is only $0.02^{+0.08}_{-0.02}$ in the log, and that D/H is not consistent with $^7$Li/H. In Fig. 32 we show their primordial $^7$Li/H value that includes all their corrections, including their depletion correction. Vangioni-Flam, Coc & Cassé (2000) also believe that the $^7$Li depletion is small, and hence that $^7$Li/H rather than D/H, gives the best $\eta$.

We prefer the $\eta$ and $\Omega_b h^2$ values from D/H rather than the lower values from $^4$He and $^7$Li for several reasons. The deuterium abundance is more sensitive to $\eta$ that the abundances of the other light nuclei (Fig. 32). The D/H that we see is likely the primordial value (§9) and does not need corrections D creation or destruction. No ionization corrections are needed. Over the last eight years we have established that deuterium is seen in the spectra of a few QSOs, and D/H can be measured to approximately 10% accuracy in favorable cases. The excess dispersion in the D/H values can be explained if some of the measurement errors have been underestimated. We account for this dispersion in our estimates of the error on the primordial D/H value, the $\eta$ value and the other deduced parameters. The dispersion is not enough to include the lower $\eta$ values preferred by $^4$He and $^7$Li. The D/H value from Q1243+3047 is similar to that from HS 0105+1619 and the mean D/H towards the QSOs is very similar to the primordial D/H we expect using a simple model of with Galactic chemical evolution to estimate the depletion in the LISM (§9.4).

Our confidence in the $\eta$ and $\Omega_b h^2$ from D/H is increased by the agreement with the $\Omega_b h^2$ from the anisotropy of the CMB, but this does not lessen the need for improved primordial abundance measurements. Systematic errors are important, or dominant, in most measurement methods, and many error terms are poorly known because they are hard to estimate.

### 10.2. *Comparison with other measurements of the baryon density*

Aside from using the light element abundances, the cosmological baryon density has been measured in a variety of other ways. These methods include the amount of H in the intergalactic medium at redshift $z \simeq 3$, the fraction of baryons in clusters of galaxies, and most recently and with the most accuracy, the variation of the anisotropy of the cosmic microwave background on angles of under one degree.

The estimates of $\Omega_b h^2$ from different CMB experiments, listed in Table 7, are consistent with each other and with the $\Omega_b h^2$ from D/H and SBBN. The first results from BOOMERANG (de Bernardis *et al.* 2000) indicated a much larger value of $\Omega_b h^2 = 0.036 \pm 0.005$, however, Netterfield *et al.* (2002) have since used revised the pointing solutions and include data on smaller angular scales. They find $\Omega_b h^2 = 0.022^{+0.004}_{-0.003}$ using "weak priors" which constrain the age of the universe to $> 10$ Gyr and the Hubble constant to $0.45 < h < 0.9$. For the same instrument, de Bernardis *et al.* (2002) find $\Omega_b h^2 = 0.022^{+0.004}_{-0.003}$, $0.020^{+0.004}_{-0.004}$ and $0.019^{+0.005}_{-0.004}$ in three complementary calculations. Analyzing the measurements from the first season of observations with the Degree Angular Scale Interferometer (DASI), Pryke *et al.* (2002) report a very similar value, with similar precision: $\Omega_b h^2 = 0.022^{+0.004}_{-0.003}$. The results from a third experiment, MAXIMA-I (Lee *et al.* 2001; Stompor *et al.* 2001) are consistent. Early measurement on the CMB anisotropy in smaller angular scales by the Cosmic Background Imager (CBI) had a maximum likelihood with a lower $\Omega_b h^2 = 0.009$, and this likelihood dropped by a factor of two for $\Omega_b h^2 = 0.019$, and a factor of 3 for $\Omega_b h^2 = 0.03$. Later measurements covering 40 square degrees on the sky give much more precision. Sievers *et al.* (2002) include the COBE-DMR results and find $\Omega_b h^2 = 0.022^{+0.15}_{-0.009}$.

Other methods of measuring the $\Omega_b$ have lower accuracy. The Ly$\alpha$ forest at redshifts $z \simeq 3$ typically indicates higher $\Omega_b h^2$ values (e.g. Hue *et al.* 2002), while the baryon fraction in clusters of galaxies gives consistent values. For example, Steigman (2002) multiplied the $\Omega_m$ derived from SnIa, assuming the universe is flat, by the baryon fraction in clusters of galaxies to obtain $\Omega_b h^2 = 0.019^{+0.007}_{-0.005}$.

The relevance of D/H measurements is changing. Today SBBN and D/H gives the best estimate of $\Omega_b h^2$. However, as CMB measurements improve, the $\Omega_b h^2$ from the CMB will be as accurate as that from the SBBN. When we use $\Omega_b h^2$ from the CMB in SBBN, the D/H is predicted with no free parameters, and hence the main value of D/H will become to test the physics in SBBN (Kaplinghat & Turner 2001; Cyburt, Fields & Olive 2001; Steigman, Kneller & Zentner 2002; Abazajian 2002). Such tests can be made now, comparing the abundances of the light nuclei, but the measurement errors are not well established, and hence the precision will improve when $\Omega_b h^2$ comes from the CMB and we can use D/H alone to test the physics in SBBN.

## 11. SUMMARY

In this paper, we have presented the detection of D towards Q1243+3047. We measured D/H and obtained an accuracy nearly as good as the best previous measurements. The value is slightly lower than the previous mean and hence our best estimate for the cosmological baryon density from SBBN is slightly higher.

The most conspicuous absorption system in the optical spectrum of Q1243+3047 makes a strong Lyman break, and we found D in the main component of that system. The absorption system has a total column density $\log \mathrm{N_{HI}} = 19.73 \pm 0.04\,\mathrm{cm^{-2}}$ in two main components, sep-

arated by approximately 13 km s$^{-1}$. The separation is not well determined, because the second component contains only approximately 12% of the H I, D I and O I, and hence in no case does it make a distinct line. It makes the O I slightly asymmetric, and it accounts for a portion of the absorption at velocities between the main H and the main D, but its only effect on the H I lines is to make them slightly wider on the red side. In total the absorption system has at least seven components, but only components 1 and 2 show O I, and we have seen that nearly all of the H I is confined to $-40 < v < 40$ km s$^{-1}$. The other components have log N$_{\rm HI}\simeq$ 16 cm$^{-2}$ and with one exception, they have no effect on the D/H measurement.

The column density of the D I in the main component, D-1, is well determined, since we see five transitions from this absorber, and several of them are well separated from other lines, giving accurate $b$-values, redshift and log N$_{\rm DI}$. The column density in the second component, D-2, is less well determined because its velocity and $b$-value are not well known. We explored a variety of models for the relevant portions of the spectrum, and found the range of parameters that gave the lowest $\chi^2$ values. Some acceptable models have 7% of their N$_{\rm DI}$ in the D-2 component, while others have 28%, the maximum allowed by the spectrum. The range for the column density of D-2 gives the range in the total D column density. This range arises because the absorption near D-2 can be either D, or H I from component H-3 that has log N$_{\rm HI}$= 15.90$\pm$0.03 cm$^{-2}$, $b = 17.0 \pm 1.0$ km s$^{-1}$ and $v = -44.3 \pm 7$ km s$^{-1}$. The $b$-value and $v$ are not very well known for H-3. As the $b$-value increases, or the $v$ decreases, H-3 absorbs more near D-2, and the column in D-2 decreases.

The line near D-1 is clearly H or D because it makes a Lyman series, and with $b = 9.2 \pm 0.2$ km s$^{-1}$, it is much narrower than typical H lines. Both the velocity of the D-1 lines and their width indicate that the line is D and not H. Comparison with the width of the O I line gives T $= 5500 \pm 400$ K which is cooler than we expect, but there is more uncertainty here than indicated by the quoted error because the O I and D I are slightly separated in velocity. We are not as certain as we were for PKS 1937–1009, Q1009+2956, Q0130–4021, and HS 0105+1619 that we have detected D, because for Q1243+3047 all the H I lines are saturated, and there is extra absorption in other components on either side of the main H I, and hence we know little about the velocity distribution of the H I. We can not make a detailed comparison the H I and D I velocity structures that would prove that all of D-1 is D.

While the main error in the D column density comes from the uncertain velocity structure, the main error on the H column density comes from the uncertain continuum shape. The Ly$\alpha$ line alone gives the best constraints on the log N$_{\rm HI}$ and it is in the short wavelength side of the Ly$\alpha$ emission line, where the continuum level is especially hard to reconstruct. Had the Ly$\alpha$ line been well removed from the emission line, the error on the log N$_{\rm HI}$ might have been much less.

We determined the log N$_{\rm HI}$ by fitting the continuum, Ly$\alpha$ forest and the main Ly$\alpha$ line simultaneously. We model the continuum with smooth curves represented by B-splines, and we use an optimizing code to vary the hundreds of parameters in the model. We re-started the optimization thousands of times, using different initial values for the parameters. All models with the lowest $\chi^2$ values have log N$_{\rm HI}$= 19.73 cm$^{-2}$, which we use as the best fit value. The error on log N$_{\rm HI}$ is harder to estimate. The change in $\chi^2$ values suggests that the $1\sigma$ error is near 0.005, but we reject this error as too small, because we are unsure if we have adequately explored the parameter space or range of models that might be consistent with the spectrum. Instead, we find the range of log N$_{\rm HI}$ values that give models with acceptable $\chi^2$ values, and we represent the log N$_{\rm HI}$ error with a normal distribution chosen to give a 20% chance that the log N$_{\rm HI}$ value is outside the range of acceptable models. The errors on the H I and D I are then comparable.

There are now measurements or limits on D/H towards seven QSOs, all listed in Table 5. In the appendix, we explain why measurements towards two other QSOs are no longer considered useful, and why we will not use measurements towards Q0347–3819, because the D line is not seen, and the velocity structure is too uncertain. Ignoring the one consistent limit, there are then measurements to five QSOs, four from our group.

These five measurements have a larger dispersion than we expect given their quoted measurement errors. There is only a 1.5% chance of a larger $\chi^2$ value by chance. We suspect that the dispersion is large because one or more of the D/H values is inaccurate, or has errors that have been underestimated. The work we present here on Q1243+3047 has reinforced this belief, because we have found that it is surprisingly hard to obtain a reliable D/H measurement. Many details are relevant (§9.2) and can change the value or the error estimate, and we must attempt to model all D/H values that might be consistent with the spectrum, and not stop with the simplest models.

The five D/H measurements do not correlate with metal abundance, but instead there is a correlation with log N$_{\rm HI}$ that is not expected from cosmology or astrophysics. We suspect that this correlation is an artifact, a chance ordering of the D/H values, that themselves show excess dispersion. Even though we suspect that some of the D/H measurements have larger errors than have been quoted, if the relative size of the errors are indicative of the real errors, we can use the weighted mean D/H from the five QSOs as the best cosmological D/H. For the error, we use the error on the mean, and not the weighted mean, because the former better represents the dispersion. The best cosmological D/H is $0.6\sigma$ lower than the value that we quoted in O'Meara *et al.* (2001) because the two new measurements are both below that value. The error is unchanged, because the larger number of measurements compensates for the increased dispersion.

The lower value for the cosmological D/H increases the tension with the primordial abundances of $^4$He and $^7$Li, both of which prefer lower values for $\eta$ and $\Omega_b h^2$. However, considering the difficulties in obtaining these primordial abundances, we consider that the relative abundances of the elements are consistent with SBBN.

For several decades now most measurements have given less $^4$He than we predict, although the dispersion of those measurements suggests that this difference is because of systematic errors. A recent estimate of the primordial $^3$He abundance by Bania *et al.* (2002) agrees exactly with D/H,

but they rely on one measurement and we still do not understand the change in $^3$He caused by Galactic chemical evolution. The abundance of $^7$Li in halo stars is a factor of 3 – 4 less than predicted. Significant $^7$Li may have been destroyed in these stars, although the amount of destruction implied by SBBN and D/H is near the maximum allowed. There is a clear need for more work on all four nuclei.

We believe that Deuterium is the best baryometer (Schramm and Turner 1998) among the light nuclei for the reason given at the end of §10.1. The agreement between the $\Omega_b h^2$ from D/H and that from the CMB adds confidence. These two $\Omega_b h^2$ measurements use very different physics, at very different epochs in the universe. The agreement implies that we understand the main physical processes that effect the observations of both SBBN and the CMB anisotropies.

### 11.1. *New methods used in this paper*

For Q1243+3047, we have attempted to improve the methods that we use to measure D/H. We employed a more accurate relative flux calibration, a more thorough explorations of the models that can represent the D and H absorption, more realistic continuum fitting and better representation of the Ly$\alpha$ forest and other blended absorption. The D/H value and the errors should be more reliable.

We have paid much more attention to the accuracy of the relative flux calibration of the HIRES spectra of Q1243+3047 than we did for any of our past publications. We have several low resolution spectra from the Lick Kast spectrograph, and also a spectrum from ESI. These spectra have allowed us to compare several methods of flux calibrating our HIRES spectra, and to verify that we get similar results if we start with different calibration spectra.

Our continuum fitting procedure is more general than the methods we used for our measurement of D/H in other QSOs. For PKS 1937–1009 and Q1009+2956, we fit the continuum twice; once as a smooth curve passing through the highest flux levels, and again as one smooth curve for each portion of the spectrum which was adjusted to give a good fit. For HS 0105+1619, the continuum was a single smooth curve which passed through the high points in the flux which appeared to be least absorbed by the Ly$\alpha$ forest. We estimated the errors by moving this curve up and down by a factor, such that it was below the flux in many places, or above the flux in all places. The B-spline continua that we fit to Q1243+3047 should give make our $N_{HI}$ estimate more reliable. The B-spline continuum model allows for a wide variety of smooth shapes, and we are able to fit the continuum parameters simultaneously with the absorption line parameters. In addition, the B-spline gives us the ability localize continuum degrees of freedom in wavelength, which we have had difficulty doing in past work. These continuum can be adjusted iteratively to allow for the effects of line absorption, and hence we no longer have to require that the flux is at the continuum level in some pixels.

For Q1243+3047, we fit the continuum, Ly$\alpha$ forest and the DLA all simultaneously. For HS 0105+1619, we fitted the continuum before and independently of the Ly$\alpha$ forest and the DLA. When we used methods like those that we used for HS 0105+1619 on Q1243+3047, we found a significantly lower $N_{HI}$ value, probably because that method required that the flux in at least a few pixels is at the continuum level. We have seen here that the continuum level, the Ly$\alpha$ forest and the DLA are connected in a complex way. In contrast to HS 0105+1619, where we may have use too few degrees of freedom to model the continuum, for PKS 1937–1009 and Q1009+2956, we may have allowed too many degrees of freedom.

For Q1243+3047, we have also attempted a more thorough exploration of the models that might represent the spectrum. For PKS 1937–1009 and Q1009+2956, we used a minimization method to find the optimum parameters. Here, for the log $N_{DI}$, we use a full grid search, where each parameter takes on every allowed value, ensuring a thorough search.

For Q1243+3047, we have also used different ways of estimating the measurement errors. For PKS 1937–1009 and Q1009+2956, we used the $\delta\chi^2$ method that we used here for the log $N_{DI}$ alone. For HS 0105+1619, we quoted the error on log $N_{HI}$ of 0.009 cm$^{-2}$, compared to 0.04 cm$^{-2}$ for Q1243+3047. The smaller error for HS 0105+1619 is the weighted mean of three estimates of log $N_{HI}$ from different parts of the Ly$\alpha$ line. It is reasonable that the value is smaller than for Q1243+3047 because the DLA suffers less contamination near its core. To estimate the error from the continuum, we shift the continuum up or down by some factor, but we did not change its shape.

### 11.2. *Five Outstanding Issues*

We end with six outstanding issues. Some are specific to our D/H measurement from Q1243+3047 and others are long standing.

**Velocity offsets.** The O I absorption is centered 2.8 km s$^{-1}$ away from the center of the D absorption, not enough to change the identification of the D, but enough to raise concerns that we may have misunderstood the velocity structure of the absorption system (§5.1). The deepest components of C II and S II are also offset from O-1 by 2 km s$^{-1}$, in the other direction from the D-1 component. These offsets make it to estimate the column densities of different ions in the same gas, and hence the ionization is uncertain.

**Missing D components.** The main error on the log $N_{DI}$ comes from the amount of D in the component near 13 km s$^{-1}$. This component is hard to recognize and fit because it is weak and blended with the main component (Fig. 6). There might be D in other components that we have mistakenly modeled as H (§4.2.6). We have not included this possibility in the log $N_{DI}$ error because we do not know how to estimate the chance that it has occurred. This additional D could be >10% of the total if these components have [O/H] $< -3$.

**Accuracy of the log $N_{HI}$ error.** We spent considerable time investigating and debating the error associated with log $N_{HI}$ (§6). We mentioned three such error estimates in this paper: the covariance matrix from the optimized fits, the $\delta\chi^2$ method, and the range of log $N_{HI}$ that gave fits with acceptable $\chi^2$. They gave very different errors: 0.0002, 0.005 and 0.04 cm$^{-2}$ respectively. We know that our estimate from the covariance matrix is unreliable, and we mention it only because it is the standard

error quoted in most QSO absorption line studies.

The error that we use, from the range of acceptable fits, is unconventional. It could be in error, perhaps by a factor of two, for several reasons. The largest acceptable $\chi^2$ value might be incorrect (§6.5.4), we may have been over generous in allowing Ly$\alpha$ forest lines with $b = 150$ km s$^{-1}$ (§6.5.2), or we may have considered too narrow or too wide a range of Ly$\alpha$ forest (§6.5.2) or continuum shapes (§6.5.3).

**Dispersion in the D/H values.** While we suspect that the excess dispersion arises from underestimated measurement errors, and we discuss circumstantial evidence for this (§9.2, 9.3, & 11.1) we will not know whether this is correct until more reliable measurements are made.

We are struck that the D/H values and their errors depend more on the choice of the models that we use to estimate D/H, than upon the details of the fit to the data and the $\chi^2$ value (§9.2). A vital role of high S/N spectra is to guide us to examine an appropriate set of models. The errors on D/H values are hard to estimate because it is hard to know whether we have explored a full range of models.

**Correlation of D/H with log $N_{HI}$.** The correlation (Fig. 31) looks rather impressive, because all five measurements, and the limit, allow a monotonic decrease of D/H with increasing log $N_{HI}$. We suspect the correlation is spurious, and a random accident of the measurement errors. We do not know of any single systematic error that could explain all of the effect (§9.5). Rather, a variety of errors may be involved.

**The Lack of Precise Agreement of the Measured Abundances in SBBN.** The measurements of the light nuclei abundances have preferred slightly different $\eta$ values since our first measurement of D/H (Tytler, Fan & Burles 1996). Although Izotov & Thuan (1998) reported higher $Y_p$ values that were closer to the predictions from SBBN and D/H, our D/H values have decreased over the years, exacerbating the difference in the favored $\eta$ values. There are excellent reasons to believe that measurement problems account for the lack of precise agreement.

## 12. ACKNOWLEDGMENTS

This work was funded in part by NSF grant AST-9900842. The flux calibration was funded in part by NASA grant NAG5-9224.

The spectra were obtained from the Lick Observatory, and the W.M. Keck observatory, which is managed by a partnership among the University of California, Caltech and NASA. The Observatory was made possible by the generous financial support of the W.M. Keck foundation. We are grateful to Steve Vogt, the PI for the Keck HIRES instrument which enabled our work on D/H, to the W.M. Keck Observatory staff, to the Lick Observatory staff, to Tom Barlow, who wrote the software used to extract HIRES spectra, and to Ann Boesgaard, George Fuller, Toshitaka Kajino, Sergei Levshakov, Mike Norman, Nikos Prantzos, Jason Prochaska, Gary Steigman and Art Wolfe for helpful discussions and comments.

## 13. APPENDIX I: B-SPLINE CONTINUUM MODEL

We model the continuum level with a B-spline curve. A B-spline is defined by a set of control points, $P_0, P_1, \ldots, P_n$, $n > 3$ where $n+1$ is the number of control points defining the curve. The B-spline passes near to the control points, but does not generally pass through them. A B-spline is defined by the control points as a series of $n-2$ piecewise parametric polynomial segments. The $i$'th segment is given by

$$C_i(t) = \frac{1}{6}[t^3\ t^2\ t\ 1] \begin{bmatrix} -1 & 3 & -3 & 1 \\ 3 & -6 & 3 & 0 \\ -3 & 0 & 3 & 0 \\ 1 & 4 & 1 & 0 \end{bmatrix} \begin{bmatrix} P_{i-1} \\ P_i \\ P_{i+1} \\ P_{i+2} \end{bmatrix} \quad (6)$$

where $t$ is the parametric variable and ranges from 0 to 1. The full B-spline curve, including the joints between segments, has continuity of order two. That is the curve itself, and it's first and second derivatives are continuous.

In the past we have defined continuum levels with Chebyshev polynomials and with cubic splines, which are the options available in the `IRAF` task `continuum`. We decided against using such representations of the continuum in this work because they both define global curves – if you change one control point in a cubic spline or a single coefficient in a polynomial the *entire* curve is affected. In contrast, when $P_i$ is changed, only the B-spline segments between $C_{i-2}(t)$ and $C_{i+1}(t)$ are affected. This locality has two advantages. First, it is easy to define the continuum over a large wavelength range in a piecewise fashion e.g. modifications to the emission line continuum do not mess up the continuum level defined near the Lyman limit. Secondly, it greatly simplifies the task of efficiently computing the continuum changes that occur as a result of changing a single control point, as often occurs during non-linear optimizations.

## 14. APPENDIX II: OPTIMIZER

Here we describe the code we used to vary the parameters of a model for the spectrum. In our previous absorption line work, we have usually fit absorption line parameters using the $\chi^2$ optimize `VPFIT`, which was kindly made available to us by R.F. Carswell and J. Webb and collaborators. We were unable to use `VPFIT` for this work because we desired to optimize both our continuum and absorption line models simultaneously. In addition, we wanted to be able to optimize many hundreds of parameters simultaneously, which we had difficulty doing with standard tools. The optimizer we developed to address these issues implements the Levenberg-Marquardt algorithm where we regularize the normal equations by inverting the curvature matrix by means of a truncated singular value decomposition (SVD).

Our algorithm is based on the Press *et al.* (1992) routine `mrqmin`, and we refer the reader to Press *et al.* for a general description of the Levenberg-Marquardt (LM) algorithm, which we will not repeat here. We only describe the differences between our algorithm and the algorithm implemented by `mrqmin`.

Using the Press *et al.* notation, a key step in the LM algorithm is to solve the following set of linear equations for the changes $\delta a_l$ that need to be applied to the parameter vector $a_l$ during the next iteration of the algorithm

$$\sum_{l=1}^{M} \alpha_{kl} \delta a_l = \beta_k \quad (7)$$

where M is size of the parameter vector. The curvature matrix $\alpha$ is defined as

$$\alpha_{kl} = \frac{1}{2}\frac{\partial^2\chi^2}{\partial a_k \partial a_l} \tag{8}$$

and $\beta$ is given by

$$\beta_k = -\frac{1}{2}\frac{\partial\chi^2}{\partial a_k} \tag{9}$$

In the most implementations of the LM algorithm, Equation 7 is solved by direct inversion of the curvature matrix. For example, `mrqmin` does this by Gauss-Jordan elimination.

The problem with a direct solution of Equation 7 is that when fitting absorption lines the curvature matrix is frequently ill-conditioned. When $\alpha$ has high condition number, a direct inversion gives a solution vector $\delta a_l$ that is usually nonsense. As a result, the LM algorithm will fail to find acceptable parameter updates and will stop.

Unfortunately, it is very easy for to get an ill-conditioned $\alpha$ during an absorption line optimization – all that is required is a pair of nearly degenerate parameters. In practice this seems to occur when fitting several heavily blended lines, or when both broad lines and continuum degrees of freedom are in the parameter set. There are likely many other scenarios which result in an ill-conditioned $\alpha$, as we have observed that the LM algorithm will almost always have a few iterations with an ill-conditioned $\alpha$ if the number of optimized parameters is large enough. The critical number of parameters appears to be something in the range of 30-50 though we have not investigated this carefully. We just note that in the course of this work an ill-conditioned $\alpha$ occurred frequently enough to make the standard LM algorithm nearly useless.

In most situations when the curvature matrix is ill-conditioned, there are still parameter updates $\delta a_l$ available that would significantly improve the $\chi^2$ between the model being optimized and the underlying data. To find these, and to thus improve the performance of our optimizer, our algorithm regularizes $\alpha_{kl}$ before solving Equation 7. We do this by inverting $\alpha_{kl}$ via a truncated singular value decomposition. Briefly, we compute the SVD of the $\alpha$ using the `LAPACK` routine `dgesdd`, which computes orthogonal matrixes $U, V$ and the diagonal matrix $\Sigma = \mathrm{Diag}(\sigma_1, \ldots, \sigma_n)$. $U, V$ and $\Sigma$ are defined such that

$$\alpha = U\Sigma V^* \tag{10}$$

Because $U$ and $V$ are orthogonal and $\Sigma$ is diagonal it is trivial to invert $\alpha$ once it's SVD is known

$$\alpha^{-1} = V\Sigma^{-1}U^* \tag{11}$$

which works as long as all of the $\sigma_k$ are non-zero. The SVD (Equation 10) always exists, even if $\alpha$ is ill-conditioned or even singular. Unfortunately, if $\alpha$ is ill-conditioned, Equation 11 does no better than direct methods for computing $\alpha^{-1}$. However, the magnitude of the $\sigma_k$ tell us which of the orthogonal vectors in $U$ are responsible for the near singular behavior. The standard trick is to compute $\alpha^{-1}$ via

$$\alpha^{-1} = V\Sigma^{+}U^* \tag{12}$$

where

$$\Sigma^{+} = \mathrm{Diag}(\sigma_k^{+}), \qquad \sigma_k^{+} = \begin{cases} 1/\sigma_k & \text{if} \sigma_k > h \\ 0 & \text{otherwise.} \end{cases} \tag{13}$$

In this scheme $h$ is called the regularization parameter. Setting it is something of a black art. If $h$ is set too small, the near singular components of $U$ will corrupt $\alpha^{-1}$. If $h$ is set too large, otherwise good component vectors of $U$ will not be updated, and the optimizer will perform poorly. We could find no guidance from the literature on an appropriate value for $h$ – the general advice given is too experiment and see what works for the application. This is exactly what we did, and in our algorithm $h = 10^{-8}$. Our entire algorithm is implemented in double precision.

This is the algorithm that was used for all of the optimizations performed in this work. This optimizer works very well in practice, and we have routinely performed successful optimizations of over 500 parameters, many of which were highly blended Ly$\alpha$ forest lines.

### 14.1. *Error estimates*

The standard way to estimate the errors in the fitted parameters is to estimate the covariance matrix $C$ from the curvature matrix $\alpha$

$$C = \alpha^{-1} \tag{14}$$

The parameter errors are then just given by the square root of the diagonals of $C$.

This is exactly the error estimate that we use in our optimizer. We directly invert $\alpha$ using Gauss-Jordan elimination instead of using the truncated SVD regularization described above. This is because the validity of an approximate inverse is easily tested when updating parameter values: if the solution to Equation 7 results in a better $\chi^2$, the solution has some value. However, we are not sure how an approximate inverse affects the errors inferred from the covariance matrix, so we just use a direct method.

Note that the estimated errors are not likely to be valid when $\alpha$ is ill-conditioned. In practice, they generally appear to be much to small when the curvature matrix is ill-conditioned. We did a small amount of Monte-Carlo testing which indicated that the estimated covariance matrix appeared to be accurate when optimizing a small number of lines with a well conditioned covariance matrix. However, it appeared from the same testing that the estimated covariance matrix begins to go bad long before $\alpha$ becomes ill-conditioned enough to jeopardize the solution of Equation 7. Because we are sure that Equation 14 is a valid estimate in only very simple optimizations, we use error estimates from Equation 14 only cautiously in this work.

## 15. APPENDIX III: DISCUSSION OF OTHER D/H MEASUREMENTS

In this appendix we discuss D/H measurements and limits to other QSOs. In some cases the absorption systems are too complex, or existing spectra are inadequate to give convincing measurements or constraints. Related issues are discussed in reviews by Tytler & Burles (1997), Tytler *et al.* (2000) and Lemoine *et al.* (1999).

Towards Q0014+813 Songaila *et al.* (1994) reported an upper limit of D/H $< 25 \times 10^{-5}$ in the $z_{abs} = 3.32$ LLS. Using different spectra, Carswell *et al.* (1994) reported $< 60 \times 10^{-5}$ in the same object, and they found no reason to think that the deuterium abundance might be as high as their limit. Improved spectra (Burles, Kirkman & Tytler 1999) showed that D/H $< 35 \times 10^{-5}$. A high D/H

value is allowed, but is highly unlikely because the absorption near D is at the wrong velocity, by $17 \pm 2$ km s$^{-1}$, it is too wide, and it does not have the expected distribution of absorption in velocity, which is given by the H absorption. Instead this absorption is readily explained entirely by H (D/H $\simeq$ 0) at a different redshift.

Towards PG 1718+4807 the LLS at $z_{abs} = 0.701$ was also considered as a possible site showing a large D/H value (Webb *et al.* 1997), but others argued that this was not the most convincing interpretation of the HST spectra (Levshakov, Kegel, & Takahara 1998; Tytler *et al.* 1999). New higher resolution spectra from HST (Kirkman *et al.* 2001) show the velocity structure of the H for the first time. We found that it is unlikely that this QSO gives any useful information on D/H, because the absorption near D is at the wrong velocity and has the wrong line width to be all D. Hence it is probably mostly contaminating H.

Molaro *et al.* (1999) claimed that the z=3.514 absorption system towards AMP 08279+5255 showed low D/H, but they and Levshakov *et al.* (2000) note that since only the Ly$\alpha$ line has been observed, the hydrogen velocity structure and the H I column density are poorly known, and the D feature can be fit using H alone.

### 15.1. *Q2206–0199*

Pettini and Bowen (2001, hereafter PB) report D/H = $1.65 \pm 0.35 \times 10^{-5}$ in the $z = 2.076$ DLA towards Q2206–199. Since the D is measured in a very low S/N HST spectrum it is hard to determine whether the errors are reasonable, and whether D is seen. The reported D/H value is very low compared to the D/H we expect from Galactic chemical evolution and the D/H in the LISM (§9.4). We now discuss some ways in which the errors might have been underestimated.

We concentrate on the $N_{DI}$ which seems to be less reliable than the log $N_{HI}$. The authors solve for the $N_{DI}$ by fitting features at the position of D in three Lyman series transitions: Ly-7, Ly-9, and Ly-12. The $N_{DI}$ value depends on the $b$-value chosen for the D. The D lines are too noisy to give this $b$-value, so the authors interpolate between the widths they measure for the $b$-values of the H I and the metal lines, giving 10.6 km s$^{-1}$. We question whether this $b$-value is accurate, perhaps because the $b$-value of the H I is itself uncertain.

Although the low ion transitions such as Fe II and Al II indicate a single component nature for the gas, Prochaska & Wolfe (1997) also fit multi-component CIV and SiIV gas on either side of the $v = 0$ position of the H which shows D. These additional components may have enough H absorption to widen the Lyman lines that were used to get the $b$-value of the main H I. As such, we explore the implications of a lower $b$(D) on the range of D/H allowed by the data. If we assume the gas is cold, in the range of 300–400 K, and motions are dominated by turbulent velocities, then values of log $N_{DI}$ giving D/H $\simeq 2.9 \times 10^{-5}$ are consistent with the 1 $\sigma$ errors obtained by PB's fit to Ly-9, but not to Ly-12.

We consider the other sources of error relevant to the determination of log $N_{DI}$. In the Lyman limit region presented by PB, very few pixels reach the continuum in their normalized data. In particular, for Ly-9 and Ly-12, no pixels reach the continuum within $v \simeq 150$ km s$^{-1}$ of the position of D. Due to the high level of contamination throughout the Lyman limit, the continuum is very poorly constrained, and could contribute significant errors to the log $N_{DI}$.

Continuum placement aside, contamination also affects the determination of log $N_{DI}$ in this system. In particular we note that the fit to the contamination on the large wavelength side of the D feature in Ly-9 seems incompatible with the size of the 1 $\sigma$ errors given to the D line. Since this additional absorption adds significant optical depth at the position of D, it might change the log $N_{DI}$ by more than $2\sigma$.

Our main concern with this D/H measurement is that the HST spectra have low S/N and provide very little supporting evidence. However, the ions do show a simple velocity structure, and hence the feature may be D with the measured D/H.

### 15.2. *Q0347–3819*

D'Odorico, Dessauges-Zavadsky & Molaro (DDM, 2001) report D/H = $2.24 \pm 0.67 \times 10^{-5}$ in the z=3.025 absorption system to Q0347-3819, while Levshakov, Dessauges-Zavadsky, D'Odorico & Molaro (LDDM, 2002) report a very different value, D/H = $3.75 \pm 0.25 \times 10^{-5}$, from a sophisticated analysis of the same spectrum. We are not convinced that D has been detected in the spectrum of this QSO. The D lines are completely blended with the H lines and in no case can we see D clearly separated from the H. Hence we do not know the central velocity, velocity structure or $b$-value for the absorption near D. This absorption could be partly or predominantly H. It is hard to obtain either a secure value or a limit on D/H, because the velocity structure for this absorption system is critical and not well enough known. We will discuss this system in detail here because many of the issues are very familiar from our discussion of Q1243+3047.

The total H I column should be well determined from the damping wings of the Ly$\alpha$ line. The fits shown in Fig. 11 of LDDM seem to over-absorb in Ly$\alpha$ near $-2800$ km s$^{-1}$, and from +450 to +750 km s$^{-1}$ for Ly$\beta$ which suggests that the model has excess log $N_{HI}$ or that there might be errors in the flux calibration or continuum level.

The metal lines show many components that can contribute to the Lyman series H I lines. Several components may have enough log $N_{HI}$ to also show D. The low ions, especially $H_2$, indicate the velocity for much of the H I, and the expected D. There is absorption on the blue side of Lyman lines 8, 10 and 12 at the position expected for D, which resembles a Lyman series, and hence it may be caused by D I or H I or a combination of the two.

To determine the total log $N_{DI}$ that is associated with the total log $N_{HI}$ we need to know the velocity structure of the D and the H. DDM assumed that the H I is at the velocities of three of the components seen in the metal lines, and they assumed that the H I columns are distributed approximately like the metals. They fit the H I lines by adjusting the log $N_{HI}$ and $b$-values of these components. LDDM stated that their model may not be unique, which seems likely because their model seems to have more degrees of freedom than are needed to fit the data. We expect that two components might suffice, one to fit each side of the H Lyman series lines.

It is difficult to measure the amount of H I in the different components because their lines are all blended. This is especially true for the main component ($v = 0$, component 3 in DDM) because in no case do we see H I absorption from this component alone. The other components, which are on either side of it, account for both sides of the higher order Lyman lines.

DDM find that additional absorption is needed near the velocity expected for D. It is difficult to measure a column density for this extra absorption, whether of not it is D, because we do not know its velocity structure. LDDM demonstrate that the fit tabulated by DDM, and hence the D/H value, is not unique, and that the differences are highly significant because some of the H I, and we expect a similar proportion of the D I, is in a saturated component with an unusually low $b \simeq 2.9$ km s$^{-1}$. The log $N_{DI}$ is sensitive to the $b$-value of the D, and the proportion of the H I and D I that is in this component, neither of which can be measured.

The log $N_{DI}$ also depends on the amount of H I absorption on the red of the D position. The more flux absorbed by the H I, the less can be absorbed by the D, and hence the lower the D/H. The total log $N_{HI}$ is not changed because it is fixed by the damped Ly$\alpha$ line that is insensitive to the velocity structure. If we adjust the relative amount of H I in the two main components, both the log $N_{HI}$ and the $b$-values, which are not known, then the amount of absorption that could be D also changes. There is also a component near $-65$ km s$^{-1}$, seen in C IV and Si IV (Prochaska & Wolfe 1999), which might also have enough H I to effect the absorption on the red side of where D is expected in Ly-8, 10 and 12. The uncertainty in continuum near Ly-10 and 12, two of the three regions used to get log $N_{DI}$, and the lines blended on the blue side of the expected positions of the D lines further increase the uncertainty in the log $N_{DI}$.

DDM and LDDM get very different log $N_{DI}$ and hence D/H because they make different assumptions about the velocity structure. They both assume that the H I, and the D I, have the components at the velocities that show low ionization metal lines, and they assume that the proportion of the H I in these components is similar to that of the metals, which will not work if the metal abundances vary. DDM find that the D can be fit with two main components with $b$-values of $14.1 \pm 0.5$ and $16.2 \pm 3.0$ km s$^{-1}$. LDDM assume that most of the D has $b \simeq 2.8$ km s$^{-1}$ which produces saturated D lines that require much larger log $N_{DI}$ to explain a given amount of absorption. It is reasonable that much of the H I and hence the expected D, has $b$ closer to 2.8 than to 15 km s$^{-1}$, and hence the D/H will be larger than reported by DDM. However we do not know how much of the H I has this low $b$-value, and hence we do not know whether the D/H is lower, similar to, or high than proposed by LDDM.

LDDM tie the unknown velocity structure of the H I and D I to that of the $H_2$ and various metal lines. This is not a unique procedure because in this system the metal lines themselves differ: Fe II (1143.2, 1133.7, 1125.4) has different velocity structure from Si II 1808 and other ions. LDDM note that the Fe II lines may lack column in the main component at $v = 0$ because the Fe there is locked up in dust.

The metal abundance in the gas where D would be seen is uncertain because this gas has a very low $b$-value and there may be dust. LDDM find [Zn/H] $= -1.51 \pm 0.05$, but elements C, P and Ar are higher by 0.3 dex, while O and Si are higher by 0.7 dex. These enhancements are unexpected because Zn should be the least depleted onto dust, and we do not expect such a large enhancement of O and Si. Although LDDM quote [Si/H] $= -0.95 \pm 0.02$, we expect that the uncertainty is much larger than 0.02 dex, and we anticipate that further analysis will show that the total abundances including metals in dust, is lower than this.

We prefer not to take the DDM D/H value as a lower limit, because we do not know whether D has been seen. Before we could take the LDDM value as an upper limit we would need to know that there is at least as much H absorption near the D as they assume, and that the proportion of the D in the low $b$-value component is at least as much as they assume. This absorption system is not ideal for the measurement of D/H.

## REFERENCES


Abazajian, K.N., 2002, astro-ph/0205238
Allende Prieto, C., Lambert, D. L., & Asplund, M. 2001, ApJ, 556, L63
Arnaud, M., Evrard, A.E., 1999, MNRAS, 305, 631
Babul, A. & Katz, N. 1993, ApJ, 406, L51
Ballantyne, D. R., Ferland, G. J., & Martin, P. G. 2000, ApJ, 536, 773
Bania, T. M., Rood, R. T., & Balser, D. S. 2002, Nature, 415, 54
Bigelow, B. C. & Nelson, J. E. 1998, in Proc. SPIE Vol. 3355, p. 164-174, Optical Astronomical Instrumentation, Sandro D'Odorico; Ed., Vol. 3355, 164–174
Bludman, S. A. 1998, ApJ, 508, 535
Boesgaard, A. M. & Steigman, G. 1985, ARA&A, 23, 319
Boute, D.A. & Canizares, C.R., 1996, ApJ, 457, 565
Burles, S., Kirkman, D., & Tytler, D. 1999, ApJ, 519, 18
Burles, S., Nollett, K. M., & Turner, M. S. 2001, ApJ, 552, L1
Burles, S. & Tytler, D. 1998, ApJ, 499, 699
—. 1998, ApJ, 507, 732
Carswell, R. F., Rauch, M., Weymann, R. J., Cooke, A. J., & Webb, J. K. 1994, MNRAS, 268, L1
Charbonnel, C. 2002, Nature, 415, 27
Copi, C. J., Olive, K. A., & Schramm, D. N. 1998, Proceedings of the National Academy of Science, 95, 2758
Copi, C. J., Schramm, D. N., & Turner, M. S. 1995, SCIENCE V.267, NO.5195/JAN13, P. 192, 1995, 267, 192
Cyburt, R. H., Fields, B. D., & Olive, K. A. 2001, New Astronomy, Volume 6, Issue 4, p. 215-238., 6, 215
de Bernardis, P., Ade, P. A. R., Bock, J. J., Bond, J. R., Borrill, J., Boscaleri, A., Coble, K., Contaldi, C. R., Crill, B. P., De Troia, G., Farese, P., Ganga, K., Giacometti, M., Hivon, E., Hristov, V. V., Iacoangeli, A., Jaffe, A. H., Jones, W. C., Lange, A. E., Martinis, L., Masi, S., Mason, P., Mauskopf, P. D., Melchiorri, A., Montroy, T., Netterfield, C. B., Pascale, E., Piacentini, F., Pogosyan, D., Polenta, G., Pongetti, F., Prunet, S., Romeo, G., Ruhl, J. E., & Scaramuzzi, F. 2002, ApJ, 564, 559
de Bernardis, P., Ade, P. A. R., Bock, J. J., Bond, J. R., Borrill, J., Boscaleri, A., Coble, K., Crill, B. P., De Gasperis, G., Farese, P. C., Ferreira, P. G., Ganga, K., Giacometti, M., Hivon, E., Hristov, V. V., Iacoangeli, A., Jaffe, A. H., Lange, A. E., Martinis, L., Masi, S., Mason, P. V., Mauskopf, P. D., Melchiorri, A., Miglio, L., Montroy, T., Netterfield, C. B., Pascale, E., Piacentini, F., Pogosyan, D., Prunet, S., Rao, S., Romeo, G., Ruhl, J. E., Scaramuzzi, F., Sforna, D., & Vittorio, N. 2000, Nature, 404, 955
D'Odorico, S., Dessauges-Zavadsky, M., & Molaro, P. 2001, A&A, 368, L21
Dolgov, A. D. 2002, Phys. Rep., 370, 333
Edmunds, M. G., Henry, R. B. C., & Köppen, J. 2001, Astrophysics and Space Science Supplement, v. 277, p. 169-172 (2001)., 277, 169

Epps, H. W. & Miller, J. S. 1998, in Proc. SPIE Vol. 3355, p. 48-58, Optical Astronomical Instrumentation, Sandro D'Odorico; Ed., Vol. 3355, 48–58
Esposito, S., Mangano, G., Miele, G., & Pisanti, O. 2000, Nuclear Physics B Proceedings Supplements, Volume 85, Issue 1-3, p. 292-297., 85, 292
—. 2000, Nuclear Physics B Proceedings Supplements, Volume 81, Issue 1-3, p. 59-62., 81, 59
Everett, M. E. & Wagner, R. M. 1995, PASP, 107, 1059
Famiano, M., Vandegriff, J., Boyd, R. N., Kajino, T., & Osmer, P. 2001, ApJ, 547, L21
Famiano, M. A., Boyd, R. N., & Kajino, T. 2002, ApJ, 576, 89
Fan, X. & Tytler, D. 1994, ApJS, 94, 17
Ferland, G. J. 2000, in Astrophysical Plasmas: Codes, Models, and Observations, Proceedings of the conference held in Mexico City, October 25-29, 1999, Eds. Jane Arthur, Nancy Brickhouse, and José Franco, Revista Mexicana de Astronomía y Astrofísica (Serie de Conferencias), Volume 9, p. 153-157 POSTSCRIPT: http://www.astrosmo.unam.mx/rmaa/APCM/PSGZ/apcm_ferland.ps.gz, Vol. 9, 153–157
Fields, B. D., Olive, K. A., Silk, J., Cassé, M., & Vangioni-Flam, E. 2001, ApJ, 563, 653
Fuller, G. M. & Shi, X. 1997, ApJ, 487, L25+
Galli, D., Palla, F., Ferrini, F., & Penco, U. 1995, ApJ, 443, 536
Haardt, F. & Madau, P. 1996, ApJ, 461, 20+
Hellsten, U., Hernquist, L., Katz, N., & Weinberg, D. H. 1998, ApJ, 499, 172
Hu, E. M., Kim, T., Cowie, L. L., Songaila, A., & Rauch, M. 1995, AJ, 110, 1526
Hui, L., Haiman, Z., Zaldarriaga, M., Alexander, T., 2002, ApJ, 564, 525
Izotov, Y. I. & Thuan, T. X. 1998, ApJ, 500, 188
Jedamzik, K. 2002, Planet. Space Sci., 50, 1239
Jedamzik, K. & Fuller, G. M. 1997, ApJ, 483, 560
Kainulainen, K., Kurki-Suonio, H., & Sihvola, E. 1999, Phys. Rev. D, 59, 83505
Kaplinghat, M. & Turner, M. S. 2001, Physical Review Letters, vol. 86, Issue 3, pp. 385-388, 86, 385
Kirkman, D. & Tytler, D. 1997, ApJ, 484, 672
Kirkman, D., Tytler, D., Burles, S., Lubin, D., & O'Meara, J. M. 2000, ApJ, 529, 655
Kirkman, D., Tytler, D., O'Meara, J. M., Burles, S., Lubin, D., Suzuki, N., Carswell, R. F., Turner, M. S., & Wampler, E. J. 2001, ApJ, 559, 23
Kolb, E. W. & Turner, M. S. 1990, The Early Universe (Frontiers in Physics, Reading, MA: Addison-Wesley, 1988, 1990)
Kurki-Suonio, H. 2000, in IAU Symposium, Vol. 198, 25–+
Lee, A. T., Ade, P., Balbi, A., Bock, J., Borrill, J., Boscaleri, A., de Bernardis, P., Ferreira, P. G., Hanany, S., Hristov, V. V., Jaffe, A. H., Mauskopf, P. D., Netterfield, C. B., Pascale, E., Rabii, B., Richards, P. L., Smoot, G. F., Stompor, R., Winant, C. D., & Wu, J. H. P. 2001, ApJ, 561, L1
Lemoine, M., Audouze, J., Ben Jaffel, L., Feldman, P., Ferlet, R., Hebrard, G., Jenkins, E. B., Mallouris, C., Moos, W., Sembach, K., Sonneborn, G., Vidal-Madjar, A., & York, D. G. 1999, New Astronomy, vol. 4, no. 4, p. 231-243., 4, 231
Levshakov, S. A., Agafonova, I. I., D'Odorico, S., Wolfe, A. M., Dessauges-Zavadsky, M., & Molaro, P. 2003, ApJ, 582, 596
Levshakov, S. A., Agafonova, I. I., & Kegel, W. H. 2000, A&A, 355, L1
Levshakov, S. A., Dessauges-Zavadsky, M., D'Odorico, S., & Molaro, P. 2002, ApJ, 565, 696
Levshakov, S. A., Kegel, W. H., & Takahara, F. 1998, A&A, 336, L29
Levshakov, S. A., Tytler, D., & Burles S. 2000 in *Early Universe: Cosmological Problems and Instrumental Techniques* proceedings of the Gamov Memorial Intern. Conf. St. Petersburg, Aug. 23-28, 1999 and *A & A Transactions*, Vol. 19, No. 3 – 4, 385-396, astro-ph/9812114
Lopez, R. E. & Turner, M. S. 1999, Phys. Rev. D, 59, 103502
Lubowich, D. A., Pasachoff, J. M., Balonek, T. J., Millar, T. J., Tremonti, C., Roberts, H., & Galloway, R. P. 2000, Nature, 405, 1025
Molaro, P., Bonifacio, P., Centurion, M., & Vladilo, G. 1999, A&A, 349, L13
Netterfield, C. B., Ade, P. A. R., Bock, J. J., Bond, J. R., Borrill, J., Boscaleri, A., Coble, K., Contaldi, C. R., Crill, B. P., de Bernardis, P., Farese, P., Ganga, K., Giacometti, M., Hivon, E., Hristov, V. V., Iacoangeli, A., Jaffe, A. H., Jones, W. C., Lange, A. E., Martinis, L., Masi, S., Mason, P., Mauskopf, P. D., Melchiorri, A., Montroy, T., Pascale, E., Piacentini, F., Pogosyan, D., Pongetti, F., Prunet, S., Romeo, G., Ruhl, J. E., & Scaramuzzi, F. 2002, ApJ, 571, 604
Nollett, K. M. & Burles, S. 2000, Phys. Rev. D, 61, 123505
Olive, K. A. & Skillman, E. D. 2001, New Astronomy, Volume 6, Issue 3, p. 119-150., 6, 119
Olive, K. A., Steigman, G., & Skillman, E. D. 1997, ApJ, 483, 788
Olive, K. A., Steigman, G., & Walker, T. P. 2000, Phys. Rep., 333, 389
Oliveira, C. M., Hebrard, G., Howk, J. C., Kruk, J. W., Chayer, P., & Moos, H. W. 2002, in eprint arXiv:astro-ph/0212506, 12506–+
O'Meara, J. M., Tytler, D., Kirkman, D., Suzuki, N., Prochaska, J. X., Lubin, D., & Wolfe, A. M. 2001, ApJ, 552, 718
Ostriker, J. P. & Tinsley, B. M. 1975, ApJ, 201, L51+
Padin, S. *et al.* 2001 ApJ, 549, L1
Pagel, B. E. J. 2000, Phys. Rep., 333, 433
Peimbert, M., Peimbert, A., Luridiana, V., & Ruiz, M. T. 2002, in eprint arXiv:astro-ph/0211497, 11497–+
Peroux, C., Dessauges-Zavadsky, M., McMahon, R. G., D'Odorico, S. 2002, in SF2A-2002: Semaine de l'Astrophysique Francaise, meeting in Paris, June 2002, eds. F. Combes & D. Barret, (EdP-Science Editions de Physique Conference Series)
Pettini, M. & Bowen, D. V. 2001, ApJ, 560, 41
Pettini, M., Hunstead, R. W., Smith, L. J., & Mar, D. P. 1990, MNRAS, 246, 545
Pettini, M., Smith, L. J., King, D. L., & Hunstead, R. W. 1997, ApJ, 486, 665
Pinsonneault, M. H., Steigman, G., Walker, T. P., & Narayanan, V. K. 2002, ApJ, 574, 398
Prantzos, N. 1996, A&A, 310, 106
Prantzos, N. & Ishimaru, Y. 2001, A&A, 376, 751
Prantzos, N. & Silk, J. 1998, ApJ, 507, 229
Press, W. H., Teukolsky, S. A., Vetterling, W. T., & Flannery, B. P. 1992, Numerical recipes in C. The art of scientific computing (Cambridge: University Press, —c1992, 2nd ed.)
—. 1992, Numerical recipes in FORTRAN. The art of scientific computing (Cambridge: University Press, —c1992, 2nd ed.)
Prochaska, J. X. 1999, ApJ, 511, L71
Prochaska, J. X., Howk, J. C., O'Meara, J. M., Tytler, D., Wolfe, A. M., Kirkman, D., Lubin, D., & Suzuki, N. 2002, ApJ, 571, 693
Prochaska, J. X. & Wolfe, A. M. 1997, ApJ, 474, 140
—. 1999, ApJS, 121, 369
Pruet, J., Guiles, S., & Fuller, G. M. 2002, ApJ, 580, 368
Pryke, C., Halverson, N. W., Leitch, E. M., Kovac, J., Carlstrom, J. E., Holzapfel, W. L., & Dragovan, M. 2002, ApJ, 568, 46
Rauch, M., Miralda-Escude, J., Sargent, W.L.W., Barlow, T.A., Weinberg, D.H., Hernquist, L., Jatz, N., Cen, R., & Ostriker, J.P., 1997, ApJ, 489, 7
Rines, K., Forman, W., Pen, U., Jones, C., & Burg, R., 1999, ApJ, 517, 70
Ryan, S. G., Beers, T. C., Olive, K. A., Fields, B. D. & Norris, J. E. 2000 ApJ, 530, L57
Sadat, R. & Blanchard, A. 2001, A&A, 371, 19
Sanduleak, N. & Pesch, P. 1984, ApJS, 55, 517
Savin, D. W. 2002 ApJ, 530, L57
Schramm, D. N. 1998, in The Age of the Universe, Dark Matter, and Structure Formation, Proceedings from a National Academy of Sciences Colloquium, National Academy of Sciences, Washington, DC, 1998, p.42-46, 42–46
Schramm, D. N. & Turner, M. S. 1998, Reviews of Modern Physics, 70, 303
Scott, J., Bechtold, J., Dobrzycki, A., & Kulkarni, V. P. 2000, ApJS, 130, 67
Sheinis, A. I., Miller, J. S., Bolte, M., & Sutin, B. M. 2000, in Proc. SPIE Vol. 4008, p. 522-533, Optical and IR Telescope Instrumentation and Detectors, Masanori Iye; Alan F. Moorwood; Eds., Vol. 4008, 522–533
Sievers, J. L., Bond, J. R., Cartwright, J. K., Contaldi, C. R., Mason, B. S., Myers, S. T., Padin, S., Pearson, T. J., Pen, U. ., Pogosyan, D., Prunet, S., Readhead, A. C. S., Shepherd, M. C., Udomprasert, P. S., Bronfman, L., Holzapfel, W. L., & May, J. 2002, in eprint arXiv:astro-ph/0205387, 5387–+
Skillman, E. D., Televich, R. J., Kennicutt, R. C., Garnett, D. R., & Terlevich, E. 1994, ApJ, 431, 172
Songaila, A., Cowie, L. L., Hogan, C. J., & Rugers, M. 1994, Nature, 368, 599
Sonneborn, G., André, M., Oliveira, C., Hébrard, G., Howk, J. C., Tripp, T. M., Chayer, P., Friedman, S. D., Kruk, J. W., Jenkins, E. B., Lemoine, M., Moos, H. W., Oegerle, W. R., Sembach, K. R., & Vidal-Madjar, A. 2002, ApJS, 140, 51
Steigman, G. 2002, Fortschritte der Physik, vol. 50, Issue 5, pp.562-568, 50, 562
Steigman, G., Kneller, J. P., & Zentner, A. 2002, in Ionized Gaseous Nebulae, a Conference to Celebrate the 60th Birthdays of Silvia Torres-Peimbert and Manuel Peimbert, Mexico City, November 21-24, 2000 (Eds. W. J. Henney, J. Franco, M. Martos, & M. Peña) Revista Mexicana de Astronomía y Astrofísica (Serie de Conferencias) Vol. 12, pp. 265-271 (2002) (http://www.astroscu.unam.mx/~rmaa/), Vol. 12, 265–271
Steigman, G. & Tosi, M. 1992, ApJ, 401, 150

Stompor, R., Abroe, M., Ade, P., Balbi, A., Barbosa, D., Bock, J., Borrill, J., Boscaleri, A., de Bernardis, P., Ferreira, P. G., Hanany, S., Hristov, V., Jaffe, A. H., Lee, A. T., Pascale, E., Rabii, B., Richards, P. L., Smoot, G. F., Winant, C. D., & Wu, J. H. P. 2001, ApJ, 561, L7
Tinsley, B. M. 1974, ApJ, 192, 629
Tinsley, B. M. 1980, Fundamentals of Cosmic Physics, 5, 287
Turnshek, D. A. & Rao, S. M. 2002, ApJ, 572, L7
Tytler, D. & Burles, S. 1997, in Origin of matter and evolution of galaxies in the universe '96. Proceedings of an international conference held in Atami, Japan, 18-20 January 1996, Singapore: World Scientific, —c1997, edited by T. Kajino, Y. Yoshii, and S. Kubono, p. 37., 37–+
Tytler, D., Burles, S., Lu, L., Fan, X., Wolfe, A., & Savage, B. D. 1999, AJ, 117, 63
Tytler, D., Fan, X.-M., & Burles, S. 1996, Nature, 381, 207
Tytler, D., O'Meara, J. M., Suzuki, N., & Lubin, D. 2000, Particle Physics and the Universe, Proceedings of Nobel Symposium 198, Haga Slott, Enköping, Sweden, 20-25 August, 1998. Edited by L. Bergström, P. Carlson, and C. Fransson. Physica Scripta, Vol. T85, 2000., p.12, 85, 12
Vangioni-Flam, E., Coc, A., & Cassé, M. 2000, A&A, 360, 15
Vangioni-Flam, E., Olive, K. A., & Prantzos, N. 1994, ApJ, 427, 618
Vidal-Madjar, A., Lemoine, M., Ferlet, R., Hebrard, G., Koester, D., Audouze, J., Casse, M., Vangioni-Flam, E., & Webb, J. 1998, A&A, 338, 694
Vogt, S. S., Allen, S. L., Bigelow, B. C., Bresee, L., Brown, B., Cantrall, T., Conrad, A., Couture, M., Delaney, C., Epps, H. W., Hilyard, D., Hilyard, D. F., Horn, E., Jern, N., Kanto, D., Keane, M. J., Kibrick, R. I., Lewis, J. W., Osborne, J., Pardeilhan, G. H., Pfister, T., Ricketts, T., Robinson, L. B., Stover, R. J., Tucker, D., Ward, J., & Wei, M. Z. 1994, in Proc. SPIE Instrumentation in Astronomy VIII, David L. Crawford; Eric R. Craine; Eds., Volume 2198, p. 362, Vol. 2198, 362+
Walker, T. P., Steigman, G., Schramm, D. M., & Olive, K. A. Kang, H. 1991, ApJ, 376, 51
Webb, J. K., Carswell, R. F., Lanzetta, K. M., Ferlet, R., Lemoine, M., Vidal-Madjar, A., & Bowen, D. V. 1997, Nature, 388, 250
Weinberg, D.H., Miralda-Escude, J., Hernquist, L., Katz, N., 1997, ApJ, 490, 564
Whitmire, S. E. & Scherrer, R. J. 2000, PhysRev D61, 083508
Wolfe, A. M. & Prochaska, J. X. 2000, ApJ, 545, 591
Woosley, S. E. & Weaver, T. A. 1995, ApJS, 101, 181
Wu, X. & Xue, Y. 2000, MNRAS, 311, 825
Zhang, Y., Meiksin, A., Anninos, P., & Norman, M.L., 1998, ApJ, 495, 63

TABLE 1
OBSERVATIONS OF Q1243+3047

| Instrument | Date[a] | Integration Time (seconds) | Slit (arcsec) | Wavelengths Observed (Å) |
|---|---|---|---|---|
| Kast | February 13, 1997 | 3300 | 3 | 3120 – 5800 |
| Kast | May 10, 1999 | 6982 | 2 | 3137 – 7188 |
| Kast | May 11, 1999 | 7200 | 2 | 3137 – 7188 |
| Kast | May 17, 2001 | 5400 | 2 | 3191 – 5881 |
| Kast | May 17, 2001 | 5400 | 2 | 3191 – 5881 |
| ESI | January 11, 2000 | 1364 | 1 | 4000 - 10,000 |
| HIRES | April 15, 1999 | 3600 | 1.14 | 3494 – 5842 |
| HIRES | April 16, 1999 | 7200 | 1.14 | 3168 – 4705 |
| HIRES | April 17, 1999 | 8100 | 1.14 | 3168 – 4705 |
| HIRES | April 17, 1999 | 8100 | 1.14 | 3168 – 4705 |
| HIRES | March 12, 2000 | 9000 | 1.14 | 3214 – 4705 |
| HIRES | March 12, 2000 | 9000 | 1.14 | 3214 – 4705 |
| HIRES | March 13, 2000 | 7200 | 1.14 | 3214 – 4705 |
| HIRES | March 13, 2000 | 7200 | 1.14 | 3214 – 4705 |

[a]We list the local calendar date at sunset at the start of the night.

TABLE 2
RESOLUTION AND S/N OF SPECTRA

| Spectrograph | Slit (arcsec) | Pixel Width ($kms^{-1}$) | S/N[a] (3250Å) | S/N[a] (4250Å) | FWHM ($kms^{-1}$) |
|---|---|---|---|---|---|
| Kast | 2 | 105[b] | 20 | 60 | $283 \pm 25$ |
| ESI | 1 | 11.5 | – | 40 | $63.2 \pm 3.0$ |
| HIRES | 1.14 | 2.1 | 10 | 90 | $8.0 \pm 0.2$ |

[a]S/N per pixel.

[b]Mean value. We measure variation with wavelength and from spectrum to spectrum.

TABLE 3
IONS IN THE $z \simeq 2.526$ ABSORPTION SYSTEM TOWARDS Q1243+3047

| Ion | log N ($cm^{-2}$) | $b$ (km $s^{-1}$) | $z$ | $v$ (km $s^{-1}$) |
|---|---|---|---|---|
| H I total[a] | $19.73 \pm 0.04$ | ... | ... | ... |
| H I (H-3) | $15.90 \pm 0.03$ | $17.0 \pm 1.0$ | 2.525171 | $-44.3 \pm 7.0$ |
| H I (H-1) | 19.63 | $14.8 \pm 2.9$ | 2.525659 | $-2.8$ |
| H I (H-2) | 19.05 | $10.9 \pm 3.3$ | 2.525804 | 9.5 |
| H I (H-4) | $16.25 \pm 0.02$ | $25.8 \pm 0.9$ | 2.526939 | $106.0 \pm 0.7$ |
| H I (H-5) | $16.35 \pm 0.02$ | $26.6 \pm 0.5$ | 2.528108 | $205.4 \pm 0.3$ |
| D I total | $15.113^{+0.042}_{-0.026}$ | ... | ... | ... |
| D I (D-1) | $15.058 \pm 0.03$ | $9.2 \pm 0.2$ | 2.525659 | $-2.8 \pm 0.6$ |
| D I (D-2) | $14.191 \pm 0.10$ | $< 12$ | 2.525804 | $9.2^{+2}_{-3.5}$ |
| O I (O-1)[b] | 13.570 | 6.766 | 2.525692 | 0.0[c] |
| O I (O-2)[b] | 12.755 | 6.766 | 2.525848 | 13.3[c] |
| Si II | 11.884 | 3.44 | 2.525209 | $-41.0$ |
| Si II | 11.783 | 5.89 | 2.525342 | $-29.8$ |
| Si II | 12.020 | 7.85 | 2.525568 | $-10.5$ |
| Si II | 11.830 | 3.76 | 2.525635 | $-4.8$[c] |
| Si II | 12.766 | 4.46 | 2.525728 | 3.1[c] |
| Si II | 12.473 | 5.99 | 2.525885 | 16.4[c] |
| Si II | 11.508 | 3.27 | 2.525984 | 24.8 |
| Si II | 12.120 | 7.41 | 2.526083 | 33.3 |
| Si II | 11.751 | 5.97 | 2.526856 | 99.0 |
| C II | 12.521 | 3.03 | 2.525215 | $-40.5$ |
| C II | 12.987 | 11.06 | 2.525324 | $-31.2$ |
| C II | 12.693 | 9.97 | 2.525552 | $-11.9$ |
| C II | 12.956 | 7.58 | 2.525626 | $-5.6$ |
| C II | 13.344 | 5.21 | 2.525708 | 1.4[c] |
| C II | 13.260 | 7.17 | 2.525872 | 15.4[c] |
| C II | 12.921 | 12.73 | 2.525959 | 22.8 |
| C II | 13.150 | 10.40 | 2.526076 | 32.7 |
| C II | 12.916 | 10.59 | 2.526834 | 97.1 |
| Al II[d] | $< 12.2$ | 7 | ... | 0[c] |
| Si III[e] | $< 13.0$ | 7 | ... | 0[c] |
| C IV[f] | $< 12.75$ | 7 | ... | 0[c] |
| C IV | 13.190 | 38.81 | 2.525750 | 4.9 |
| C IV | 13.256 | 20.98 | 2.526171 | 40.8 |
| C IV | 13.248 | 29.53 | 2.526985 | 110.0 |
| C IV | 12.514 | 14.11 | 2.528017 | 197.7 |
| Si IV[f] | $< 12.4$ | 7 | ... | 0[c] |
| Si IV | 12.905 | 37.64 | 2.525560 | $-11.2$ |
| Si IV | 12.730 | 17.21 | 2.526145 | 38.6 |
| Si IV | 12.709 | 24.33 | 2.526944 | 106.5 |
| Si IV | 11.920 | 10.71 | 2.527978 | 194.4 |

[a] Includes components H-1 and H-2 only.

[b] Values correspond to model where the $b$ of O-1 and O-2 have been set to equal each other.

[c] The column density for this component was used to constrain the ionization in components 1 & 2.

[d] This ion was observed in the ESI spectrum only. The quoted upper limit on the column density is obtained when we fix $b = 7.0$ km $s^{-1}$, $v = 0$ km $s^{-1}$ and fit the entire region from –60 km $s^{-1}$ to +60 km $s^{-1}$.

[e] Not fit because strongly blended. We quote the maximum column near $v = 0$ for $b = 7$ km $s^{-1}$ that is consistent with the residual flux.

[f] The upper limit comes from a fit with fixed $b = 7$ km $s^{-1}$ and $v = 0$ km $s^{-1}$.

TABLE 4
INFERRED PHYSICAL CONDITIONS WHERE D/H IS MEASURED

| QSO | $\log H\ I/H$ | $\log H$ ($\mathrm{cm}^{-2}$) | Size (kpc) | Hydrogen Gas Mass ($M_\odot$) |
|---|---|---|---|---|
| PKS 1937–1009[a,b] | $-2.35, -2.29$ | 20.05,19.74 | 0.9, 0.4 | $3.9 \times 10^5$,$2.9 \times 10^4$ |
| Q1009+299[b,c] | $-2.97, -2.84$ | 19.90, 19.93 | 1.8, 1.5 | $1.1 \times 10^6$,$7.5 \times 10^6$ |
| HS 0105+1619[b,d] | $> -0.1$ | $< 19.52$ | $< 1.1$ | $< 1.6 \times 10^5$ |
| Q1243+3047[e] | $-0.69$ | 20.42 | 2.7 | $8.0 \times 10^6$ |
| Q2206–199[f] | unknown[g] | unknown | unknown | unknown |
| Q0347–3819[h] | $> -0.3$ | $< 20.93$ | 0.014 | 211 |
| Q0130–403[i] | $-3.4$ | 20.06 | 30[j] | $4.5 \times 10^8$ |

[a] We list the parameters for each of the two components, where available, from Tytler, Fan & Burles (1996); Burles & Tytler (1998a).

[b]Scaled from previous references to $J_{912} = 10^{-21}$ ergs $\mathrm{cm}^{-2}$ $\mathrm{s}^{-1}$ $\mathrm{Hz}^{-1}$ $\mathrm{sr}^{-1}$ .

[c] We list the parameters for each of the two components, where available, from Tytler & Burles (1997) and Burles & Tytler (1998b).

[d]O'Meara *et al.* 2001.

[e]This paper.

[f]Pettini & Bowen 2001.

[g]Currently, there is not enough diagnostic information to measure the ionization state in this absorber, yet it is presumably neutral, given the log $\mathrm{N_{HI}}$.

[h]Levshakov *et al.* 2002.

[i]Kirkman *et al.* 1999.

[j]Calculated from $log\ n_H = -2.9$ $\mathrm{cm}^{-3}$ from Kirkman *et al.* 2000 and $log\ n_{HI}/n_H = -3.4$ from O'Meara *et al.* 2001 .

TABLE 5
D/H MEASUREMENTS TOWARDS QSOS

| QSO | $z_{DH}$ | D/H $\pm1\sigma$ ($\times10^{-5}$) | logD/H | $X_i$[a] | $b$(D) (km s$^{-1}$) predicted | observed |
|---|---|---|---|---|---|---|
| PKS 1937–1009[b] | 3.572 | $3.25 \pm 0.3$ | $-4.49 \pm 0.04$ | $+1.65$ | $12.5 \pm 2.1$[c] | $14.0 \pm 1.0$ |
| Q1009+299[d] | 2.504 | $3.98^{+0.59}_{-0.67}$ | $-4.40^{+0.06}_{-0.08}$ | $+1.95$ | $13.5 \pm 0.5$[c] | $15.7 \pm 2.1$ |
| HS 0105+1619[e] | 2.536 | $2.54 \pm 0.23$ | $-4.596 \pm 0.040$ | $-1.00$ | $10.1 \pm 0.3$[c] | $9.85 \pm 0.42$ |
| Q1243+3047[f] | 2.525675 | $2.42^{+0.35}_{-0.25}$ | $-4.617^{+0.058}_{-0.048}$ | $-1.05$ | $11.3 \pm 1.8$ | $9.2 \pm 0.2$ |
| Q2206–199[g] | 2.0762 | $1.65 \pm 0.35$[h] | $-4.78^{+0.08}_{-0.10}$ | $-2.17$ | 10.6 | – |
| Q0347–3819[i] | 3.024855 | $3.75 \pm 0.25$[h] | $-4.43 \pm 0.03$ | $+3.35$ | 3,14.1,16.2 | – |
| Q0130–403[j] | 2.799 | $< 6.8$ | $< -4.17$ | – | $16.2 \pm 0.3$[c] | – |

[a] $X_i = (Y_i - mean)/\sigma(Y_i)$, where $Y_i = log(D/H)_i$ and we use the weighted mean of the first five QSOs, log D/H $= -4.556 \pm 0.064$.

[b] We list combined results for the two components, from Tytler, Fan & Burles (1996); Burles & Tytler (1998a).

[c] Calculated from the published data and first presented here.

[d] We list combined results for the two components, from Tytler & Burles (1997) and Burles & Tytler (1998b).

[e] O'Meara *et al.* 2001.

[f] This paper.

[g] Pettini & Bowen 2001.

[h] Discussed in the the appendix of this paper.

[i] First analyzed by D'Odorico *et al.* 2001. We quote results from Levshakov *et al.* 2002.

[j] From Kirkman *et al.* 2000.

TABLE 6
COLUMN DENSITIES AND METAL ABUNDANCES WHERE D/H IS MEASURED

| QSO | log $N_{HI}$ ($cm^{-2}$) | Element $\alpha$ | Abundance [$\alpha$/H] |
|---|---|---|---|
| PKS 1937–1009[a] | $17.86 \pm 0.02$ | Si | $-2.7, -1.9$ |
| Q1009+299[b] | $17.39 \pm 0.06$ | Si | $-2.4, -2.7$ |
| HS 0105+1619[c] | $19.422 \pm 0.009$ | O[d] | $-1.73$ |
| Q1243+3047[e] | $19.73 \pm 0.04$ | O[d] | $-2.79 \pm 0.05$ |
| Q2206–199[f] | $20.436 \pm 0.008$ | Si | $-2.23$[g] |
| Q0347–3819[h] | $20.626 \pm 0.005$ | Si | $-1$[i] |
| Q0130–403[j] | $16.66 \pm 0.02$ | Si | $-2.6$ |

[a] We list the parameters for each of the two components, where available, from Tytler, Fan & Burles (1996); Burles & Tytler (1998a).

[b] We list the parameters for each of the two components, where available, from Tytler & Burles (1997) and Burles & Tytler (1998b).

[c] O'Meara *et al.* 2001.

[d] Using log O/H = −3.31 from Allende Prieto, Lambert & Asplund (2001).

[e] This paper.

[f] Pettini & Bowen 2001.

[g] Prochaska & Wolfe 1997.

[h] Levshakov *et al.* 2002.

[i] Discussed in this paper.

[j] Kirkman *et al.* 1999.

TABLE 7
RECENT ESTIMATES OF THE BARYON DENSITY

| Method | $\Omega_b h^2$ | Ref. |
|---|---|---|
| BBN + D/H | $0.0214 \pm 0.0020$ | this paper |
| CMB:- BOOMERANG | $0.021^{+0.003}_{-0.003}$ | Netterfield *et al.* 2002 |
| CMB:- DASI | $0.022^{+0.004}_{-0.003}$ | Pryke *et al.* 2002 |
| CMB:- MAXIMA-I | $0.033 \pm 0.013$ (95%) | Stompor *et al.* 2001 |
| CMB:- CBI | $0.022^{+0.15}_{-0.009}$ | Sievers *et al.* 2002 |
| Clusters + SNIa | $0.019^{+0.007}_{-0.005}$ | Steigman 2002 |

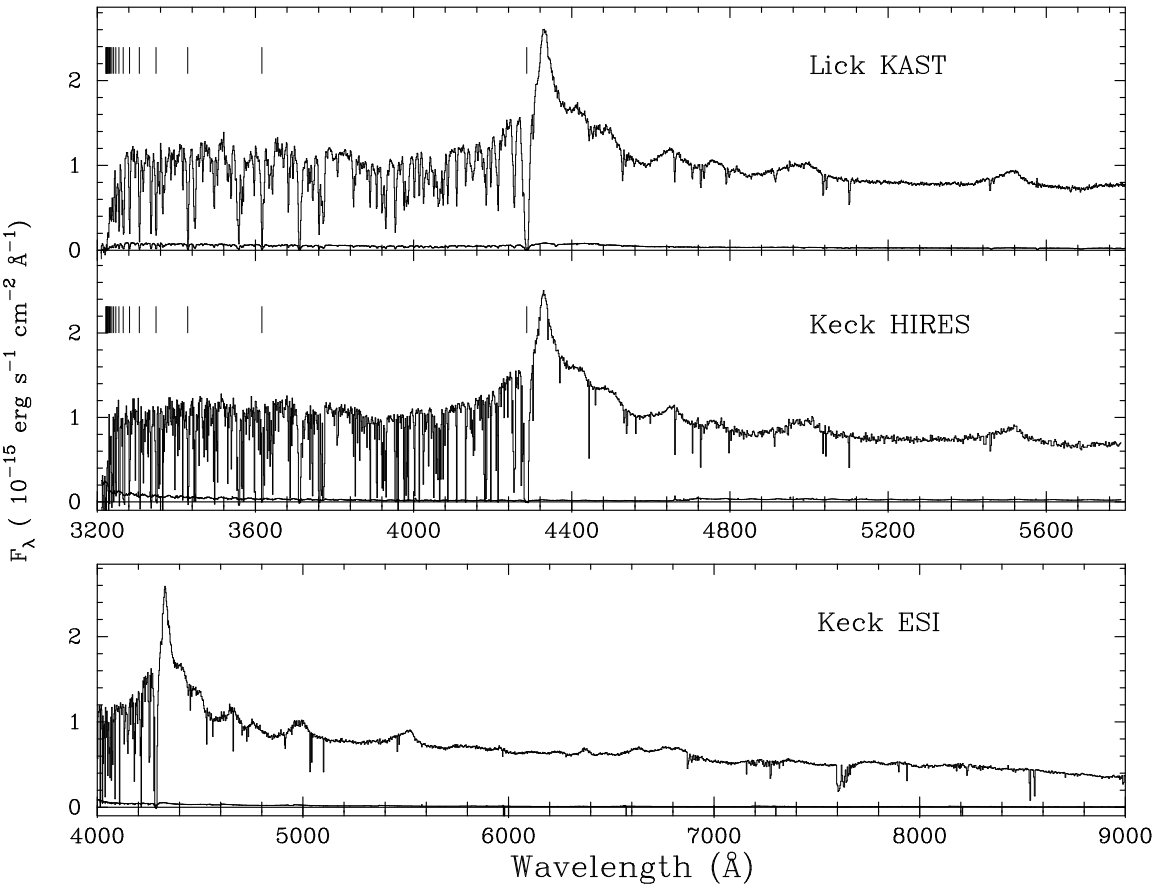


FIG. 1.— The spectra of Q1243+3047 from the KAST spectrograph (top), HIRES (middle) and ESI (bottom). We show the complete wavelength coverage for the Kast and HIRES spectra, but not for the ESI, which extends to 10,000 Å. We have applied relative flux calibration to all three spectra. The emission lines blend to give a continuously undulating continuum level from 4400 – 5000 Å. The vertical marks above the Kast and HIRES spectra show the positions of the Lyman series lines in the absorption system at $z = 2.526$ that gives the D/H value. The Ly$\alpha$ absorption line of this system, from which we get the H I column density, is near 4285 Å, just to the left of the peak of the Ly$\alpha$ emission line. We do not plot most pixels, to reduce the file size.

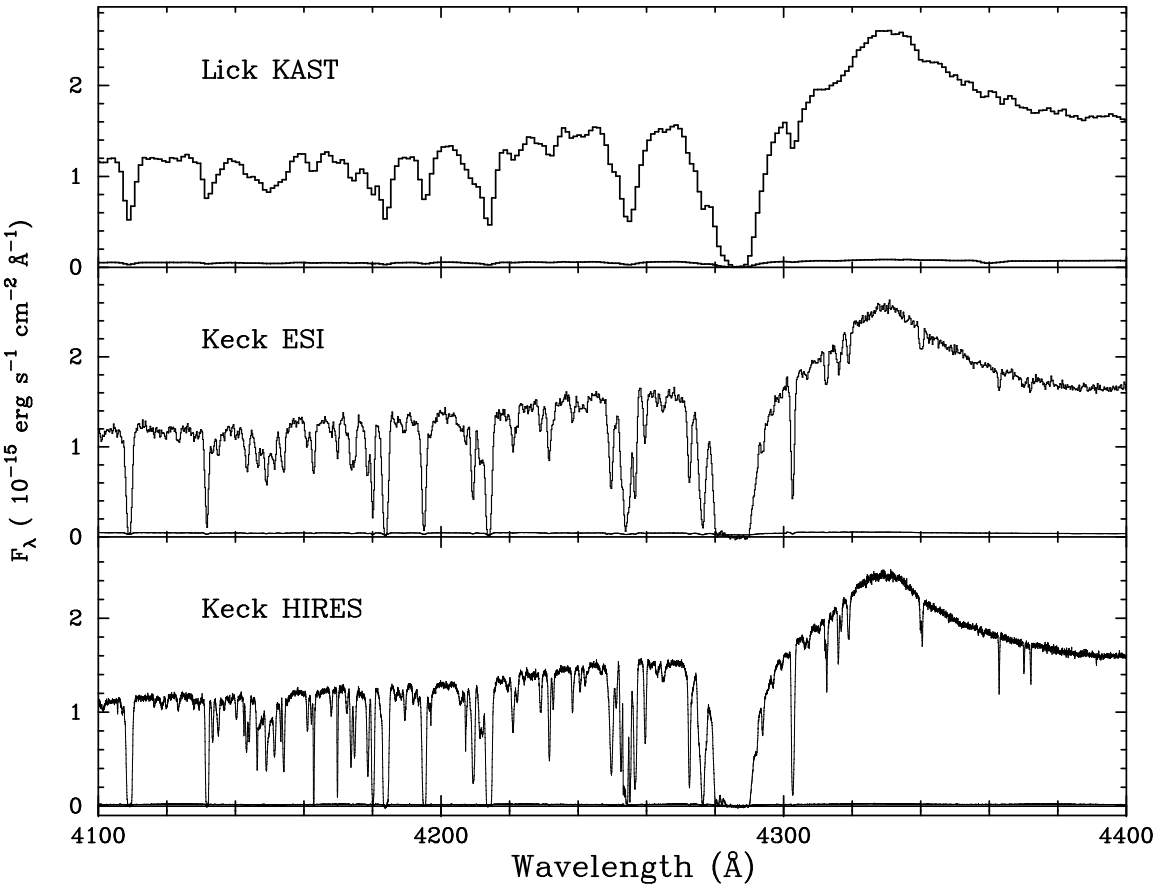


FIG. 2.— Expansion of the Kast, ESI and HIRES spectra from Figure 1. The Ly$\alpha$ absorption near 4285 Å is from the system in which we measure D/H.

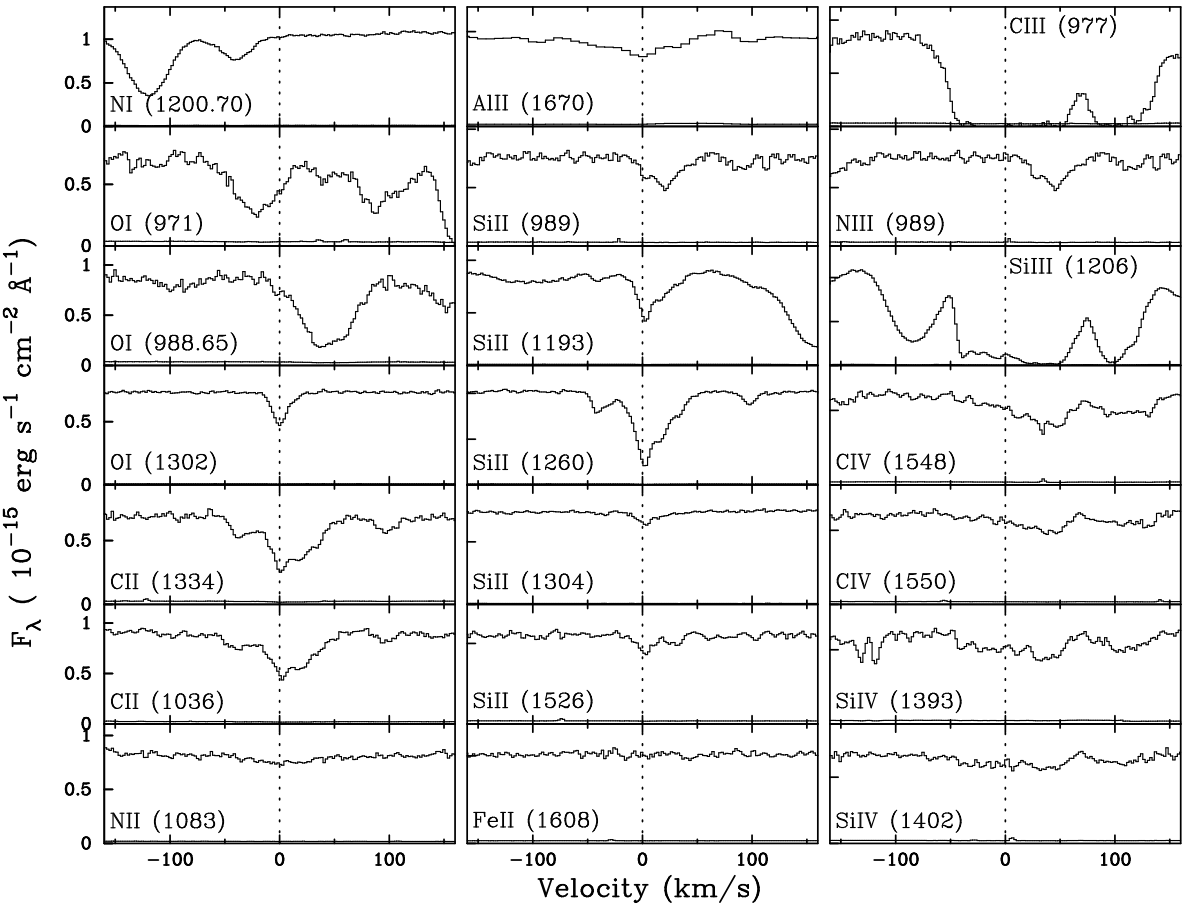


FIG. 3.— Most of the metal absorption lines near $z = 2.526$. We shifted the Al II 1670 spectrum, which is the only one from ESI, by $-16.5$ km s$^{-1}$ to correct a likely error. We see three types of components, grouped by ionization; the low ionization lines represented by O I alone, intermediate ions C II, Si II and high ionization C IV and Si IV.

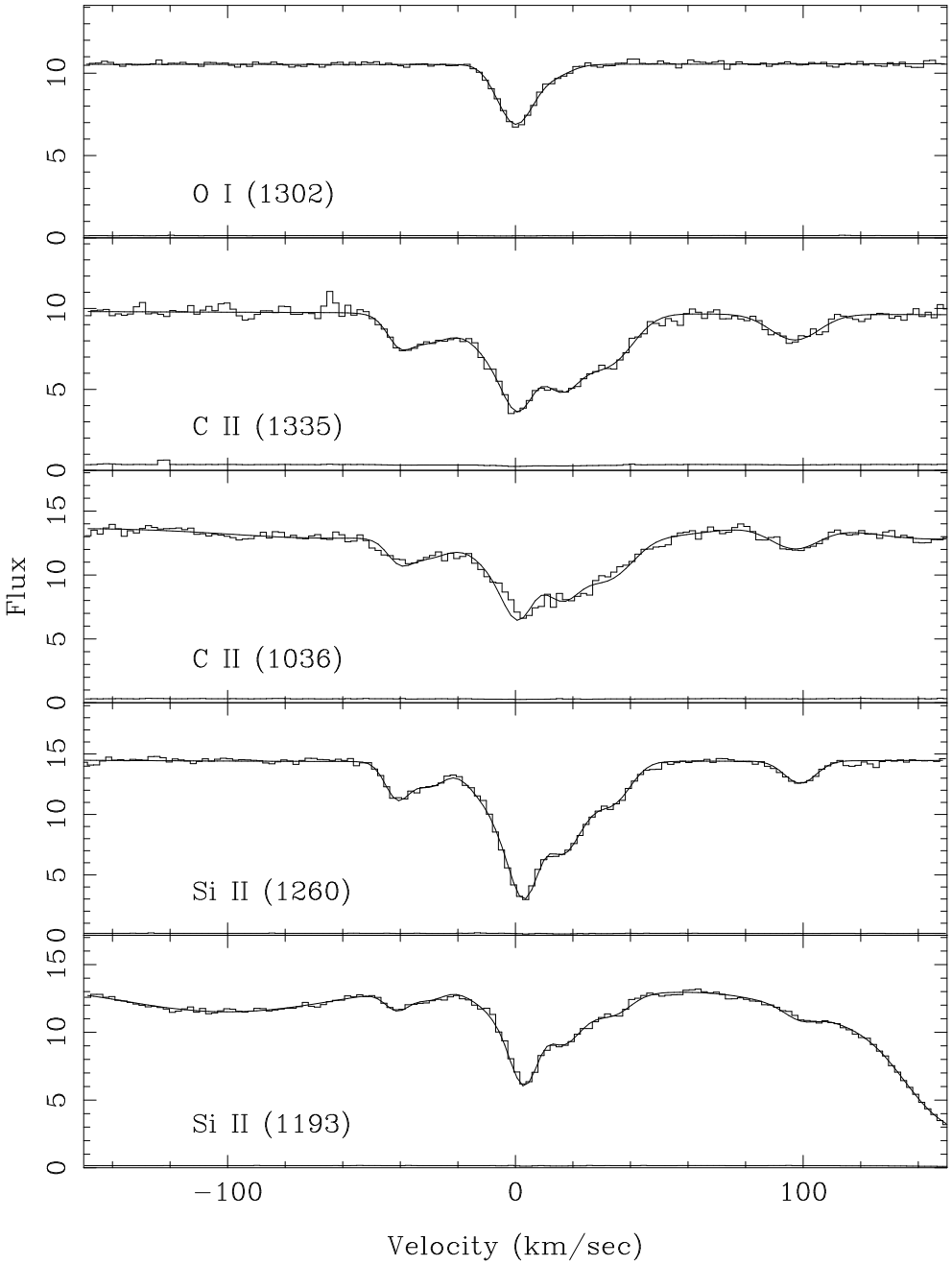


FIG. 4.— Voigt profile fits to the lines of the low ionization ions. The line parameters used to generate these profiles are given in Table 3. The data is our combined HIRES spectrum, with $1\sigma$ errors shown just above the zero flux level. Flux is in units of $10^{-16}$ erg s$^{-1}$ cm$^{-2}$ Å$^{-1}$. The O I absorption shows a well defined component 1 at $v = 0.0$ km s$^{-1}$, and additional absorption in component 2 near +13 km s$^{-1}$. C II and Si II show several components, including a main component near $v = 0$ km s$^{-1}$ for C II (1335) or 3 km s$^{-1}$ for C II (1036) and Si II, and a second component near 16 km s$^{-1}$. We see no absorption near –82 km s$^{-1}$.

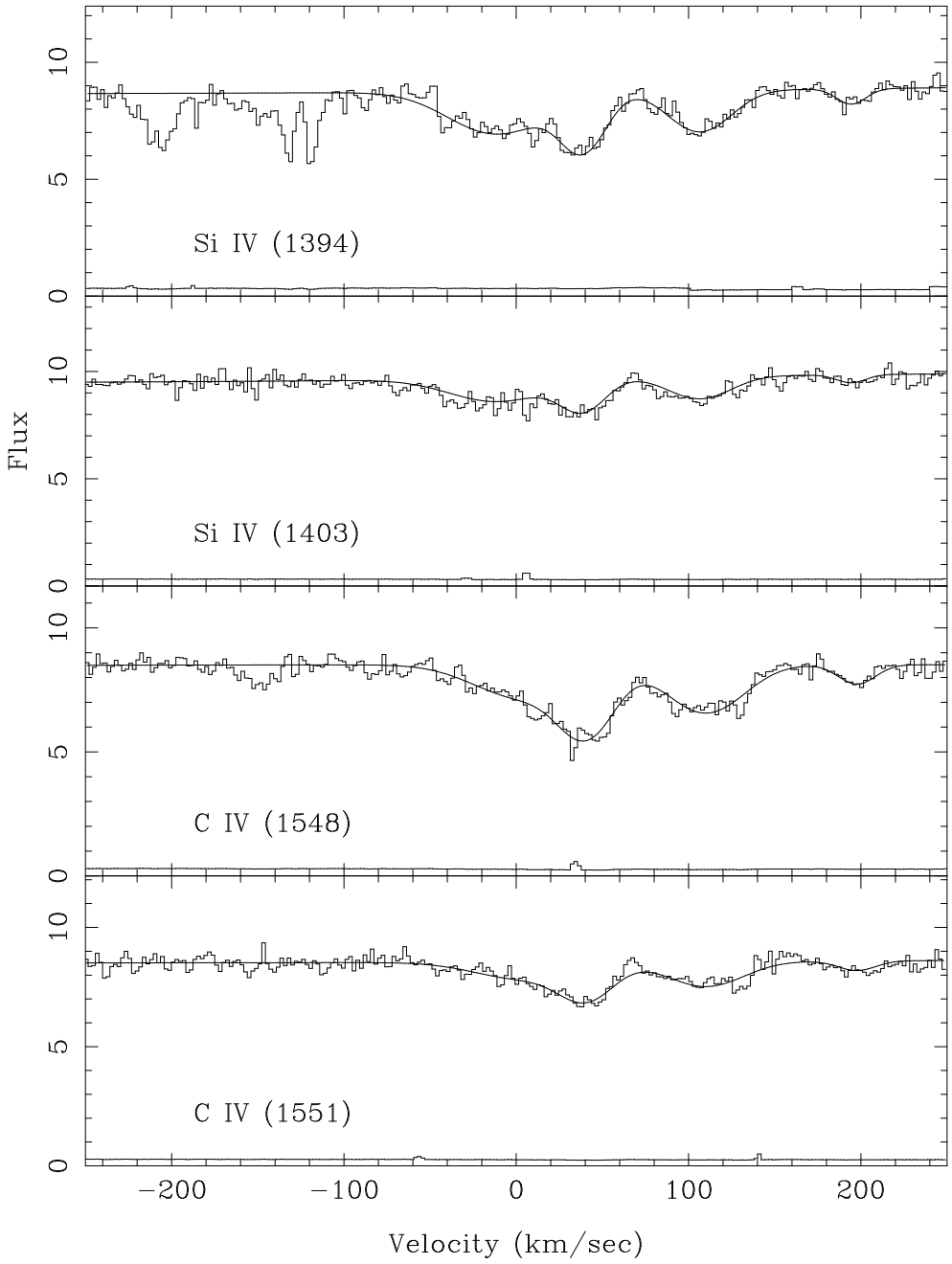


FIG. 5.— As Figure 4, but here we show the lines of the high ionization ions. Again, there is no evidence of metal line absorption near –82 km $s^{-1}$.

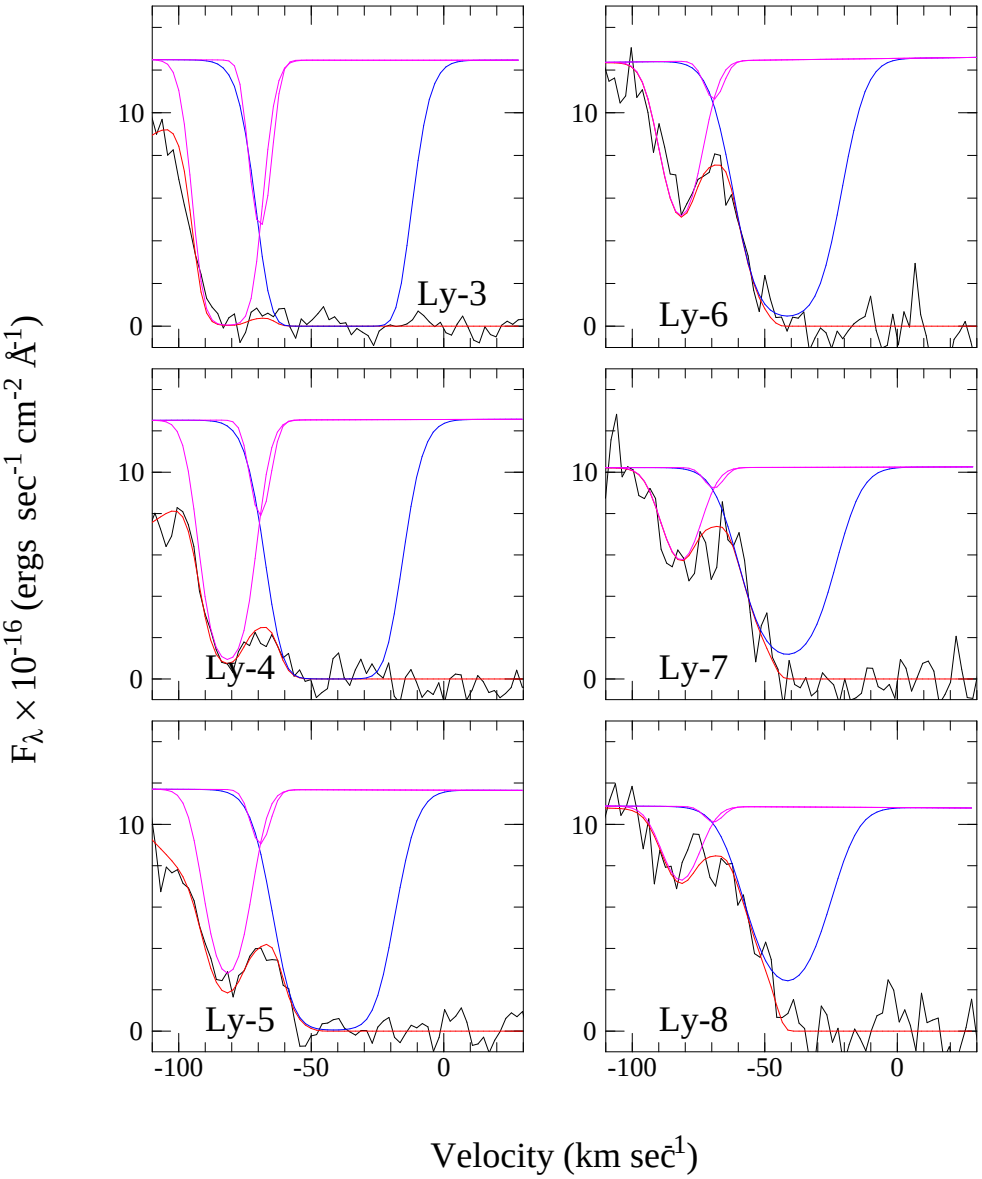


FIG. 6.— The blending of the absorption line components D-1, D-2 and H-3 in Lyman series lines 4 – 9. The two components of the D I absorption are centered at $-82$ km s$^{-1}$ and $-70$ km s$^{-1}$. H-3 is the deep broad line centered near $-40$ km s$^{-1}$. The data is our summed HIRES spectrum. Also shown is the full fit (D-1, D-2, H-3, and all other absorption associated with the system). Note that D-2 is strongly blended with both D-1 and H-3.

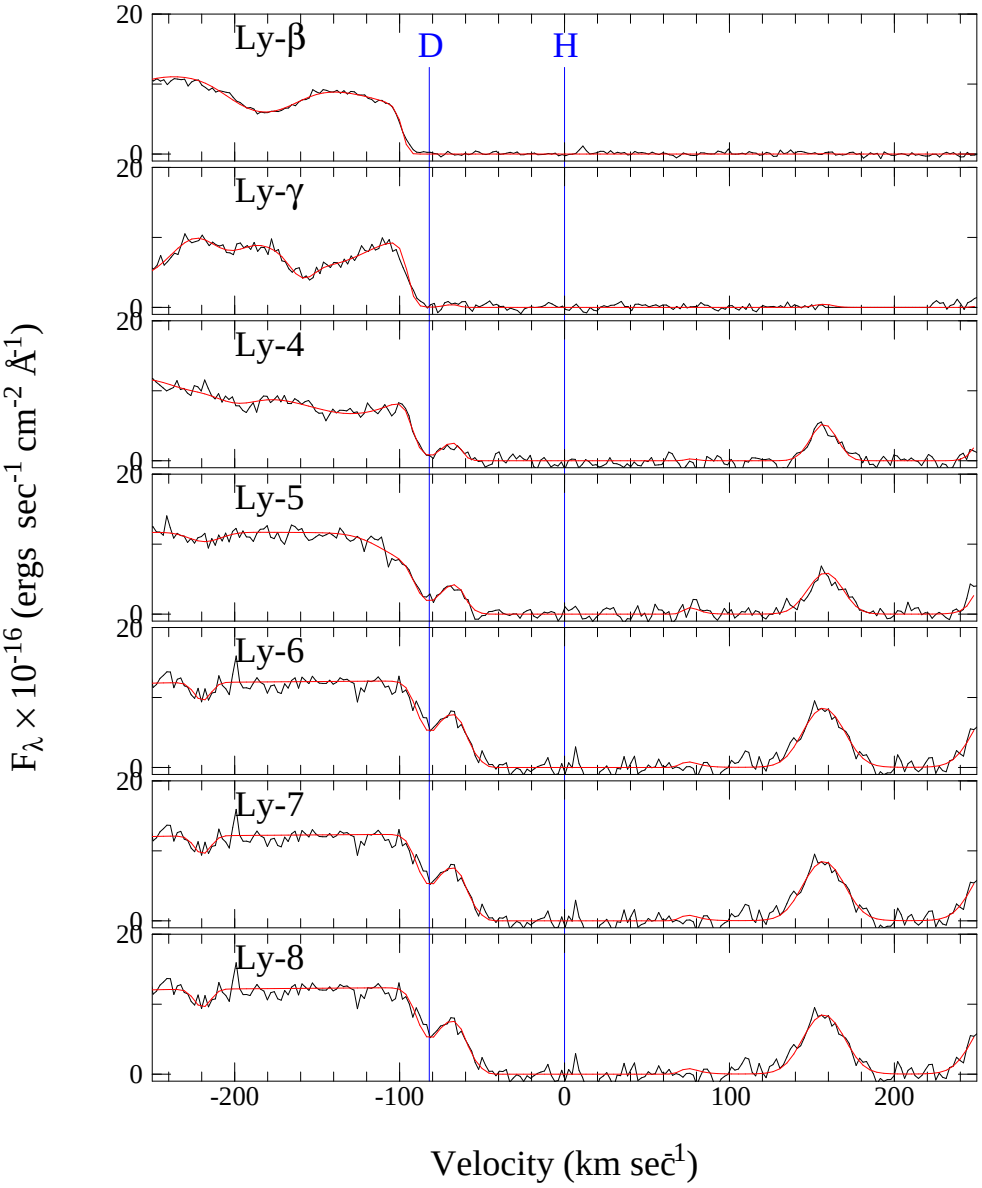


FIG. 7.— The HIRES spectrum of Ly-2 to 8, together with our model of the system, as given in Table 3.

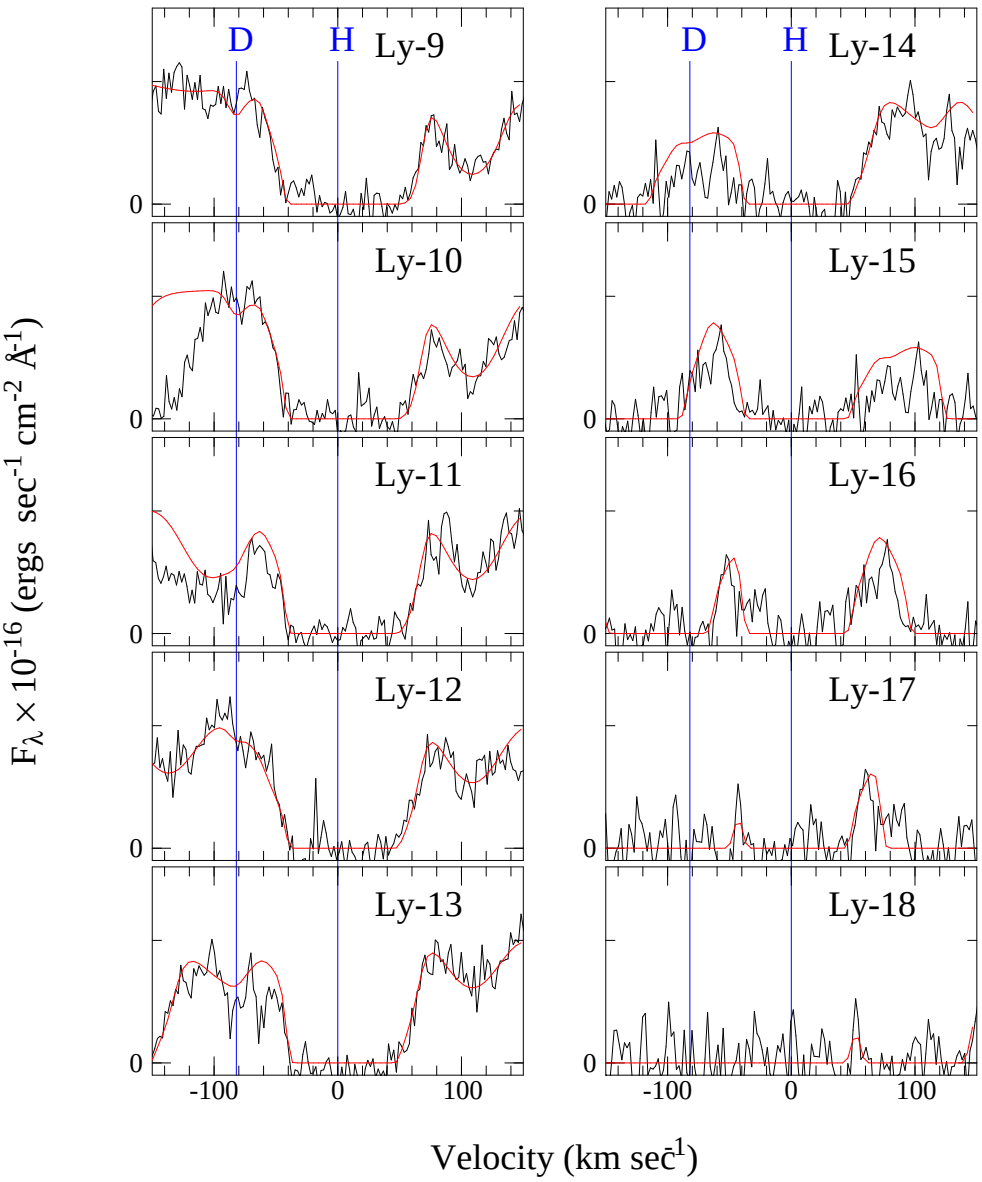


FIG. 8.— The HIRES spectrum of Ly-9 to 18, together with our model of the system, as given in Table 3.

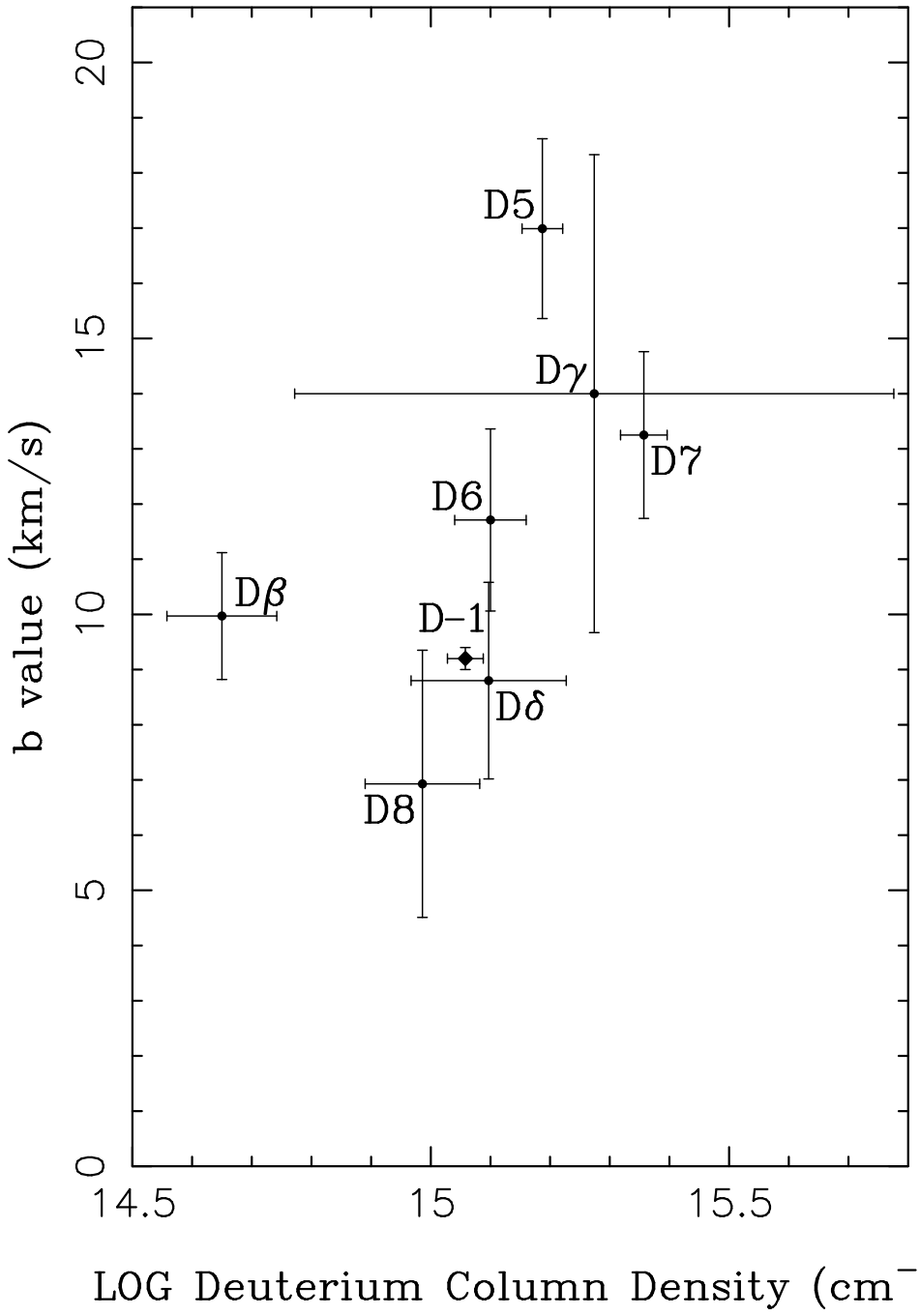


FIG. 9.— The $b$ and $N_{DI}$ values from single component fits to the individual D lines. The only free parameters in the optimizations were $b$(D) and $N_{DI}$(D). All other parameters, including $v$(D)=0, and $b$(H-3)=16.3km s$^{-1}$, were fixed during the fitting process. The displayed errors com from the estimated covariance matrix we produced during the optimization process.

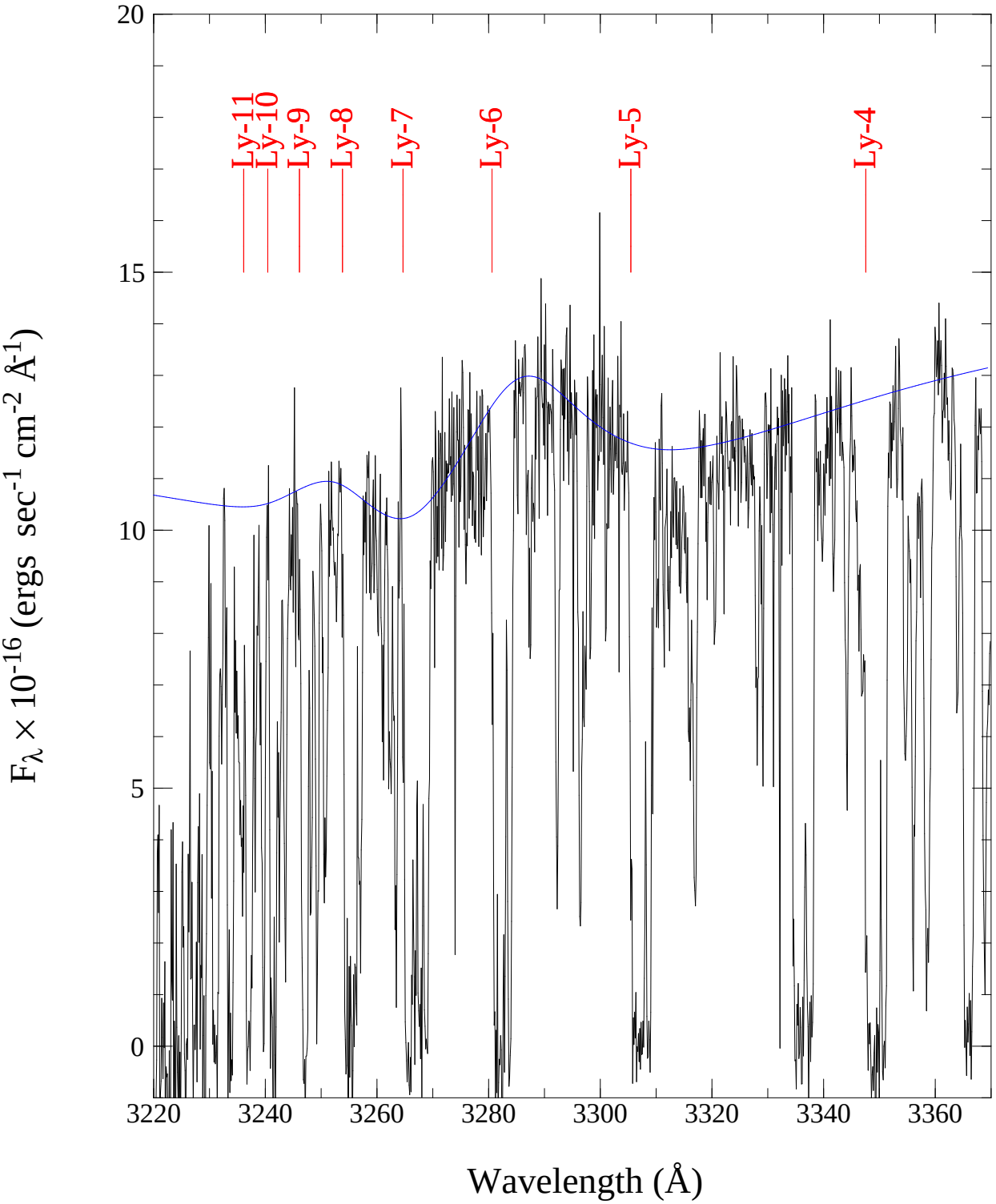


FIG. 10.— The continuum level used to construct our models of the D absorption. The positions of the Lyman series lines are marked at the top of the panel.

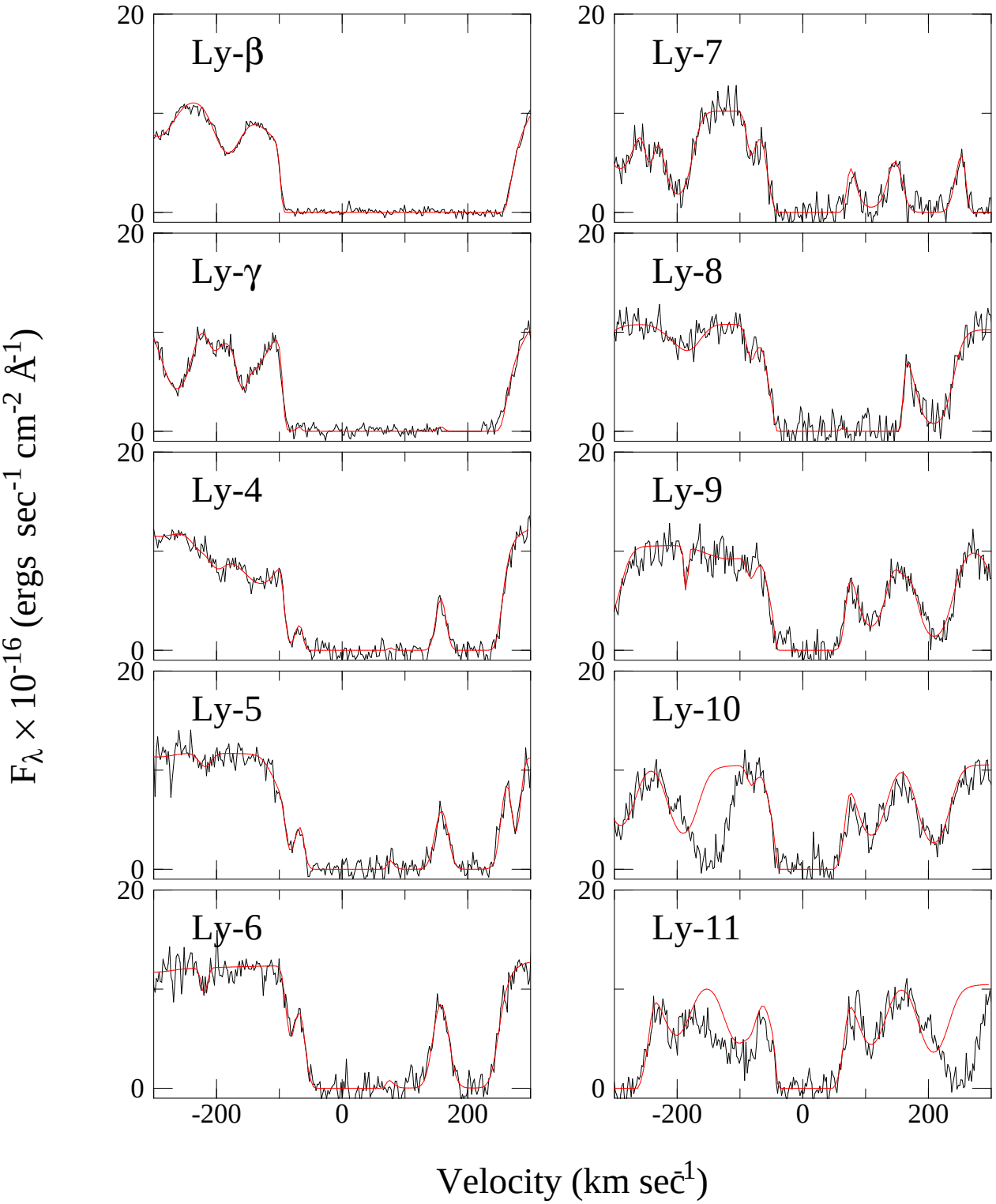


FIG. 11.— The complex continuum shown in Fig. 10 is required to obtain the fit shown here using relatively few Ly$\alpha$ forest lines.

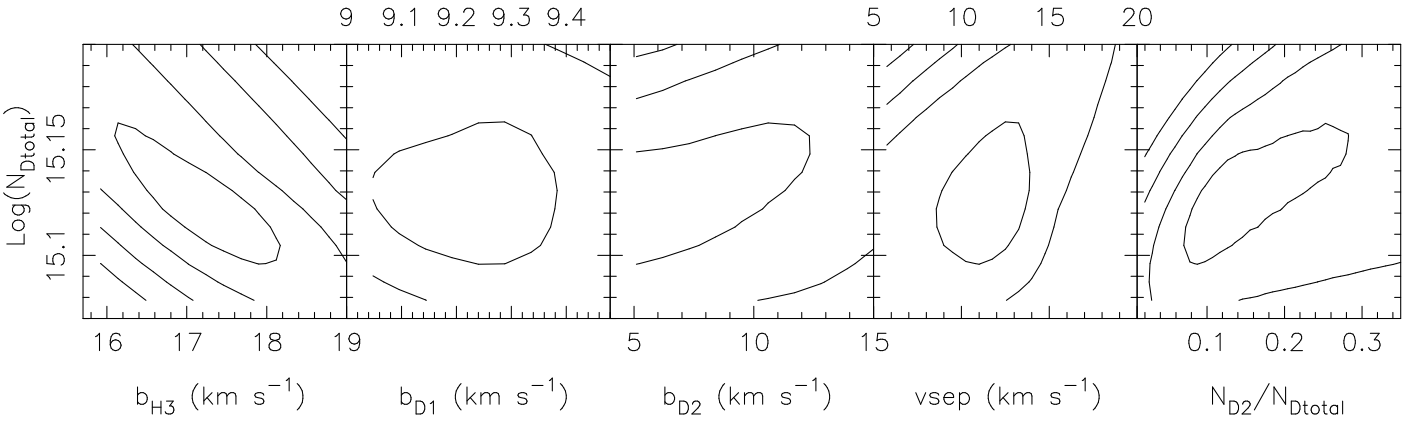


FIG. 12.— The results of our grid search to measure $N_{DI}$. We plot contours of constant $\chi^2$ for $N_{DI}$ against each of the parameters we varied in the search. The contours are at the 1,2,3, and 4 sigma levels.

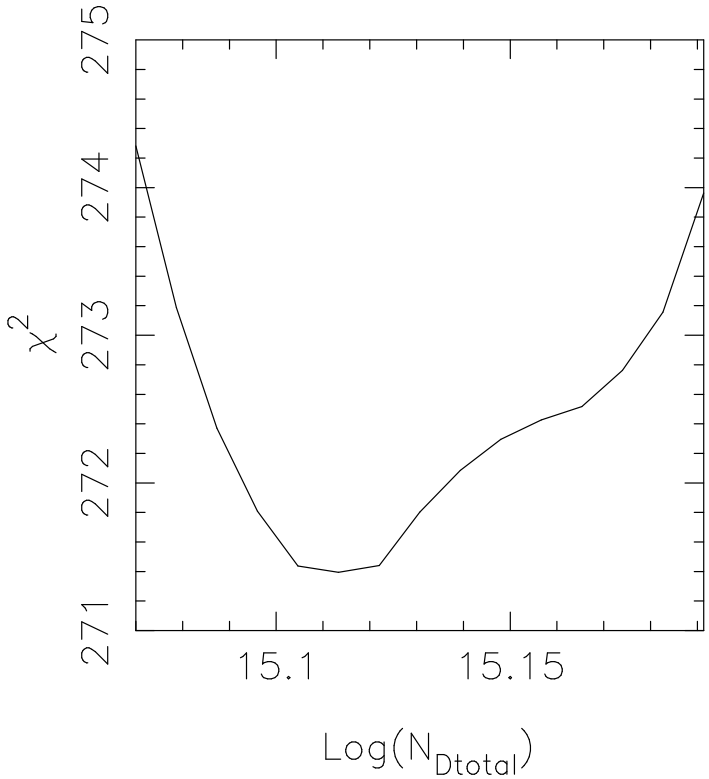


FIG. 13.— The minimum $\chi^2$ value that we found in our grid search, as a function of the total $N_{DI}$ ($cm^{-2}$) in components 1 and 2

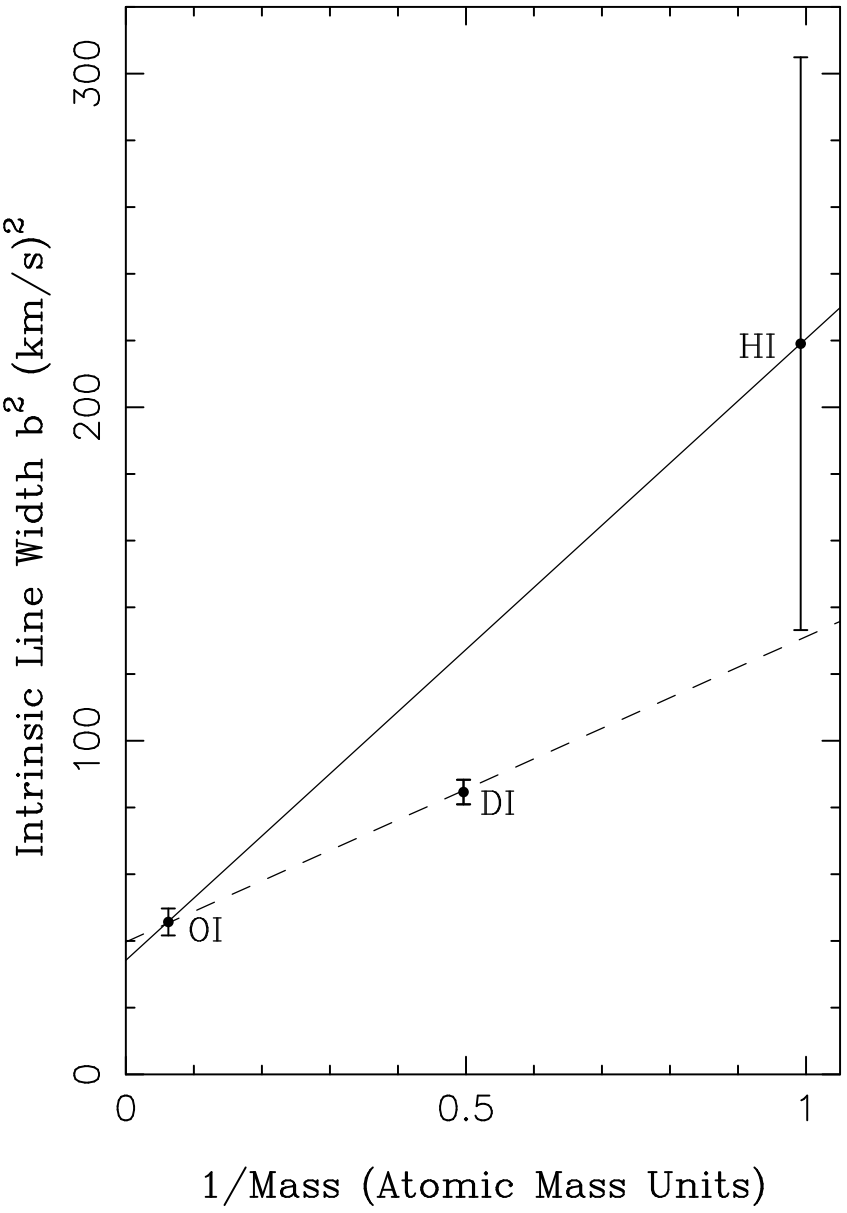


FIG. 14.— Square of the intrinsic width of the lines of ions as a function of 1/mass of the ion in atomic mass units. We plot the $b_{int}^2$ for the main components of the O I, D I and H I (components O-1, D-1 and H-1). The solid line connects the O I and H I points and ignores the D I. The slope of this line gives a temperature $T = 1.1 \pm 0.6 \times 10^4$ K and the intercept gives the turbulent velocity of $b_{turb} = 5.8 \pm 0.6$ km s$^{-1}$. The line predicts $b(D-1) = 11.3 \pm 1.8$ km s$^{-1}$. The observed $b(D-1) = 9.2 \pm 0.2$ km s$^{-1}$ is $1.2\sigma$ below, and consistent with this prediction. The dashed line that is the best fit to O, H and D. The data are also consistent with this fit, which we prefer. Although the $b$-value of the H-1 component is not well known, the data shown on this plot provide evidence that D-1 is D rather than H.

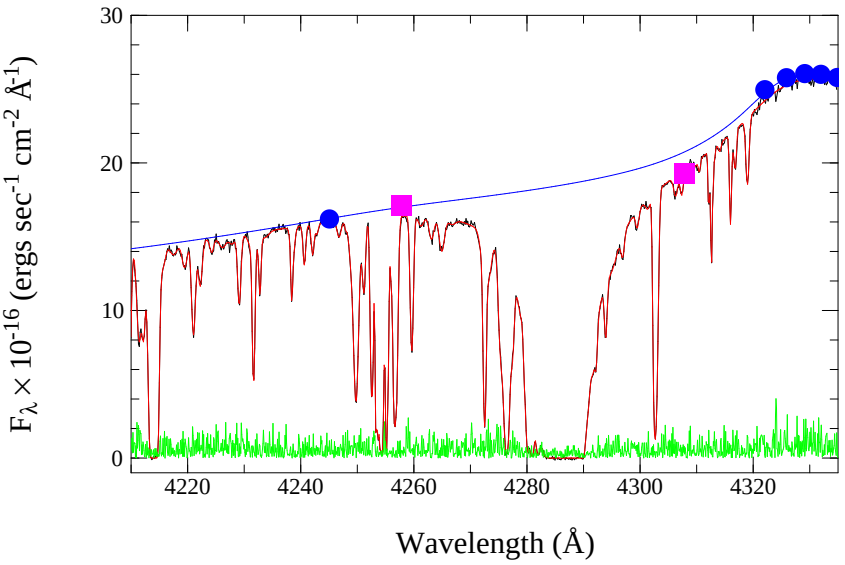


FIG. 15.— Our initial model of the spectrum 4284 Å. We show the observed data, our model and the continuum level of our model. The jagged horizontal array below 2 units of flux shows five times the absolute value of the difference between our model and the data. The squares and circles are the b-spline control points that define the continuum model. The circles are fixed in wavelength and free in flux, while the squares are free in both wavelength and flux. The $\chi^2$ for this model is 5911, with 4759 degrees of freedom.

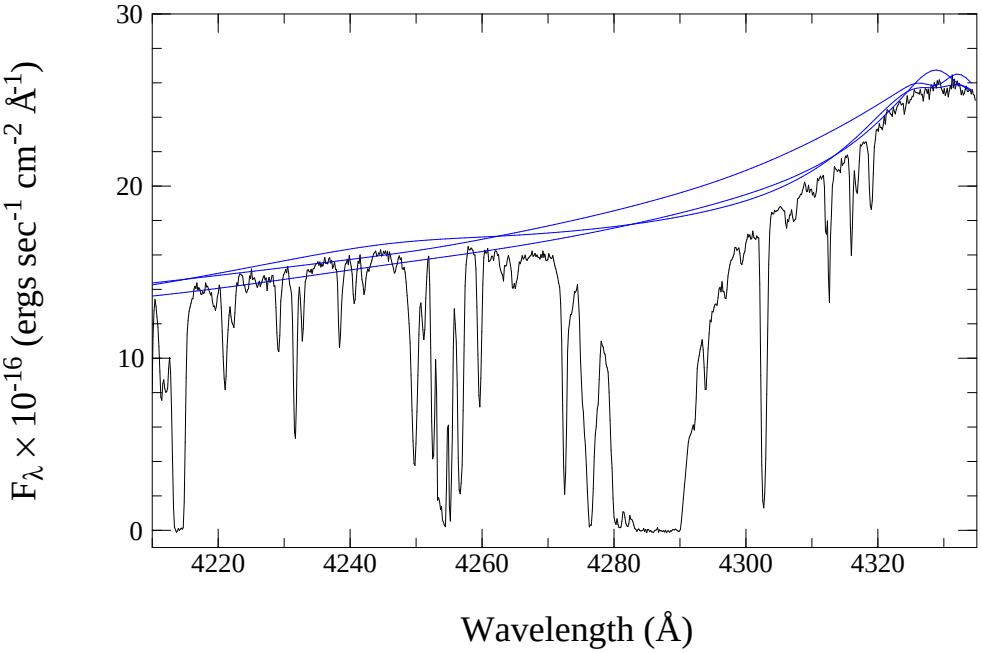


FIG. 16.— Three of the randomly generated continua used at the start of the optimization restarts that we used to estimate $N_{HI}$.

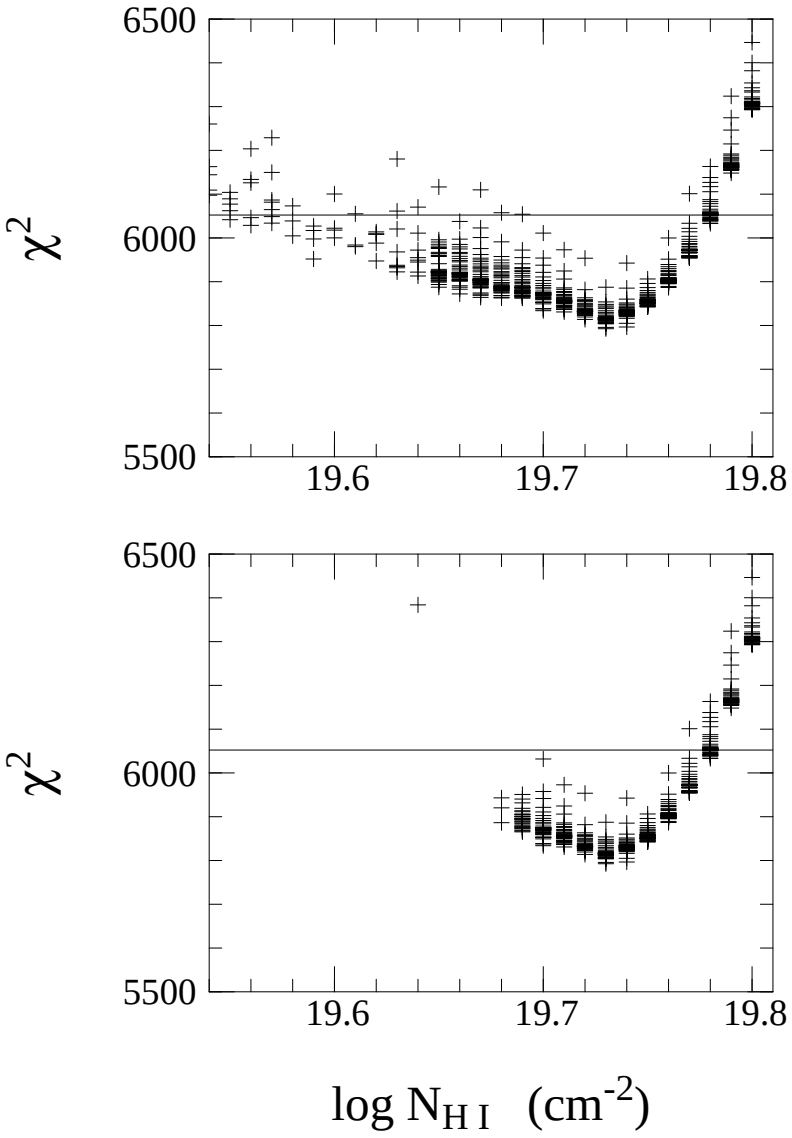


FIG. 17.— $\chi^2$ values as a function of the log $N_{HI}$ in components 1 and 2. The $\chi^2$ values are those returned by the optimization code. The results are shown for 3195 restarts. Models containing Ly$\alpha$ forest absorbers with $b > 150$ km s$^{-1}$ are excluded from the lower panel. We accept log $N_{HI}$ values that gave $\chi^2$ values below the horizontal lines at 6052.3.

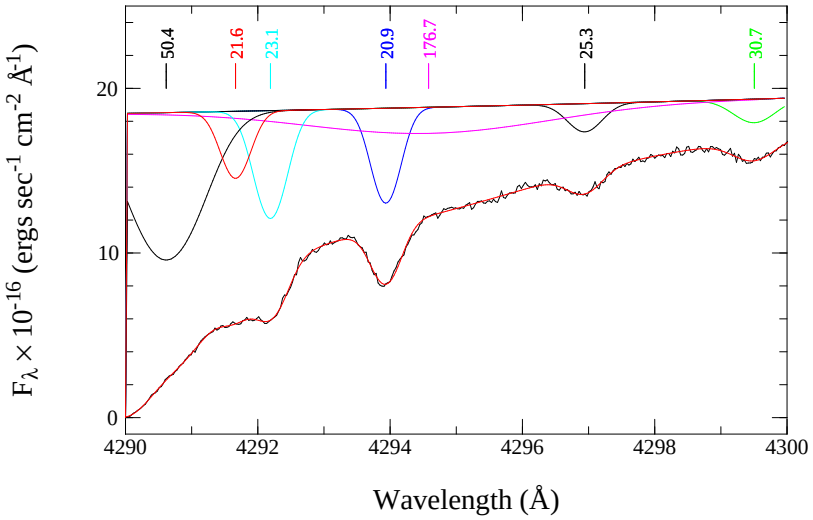


FIG. 18.— Example of a model with a wide Ly$\alpha$ forest absorption line. This model has log $N_{HI}$ = 19.67 cm$^{-2}$ and uses the Ly$\alpha$ forest lines that we show, including the wide, shallow line centered near 4294.5 Å with $b$ = 176.7 km s$^{-1}$. The line running through the spectrum is the complete model that includes the continuum level, the DLA and the Ly$\alpha$ forest lines. The optimizer restarts found a number of models, typically with log $N_{HI}$ < 19.69 cm$^{-2}$, which used similar wide Ly$\alpha$ forest lines. In these cases, it appears that the optimizer is using wide Ly$\alpha$ forest absorption to provide opacity that should be provided by the DLA or the continuum. Because such wide Ly$\alpha$ forest lines are not observed in other studies of the Ly$\alpha$ forest, we rejected models with wide Ly$\alpha$ forest lines.

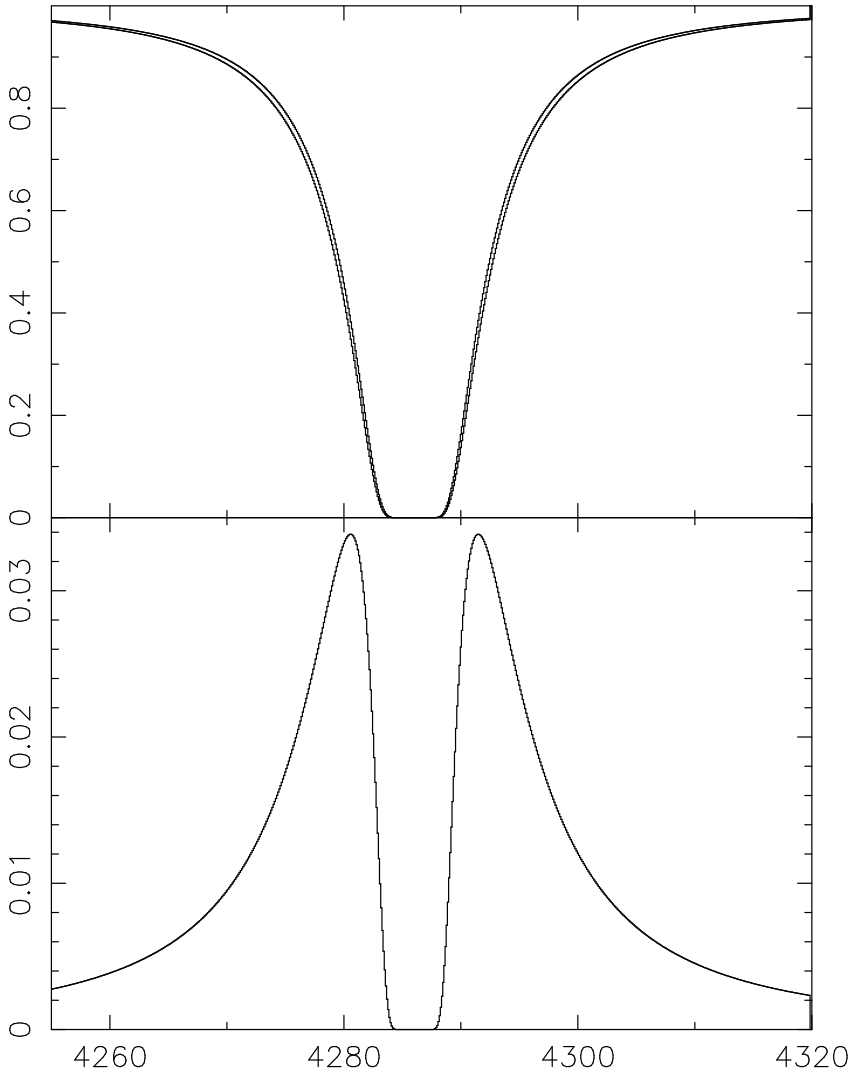


FIG. 19.— The upper panel shows the normalized in flux profiles of two absorption lines whose column densities differ by log $N_{HI} = 0.04$ $cm^{-2}$, the error we quote on the log $N_{HI}$ value for the system that shows D. The upper line has a column density of log $N_{HI} = 19.73$ $cm^{-2}$. The lower panel displays the difference in flux between these two absorption line profiles.

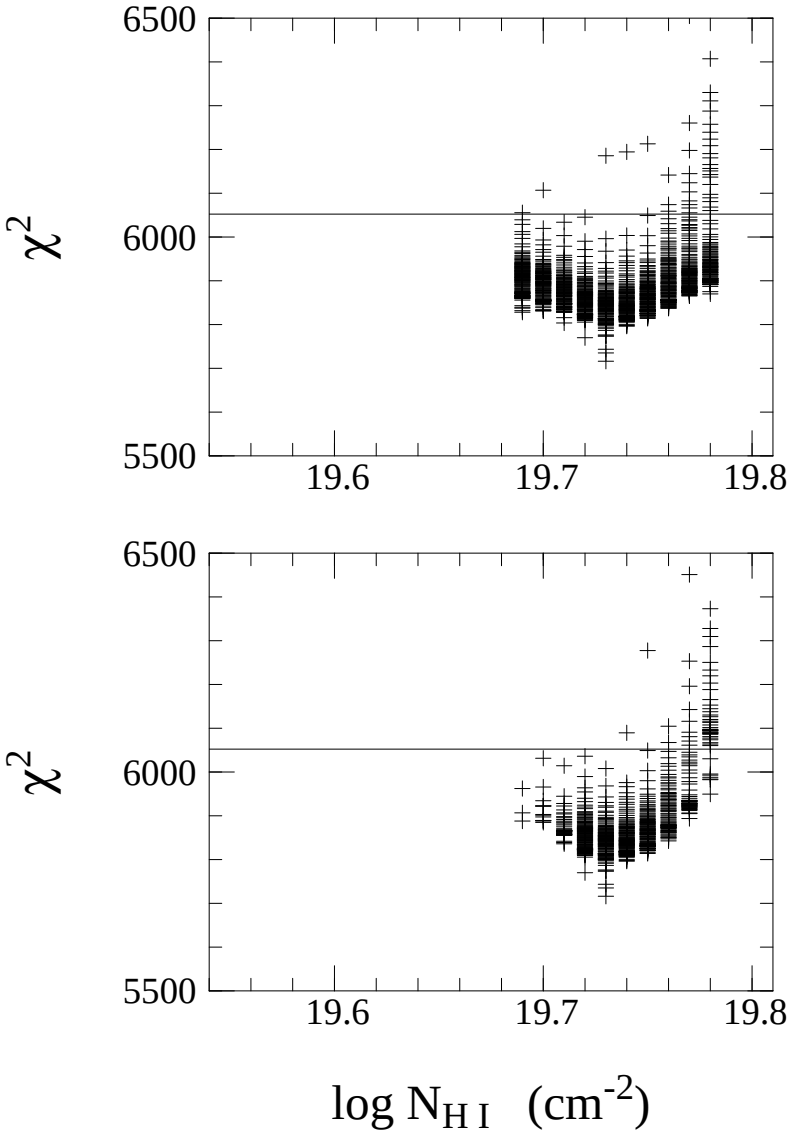


FIG. 20.— As 17, only for the 7898 optimization restarts with three continuum control points in the region between 4260 Å and 4325 Å.

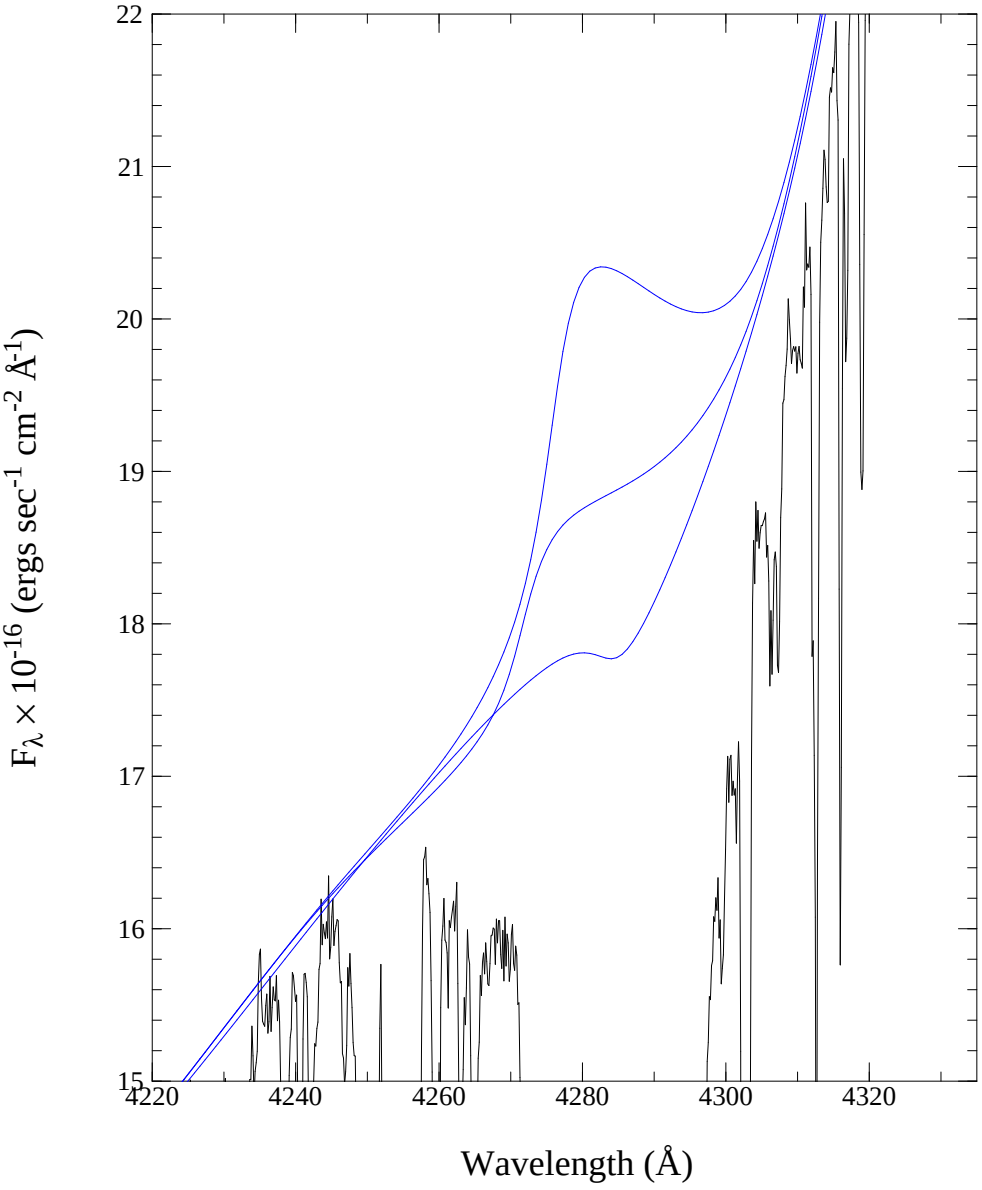


FIG. 21.— Three examples of continuum shapes that were rejected by the filter we applied to the three continuum control point models.

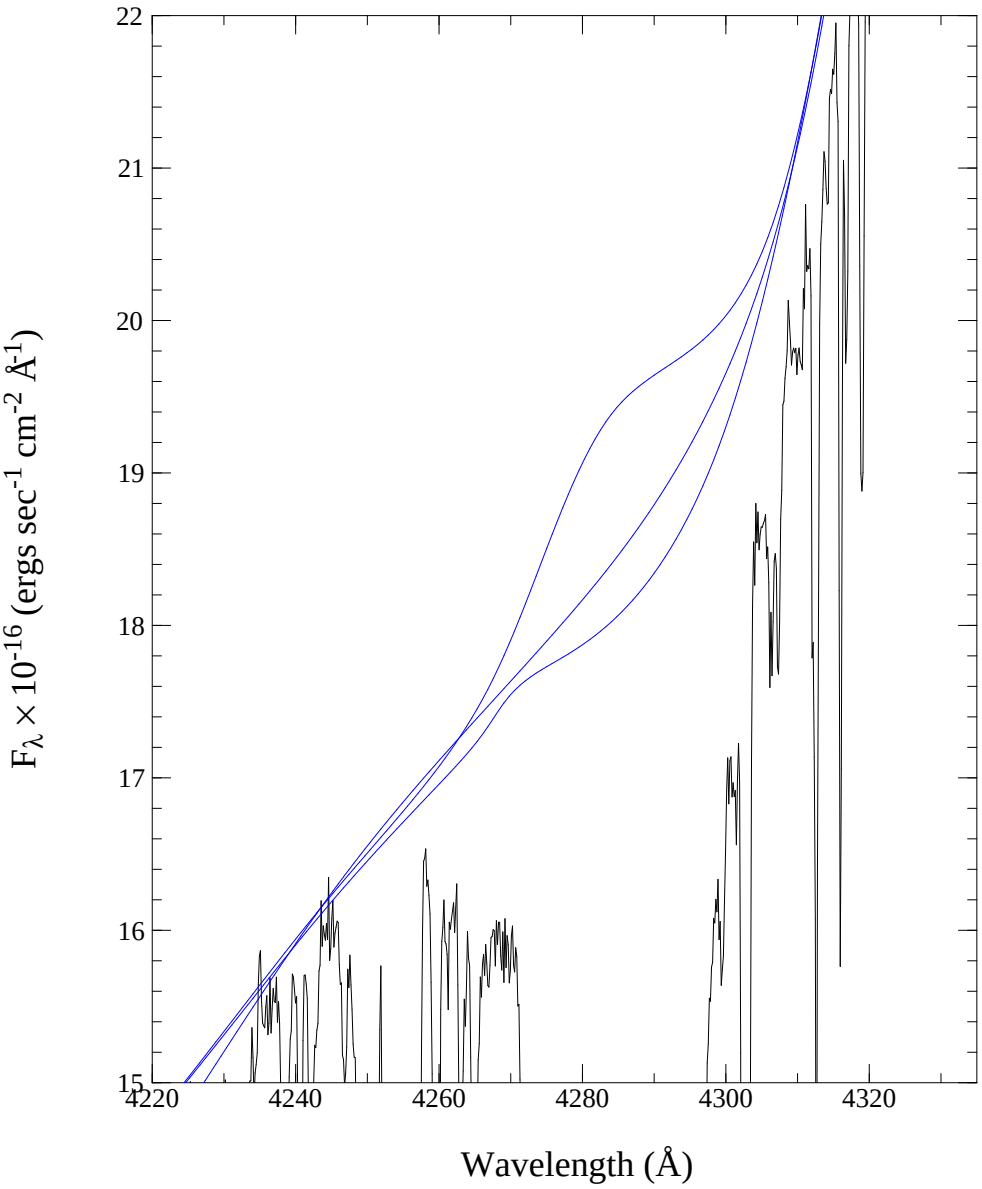


FIG. 22.— Three examples of continuum shapes that were found acceptable by the filter we applied to the three continuum control point models. The top curve is from a model with log $N_{HI} = 19.78$ cm$^{-2}$, the middle curve is from a model with log $N_{HI} = 19.73$ cm$^{-2}$, and the bottom curve is from a model with log $N_{HI} = 19.69$ cm$^{-2}$.

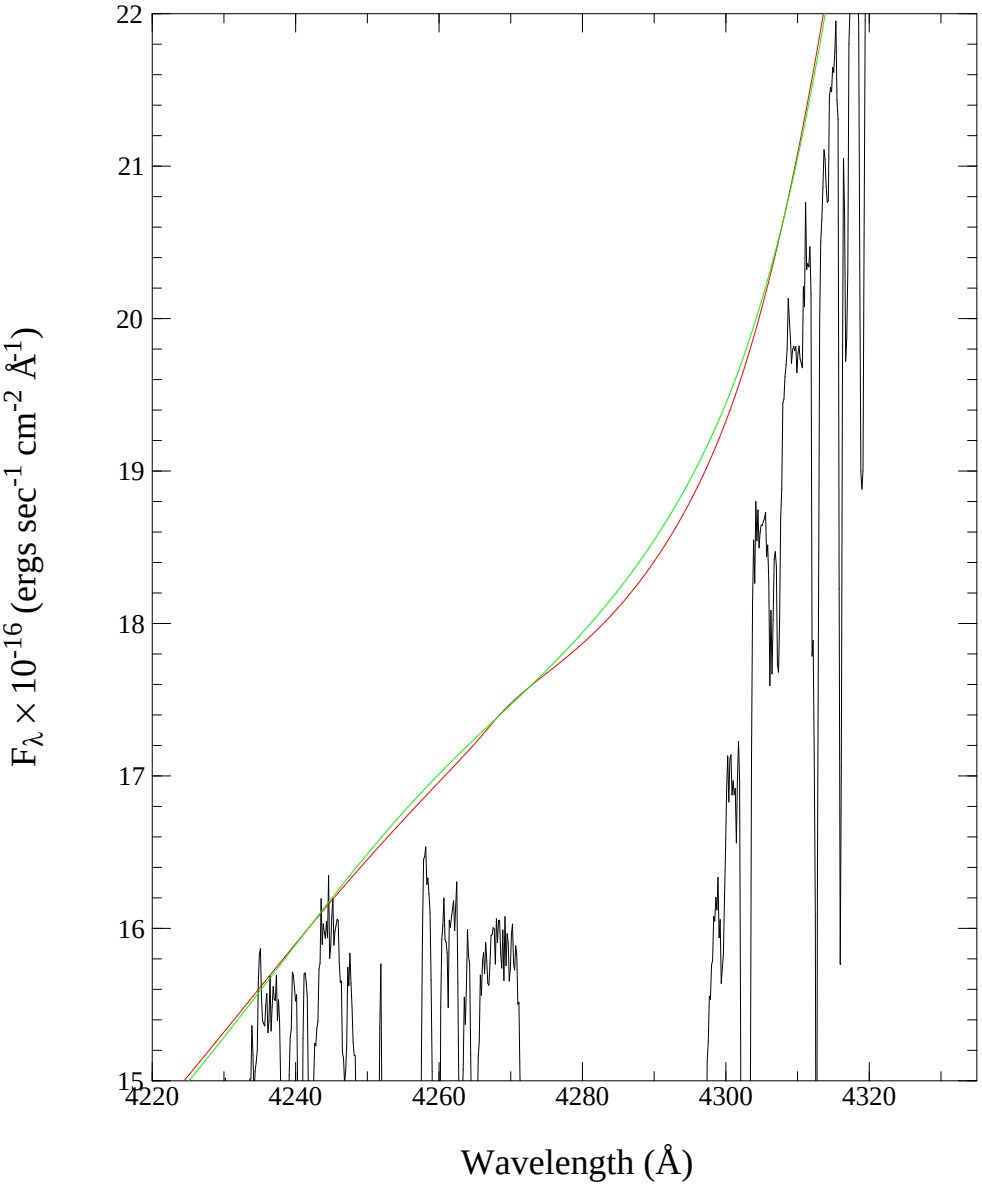


FIG. 23.— The continua for the best models we were able to find with log $N_{HI} = 19.69$ cm$^{-2}$. The continuum that is low at 4290Å is from the best model with three continuum control points in the region between 4260Å and 4325Å. The other curve is from the best model with two continuum control points.

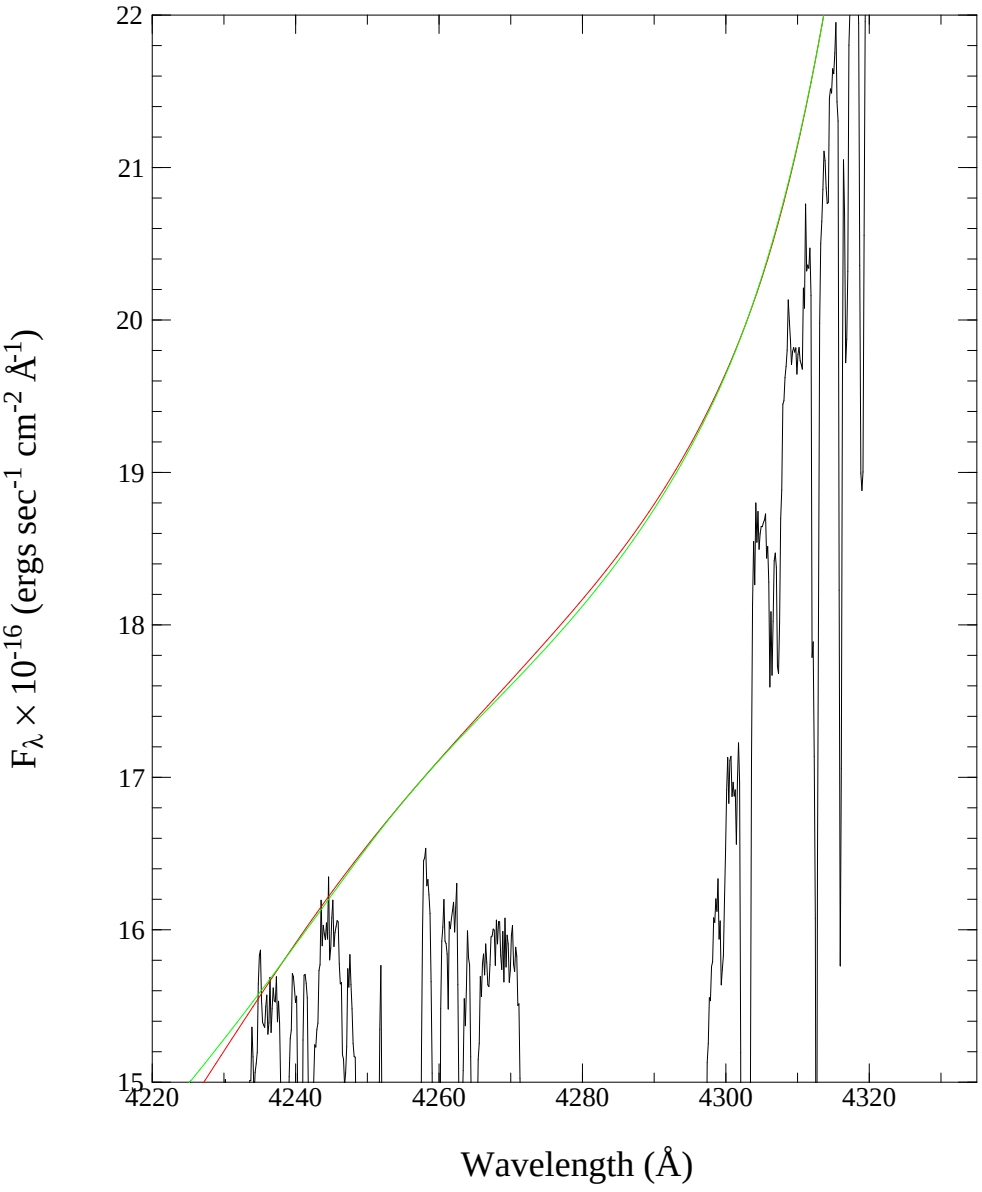


FIG. 24.— As 23, but for models with log $N_{HI} = 19.73$ cm$^{-2}$.

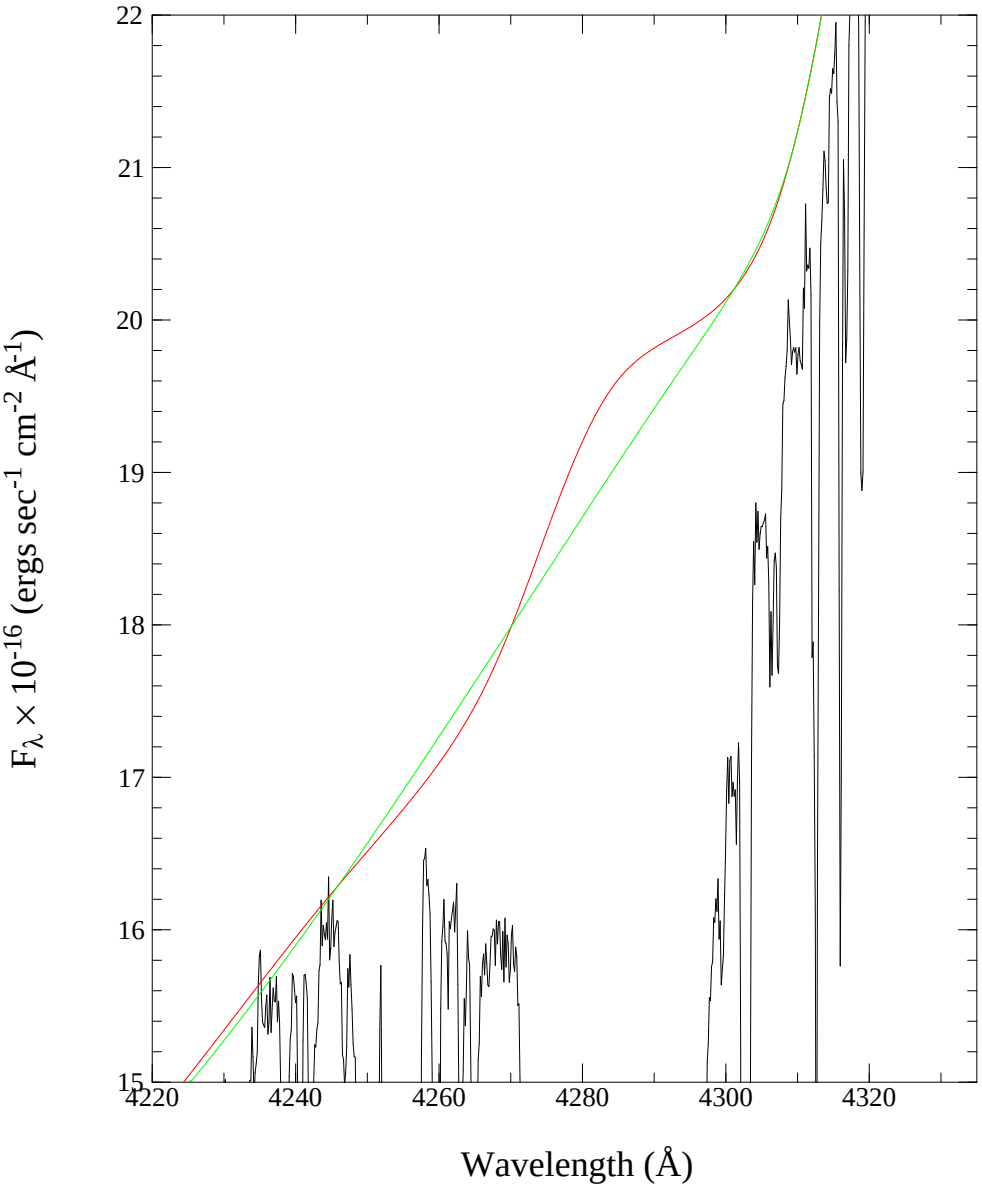


FIG. 25.— As 23, but for models with log $N_{HI} = 19.78$ cm$^{-2}$. In this case the three continuum control point model is high at 4290Å.

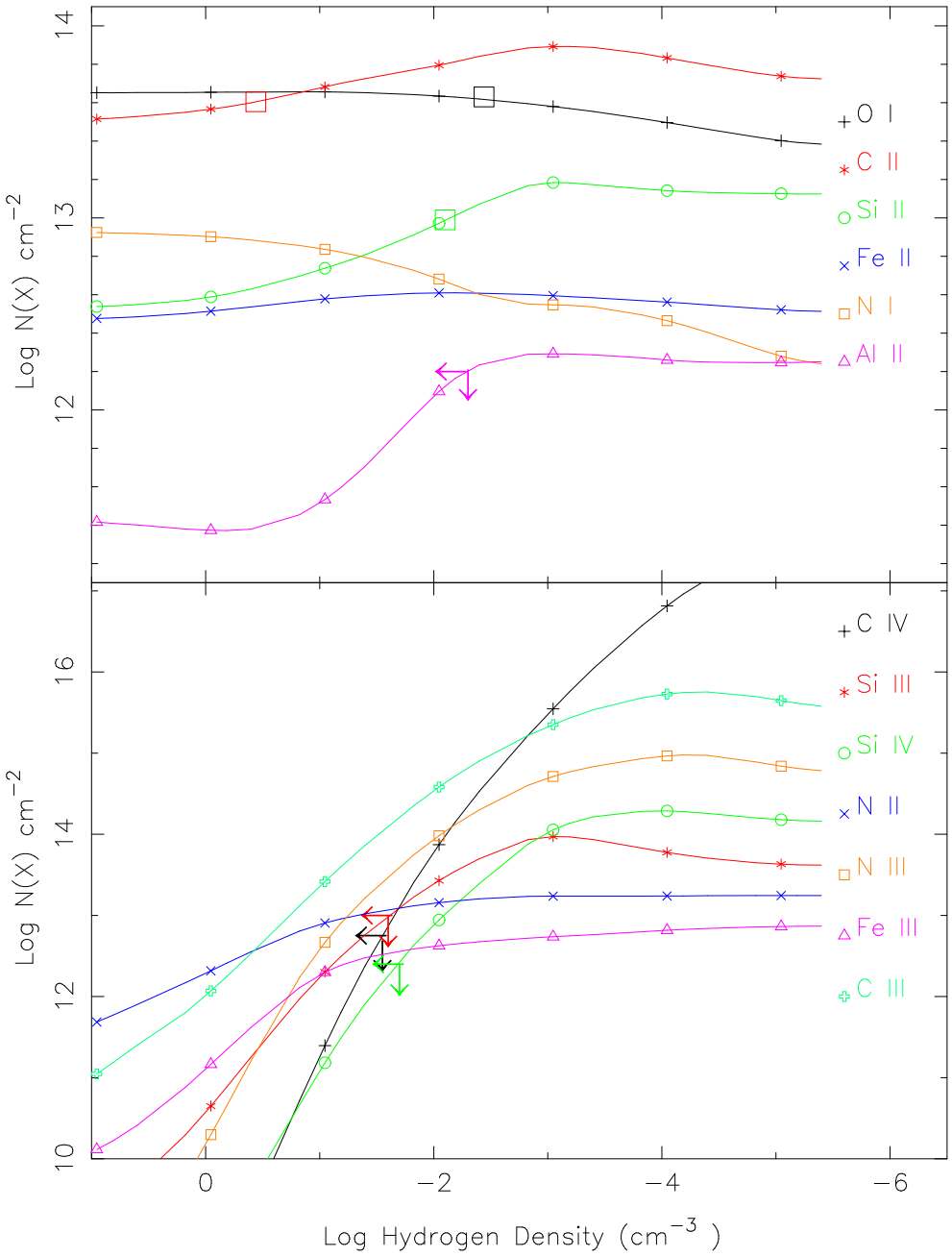


FIG. 26.— Column densities for various metal ions as a function of the hydrogen density $n_H$ for a photoionized cloud with log $N_{HI}$ = 19.73 cm$^{-2}$, a metal abundance $[X/H] = -2.77$, and a $J_{912} = 10^{-21}$ ergs cm$^{-2}$ s$^{-1}$ Hz$^{-1}$ sr$^{-1}$. Ionization increases to the right. We show solar abundance ratios. The O I column density is insensitive to the ionization. Measured column densities in components 1 & 2 are shown by the three large boxes in the upper panel, while four allowed upper limits are shown by arrows. The preferred density is $\log n_H \simeq -1.5$ cm$^{-3}$.

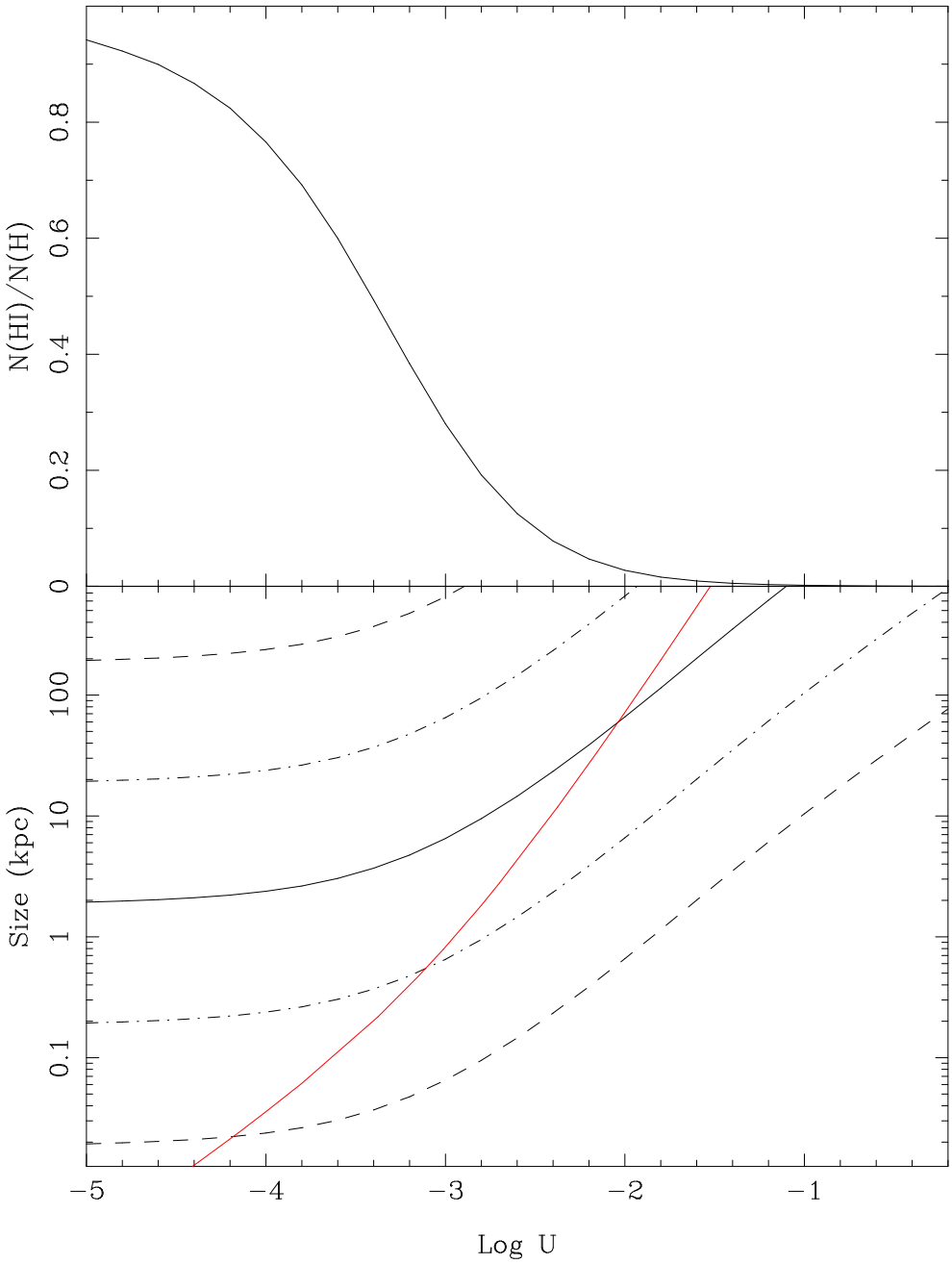


FIG. 27.— The upper panel shows the neutral fraction of the gas with log $N_{HI}$= 19.73 cm$^{-2}$ as a function of ionization parameter log $U$ as returned by Cloudy, assuming a constant Hydrogen density of $n_H = 0.01$ cm$^{-3}$. The lower panel shows the size of the absorber along the line of sight in kpc, again as a function of log $U$. In the lower panel, the solid curve that begins at 2 kpc displays the absorber size when $n_H = 0.01$ cm$^{-3}$. The $J_{912}$ increases to the right along this and other curves with the same shape. We also show curves for $n_H$ increased (lower on the plot) or decreased by a factor of 10 (dot-dashed lines) or 100 (dashed lines). The steeper curve that begins on the horizontal axis at log $U = -4.4$ shows the size when the $J_{912} = 10^{-21}$ ergs cm$^{-2}$ s$^{-1}$ Hz$^{-1}$ sr$^{-1}$. The density increases to the right along this curve. The ion column densities indicate log $U \simeq -2.84$.

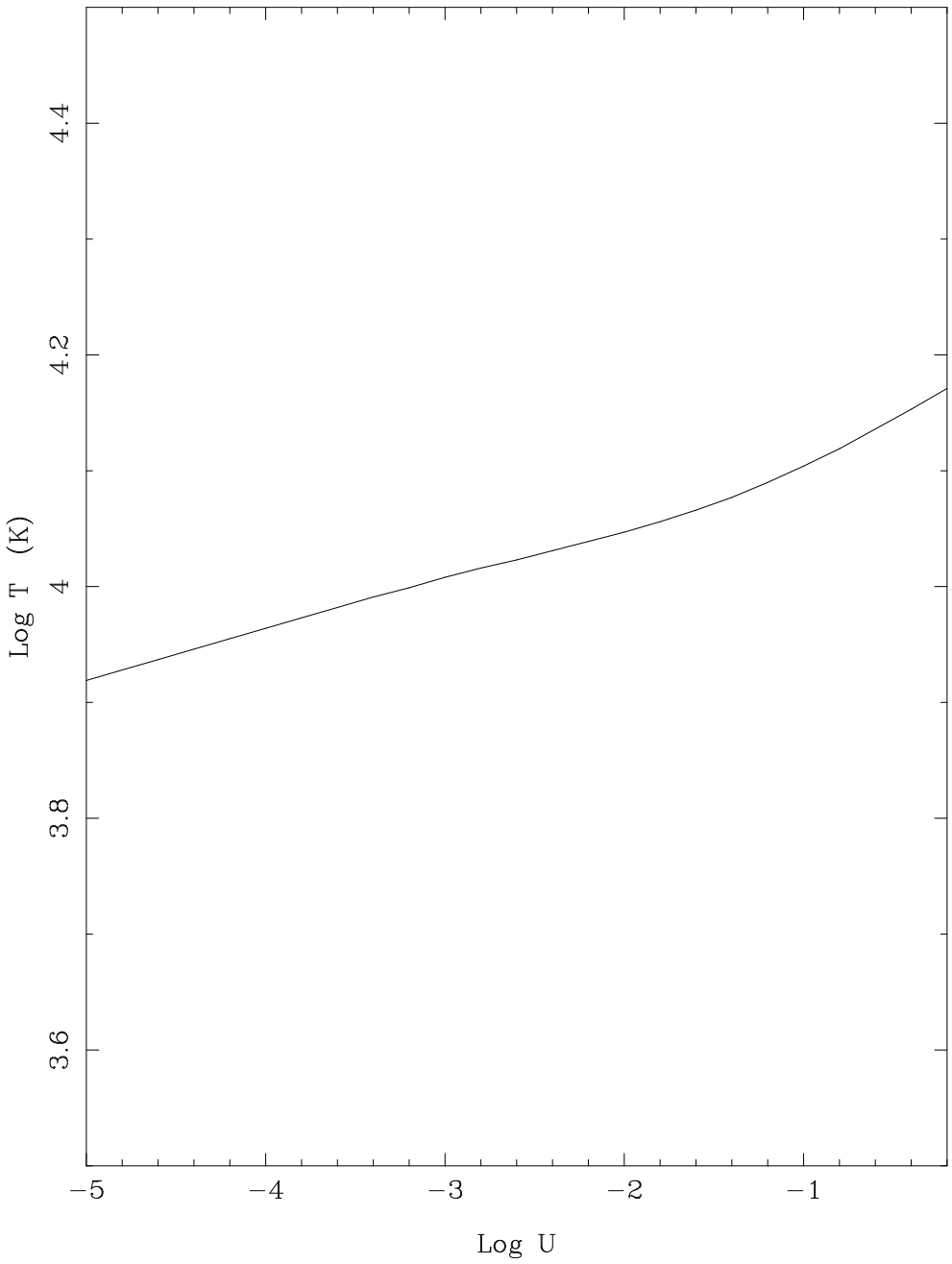


FIG. 28.— Temperature for the gas returned by Cloudy for an absorber with log $N_{HI}$= 19.73 $cm^{-2}$as a function of the ionization parameter $\log U$.

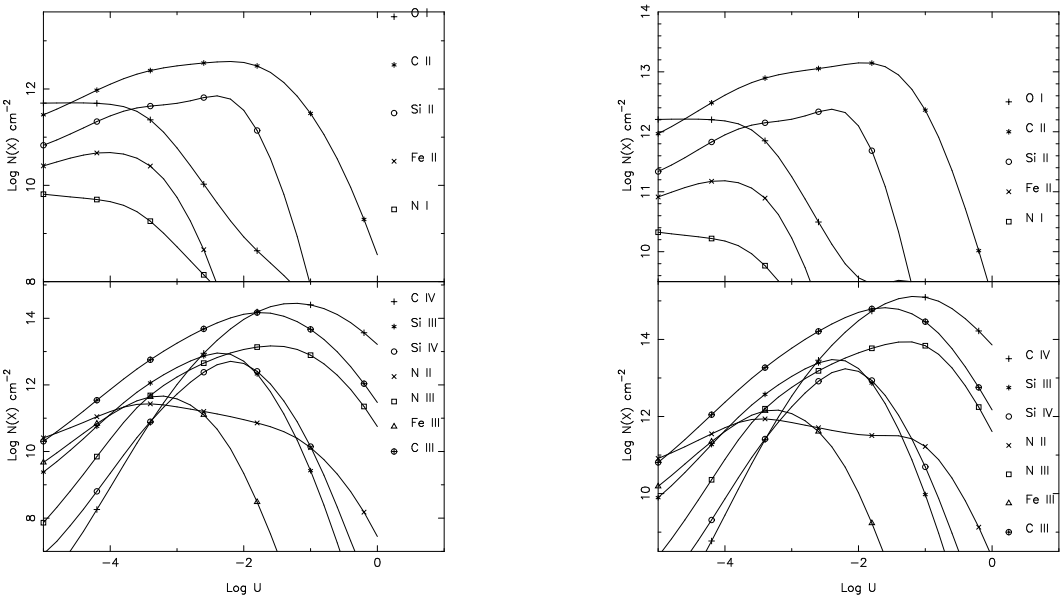


FIG. 29.— Cloudy simulations for log $N_{HI}$= 16.0cm$^{-2}$ (left panel), and log $N_{HI}$= 16.5cm$^{-2}$ (right) assuming a Hydrogen density $n_H = 0.001$ cm$^{-2}$ and a metal abundance of [X/H] = −1.5 as a function of ionization parameter $\log U$. For this figure alone, we enhanced the O and Si abundances by 0.3 dex, and lowered N by 0.45 dex to match [N/O] in DLAs and elsewhere (Prochaska *et al.* 2002; Edmunds, Henry & Koppen 2001). The results on the left are applicable to the component near –40 km s$^{-1}$ that we call component 3, while those on the right are for the component near +100 km s$^{-1}$.

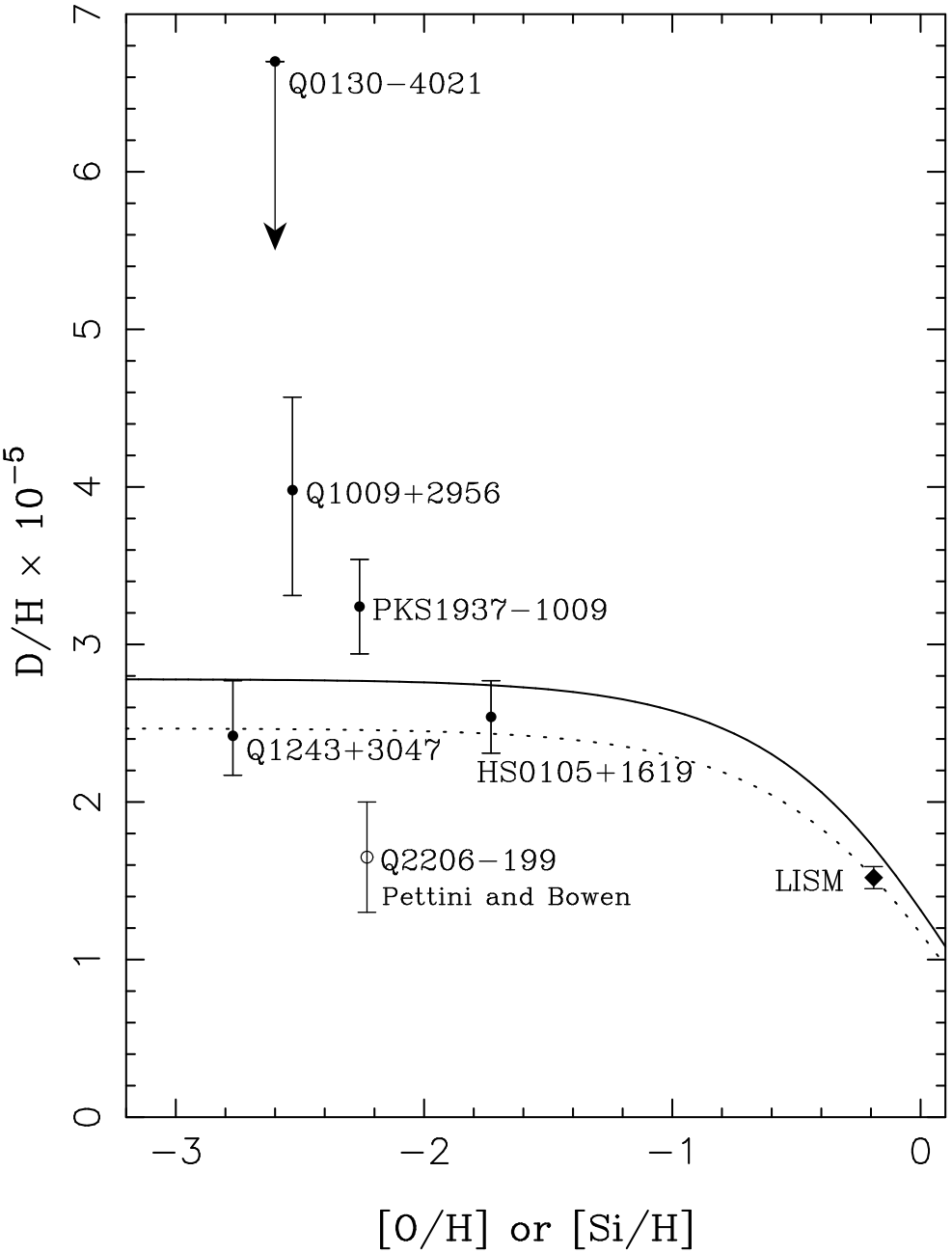


FIG. 30.— Measurements of D/H as a function of the Silicon or Oxygen abundance in the gas. The solid circles are from our group, Q2206–199 is from Pettini & Bowen (2001) and the diamond is the local interstellar medium (LISM) measurement (Oliveira *et al.* 2002). The error bars are intended to be $1\sigma$ but we suspect that in some cases they have been underestimated. The curves show a closed box model for the expected D/H evolution. The solid curve is normalized to the primordial D/H from five QSOs while the dotted curve uses the D/H value in the LISM.

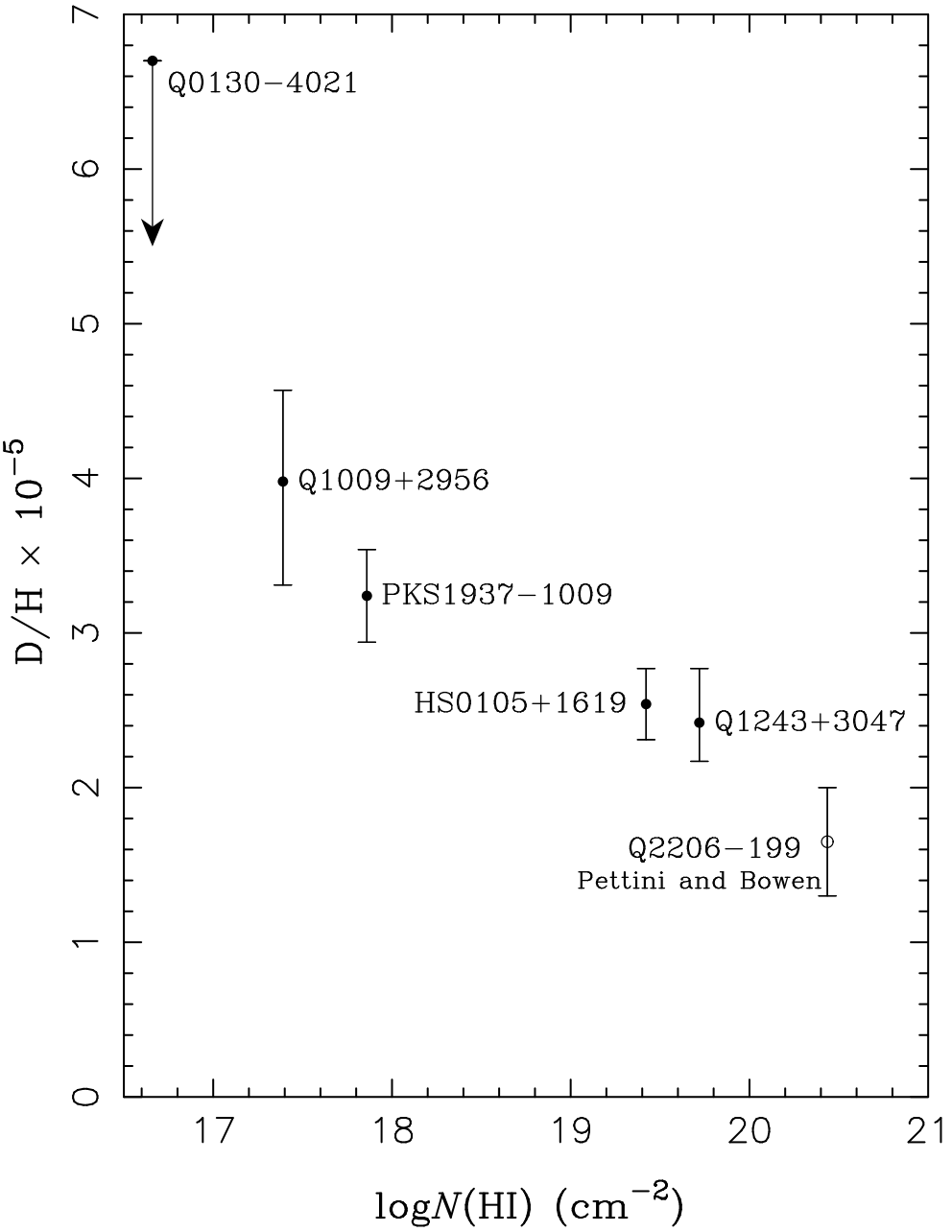


FIG. 31.— As Fig. 30 but showing D/H as a function of the H I column density. This correlation is unexpected and we believed it is an accident.

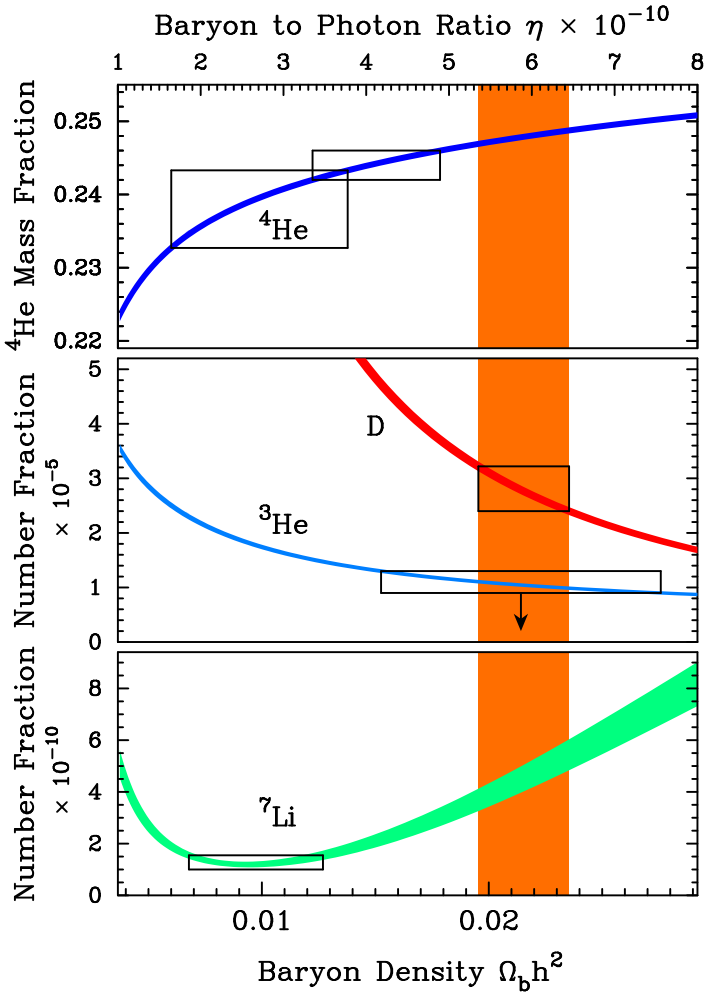


FIG. 32.— Comparison of predicted and measured abundances of four light nuclei as a function of the baryon density. The figure has three vertical panels each with a different linear scale. The curves show the abundance ratios predicted for SBBN, from the calculations by Burles, Nollett and Turner(2001). The top curve is the $^4$He mass as a fraction of the mass of all baryons, while the three lower curves are the number fractions D/H, $^3$He/H and $^7$Li/H. The vertical widths of the curves show the uncertainties in the predictions. The five boxes show measurements, where the vertical extension is the $1\sigma$ random error, and the horizontal range is adjusted to overlap the prediction curves. For $^4$He the larger box is from Olive, Steigman and Skillman (1997), and the error includes in quadrature the systematic error from Olive and Skillman (2001). The smaller $^4$He box is from Izotov & Thuan (1998). The D/H box is the mean from five QSOs from this paper. The $^3$He from Bania, Rood & Balser (2002) is an upper limit. The $^7$Li is from Ryan *et al.* (2000). We expect that all the data boxes should overlap the vertical band that covers the D/H data. They do not, probably because of systematic errors.